City Research Online

City, University of London Institutional Repository

Thermal Spray Coatings for Electromagnetic Wave Absorption and Interference Shielding: A Review and Future Challenges

Nadimul Haque Faisal,* Rehan Ahmed, Nazmi Sellami, Anil Prathuru,
James Njuguna, Federico Venturi, Tanvir Hussain, Hamed Yazdani Nezhad,
Nirmal Kumar Katiyar, Saurav Goel, Hari Upadhyaya, Shrikant Joshi,
Firdaus Muhammad-Sukki, Radhakrishna Prabhu, Tapas Mallick, Will Whittow,
and Spyros Kamnis

This review aims to consolidate scattered literature on thermally sprayed coatings with nonionizing electromagnetic (EM) wave absorption and shielding over specific wavelengths potentially useful in diverse applications (e.g., microwave to millimeter wave, solar selective, photocatalytic, interference shielding, thermal barrier-heat/emissivity). Materials EM properties such as electric permittivity, magnetic permeability, electrical conductivity, and dielectric loss are critical due to which a material can respond to absorbed, reflected, transmitted, or may excite surface electromagnetic waves at frequencies typical of electromagnetic radiations. Thermal spraying is a standard industrial practice used for depositing coatings where the sprayed layer is formed by successive impact of fully or partially molten droplets/particles of a material exposed to high or moderate temperatures and velocities. However, as an emerging novel application of an existing thermal spray techniques, some special considerations are warranted for targeted development involving relevant characterization. Key potential research areas of development relating to material selection and coating fabrication strategies and their impact on existing practices in the field are identified. The study shows a research gap in the feedstock materials design and doping, and their complex selection covered by thermally sprayed coatings that can be critical to advancing applications exploiting their electromagnetic properties.

1. Introduction

Complex values, such as magnetic permeability (μ), electrical permittivity (ε), electrical conductivity (σ), and dielectric loss, constitute the electromagnetic (EM) properties of a material. The interaction of a dielectric material with EM waves depends on the material properties such as the electric permittivity (i.e., polarization or formation of electric dipole), magnetic permeability (i.e., magnetization or formation of magnetic dipole), electrical conductivity (i.e., ability to conduct an electric current due to the presence of unbound electrons moving), and dielectric loss. This means that when EM waves (nonionizing: radio waves, microwaves, infrared, visible light, ultraviolet rays) with a velocity of $2.998 \times 10^8 \, \text{m s}^{-1}$ (in vacuum) propagate through or interact with materials, they can be absorbed, reflected, transmitted, or may excite surface EM waves (SEW).[1–3]

Figure 1 shows example applications of dielectric materials that can interact with EM waves, and how their manufacturing using coating techniques (including thermal spray) can address the technological requirements. As will be seen through this

N. H. Faisal, N. Sellami, A. Prathuru, J. Njuguna, R. Prabhu
School of Engineering
Robert Gordon University
Garthdee Road, Aberdeen AB10 7GJ, UK
E-mail: N.H.Faisal@rgu.ac.UK

The ORCID identification number(s) for the author(s) of this article can be found under https://doi.org/10.1002/adem.202200171.

R. Ahmed
School of Engineering and Physical Sciences
Heriot-Watt University
Edinburgh EH14 4AS, UK

N. Sellami, F. Muhammad-Sukki
School of Engineering and Built Environment
Edinburgh Napier University
10 Colinton Road, Edinburgh EH10 5DT, UK

F. Venturi, T. Hussain
Faculty of Engineering
University of Nottingham
Nottingham NG7 2RD, UK

Figure 1. Example applications of dielectric material that can interact with EM waves and how their manufacturing using coating techniques can address the technological requirements.

review, EM (nonionizing) wave propagation characteristics and performance of thermal spray coating materials have been investigated, which gains their properties from their microstructure as well as composition.

Thermal spraying is a standard industrial practice used for coating deposition, where the sprayed layer is formed by fully or partially molten droplets/particles of the material impacting a surface to form "splats" that are the "building blocks" for coating formation. These splats overlap due to relative motion between the thermal spray gun and the surface to cover large areas, while stacking of the splats during successive passes of the gun leads to desired coating thickness build-up. Several variant processes exist within the thermal spray family and yield a

range of gas temperatures and velocities that provide the driving force for heat up/melting and acceleration of the droplets/particles (e.g., 3,000–15 000 °C at 50 to 1000 m s^{-1} velocities: arc, flame, plasma, high-velocity oxy-fuel [HVOF], detonation spray, etc.). This can also be at cold temperature (e.g., up to 800 °C at 200 m s and 1000 m s^{-1} velocities; cold gas dynamic spraying), in which case kinetic energy plays a more dominant role in coating formation than thermal energy. Typically, in all the conventional thermal spray techniques, molten and/or semimolten droplets are propelled through a spraying gun on to the substrate and these flatten upon impact to form "splats" which are regarded as the building blocks for coating formation.[4] In case of cold spray (CS), primarily meant to deposit coatings from

H. Y. Nezhad
Department of Mechanical Engineering and Aeronautics
City, University of London
London EC1V 0HB, UK

N. K. Katiyar, S. Goel, H. Upadhyaya
School of Engineering
London South Bank University
103 Borough Road, London SE1 0AA, UK

S. Goel
Department of Mechanical Engineering
Indian Institute of Technology Guwahati
Guwahati 781039, India

S. Goel
Department of Mechanical Engineering
University of Petroleum and Energy Studies
Dehradun 248007, India

S. Joshi
Department of Engineering Science
University West
Trollhättan 46186, Sweden

T. Mallick
Environment and Sustainability Institute
University of Exeter
Penryn Campus, Cornwall TR109FE, UK

W. Whittow
Wolfson School of Mechanical, Electrical and Manufacturing Engineering
Loughborough University
Loughborough LE11 3TU, UK

S. Kamnis
Castolin Eutectic - Monitor Coatings Ltd
North Shields NE29 8SE, UK

ductile feedstock, the particles plastically deform on impact at extremely high velocity. Recent trends have been to produce thermally sprayed ceramic coatings with nanostructures or refined microstructures and precision-engineered surface textures.[5,6] Thermal spray grade powder particle shape, geometry, size, orientation, and arrangement during thermal spraying of a chosen material can affect the EM waves in an unconventional manner, thereby creating material (surface) properties which are not achievable using conventional processes.

Thermal spray coating method has been used as one of the deposition technologies for the formation of semiconducting coatings for devices, apart from other fabrication methods (e.g., molecular beam epitaxy [MBE], hydrid vapor-phase epitaxy [HVPE], liquid-phase epitaxy [LPE], metal–organic molecular beam epitaxy [MOMBE], and atomic layer deposition [ALD]). Contrarily to atomistic film deposition methods such as reactive evaporation or reactive sputtering, thermal spraying does not enable synthesis of new compounds during processing.[7] During the thermal spray-coating process, a coating is built up from powder particles (typically ranging from submicrometer to few tens of micrometers in size) and not, from atoms or molecules. Any particle used in thermal spraying remains molten in a flame for a time of milliseconds and then solidifies rapidly during a few microseconds.[4] However, some metastable phases could form due to rapid solidification of particles on impact with the substrate.

The field of coatings with EM wave absorption and shielding characteristics is an interesting subject area in which the use of thermal spraying has not advanced significantly, although there are good examples. Such coatings may be appropriate when it is desirable for the surface to behave as an EM absorber, reflector, or transmitter for single or multiple frequencies. Knowledge of the EM wave interaction behavior in thermal spray coatings (including substrate) is important because such materials can be tailored to possess microstructures and composition that will suitably respond to EM waves. When such coatings are placed into an EM field, the waves can be absorbed, emitted, transmitted, or may excite SEWs at special frequencies as demanded by the targeted functionality. In this review, the potential influence of fabrication schemes, microstructure, and composition on the EM wave performance of thermally sprayed coating materials is assessed. The influence of the microstructure as well as multicomponent alloy design on EM properties is also analyzed from the perspective of associated mechanisms.

2. Thermal Spray Coatings as a Manufacturing Route for EM Material Applications

Components for EM applications require a combination of the complex mix of properties (depending upon requirements),[8] such as good impedance matching, high thermal and electrical conductivity, high melting point, good thermal resistance, conductors and nonconductors, low environmental degradation, high strength, low density, high flexibility, lightweight, noncorrosiveness, no chemical reaction between material components, and cost-effective commercial feasibility, including mechanical strength such as hardness, fracture toughness, ductility, and yield strength. A range of materials with desirable EM properties

(metals, metal oxides, hexaferrites, carbon forms, carbon-based fillers, polymer composites, or polymer blends) do not possess ideal properties to be candidate materials as structural (substrate) elements. However, this can be overcome using a composite material system where a layer or coating of EM material (i.e., a material with desirable EM wave/matter interaction properties) can be added to the surface of a mechanically strong structural material. The thermal spray coating approach provides the opportunity to deposit different layers of EM materials on a suitable substrate. Overlay coatings such as those deposited by thermal spraying and vapor deposition on structural materials such as steel or aluminum alloys, etc., give the designer a choice to take advantage of the mechanical strength of the substrate and the EM properties of the overlay coating. Thermal spray coatings have the advantage of providing thick (few micronmeters to millimeter thicknesses) and cost-effective coatings of a range of complex engineering materials. This has enabled them to become an integral part of the aviation, transportation, power generation, chemical, and biomedical industry, which is currently worth 7.6 billion USD.[9] As will be seen later, the substrates in such thermally sprayed coatings varied from metals, alloys, glass, and ceramics to graphite; however, there is little or no evidence where lightweight polymeric substrates were considered for EM wave propagation applications. Though not a focus of current review, application of polymeric substrates (e.g., thermoplastics, which are excellent electrical and thermal insulators) is quite possible with some degree of limitations, as demonstrated by Bobzin, Wietheger, and Knoch (2021),[10] as such materials can well be combined with a high degree of design flexibility and economical mass production.

Thermal spraying is a line-of-sight process in which the coating material in the form of a powder or wire, etc., is heated and propelled to splat and form a lamella structure on the substrate or underlying coating material. HVOF, plasma spraying (PS), warm spray (WS), and CS are some of the most used processes in industries. These processes differ in the way the coating material is heated and propelled to form a coating. **Figure 2** shows some of the coating particle temperatures and velocity ranges achievable by thermal spray processes.[11] The particle velocity which can be achieved during the thermal spray process (Figure 2) ranges from $\approx$20 to $\approx$1050 m s^{-1}, which influences the mechanical, thermal, and EM properties due to the extent of the 1) designed phase transformation, for example, ratio of amorphous-to-crystalline phase for hydroxyapatite ($Ca_5(PO_4)_3(OH)$) coatings for biomedical applications[12,13] and controlled degree of eta phase (i.e., carbon-deficient form of WC that results in a harder or brittle cemented carbide) formation for sliding wear applications of WC-Co coatings,[9] etc., and 2) control of porosity during deposition.[14] Complex feedstock materials such as $BaCoTiFe_{10}O_9$, $SrFe_{12}O_9$, and hydroxyapatite[12,15,16] can be thermally sprayed using the correct powder chemistry, coating process, and coating process parameters.

Figure 3 shows a typical microstructure of a ceramic (alumina, Al_2O_3) coating deposited using the plasma spray process (Figure 3a).[17] The microstructure shows the interlamellar mechanical interlocks, pores, and other coating features. The lamellar structure becomes much finer when nanocomposite coatings of similar material are deposited using nanoparticles in a suspension, that is, suspension spray coating (Figure 3b).

ADVANCED
SCIENCE NEWS
www.advancedsciencenews.com

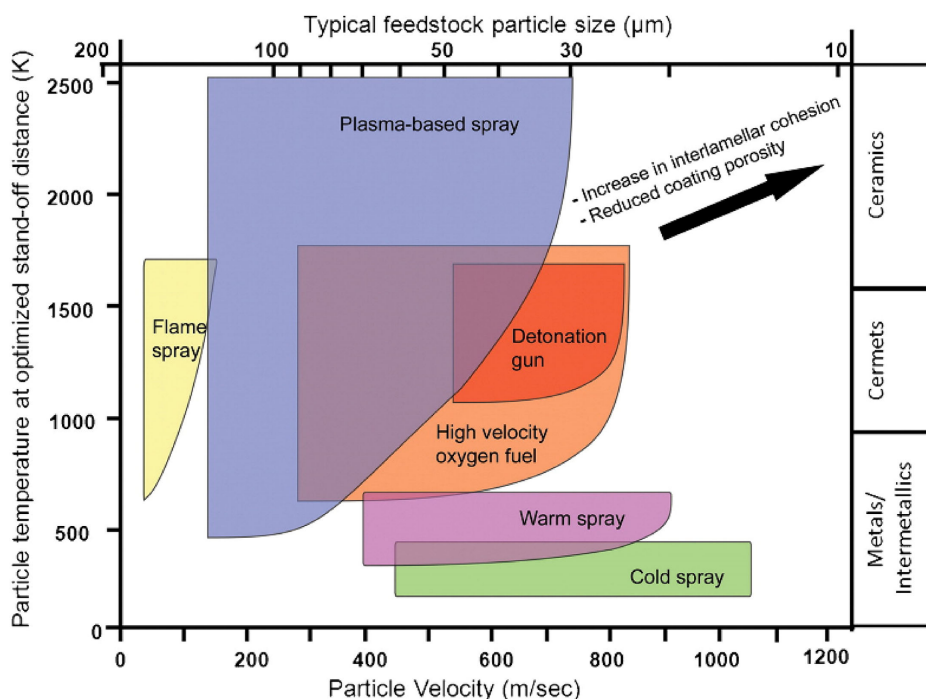ADVANCED
ENGINEERING
MATERIALS
www.aem-journal.com

Figure 2. Spectrum of thermal spray and CS processes across particle velocity and flame temperature attainable during coating deposition. Reproduced with permission.[11] Copyright 2014, Taylor and Francis.

This figure shows that the changes in powder characteristics, coating process, and process parameters can be used to achieve different engineering materials' microstructures. A similar approach is also applied to other engineering materials, that is, metals, polymers, and their composites. The lamella structure results in anisotropic mechanical properties, which are dependent upon the structure–property relationships, with major differences between the in-plane and out-of-plane directions.[9]

In the past couple of decades, the desire to use nano- or submicrometer-sized powders in thermal spraying has grown significantly, motivated by the ambition to realize coatings with refined microstructures that can plausibly yield superior properties.[18] However, the challenges associated with deploying such fine feedstocks for thermal spraying have been known for long.[19] Foremost, these fine-sized powders are characterized by poor flowability. Their relatively low momentum also precludes controlled powder delivery because of the inability of the fine particles to penetrate high-velocity gas streams that are a hallmark of virtually all industrially exploited thermal spray variants.[20] Although agglomeration of submicrometer or nano-sized powders has been attempted to overcome the above feeding-related problems, there have been reports of inhomogeneous melting,[21,22] apart from the added cost that the agglomeration step entails. Use of a suspension of fine particles in a suitable liquid medium, or of a solution of precursor salts that can lead to particle generation in situ, has been conceived primarily to address the above limitations.[18–20,23] Two variants (i.e., suspension plasma spray or suspension plasma sprayed (SPS) and solution precursor plasma spray [SPPS]) are extensively researched thermal spray techniques these days.[24] These approaches are now much better understood and found to be extremely versatile.[23–27] More recently, the possibility of utilizing a powder-liquid "hybrid" feedstock has also been demonstrated and found to be an effective pathway to create unique, function-dependent coating architectures.[24,28]

The use of thermal spray coatings, which is capable of efficiently and cost-effectively depositing continuous layers or patterned designs of conductive and isolating materials, can yield desirable dielectricity, conductance, resistance, magnetism, superconductivity, or EM properties.[5,29] In EM applications, two design factors are important, that is, 1) the choice of EM material and 2) the structure of the EM material. The thermal spray process, therefore, provides a cost-effective manufacturing route to deposit complex material compositions not only as an overlay coating but also free-standing coatings.[29,30] This offers a large range of thermally sprayed materials suitable for EM applications as a viable manufacturing route. However, this is not the only manufacturing advantage of this method. This coating process also provides the ability to control the porosity and thus the coating deposit structure. Conventionally, the coating process and process parameters are designed to minimize the porosity to improve the coating material's mechanical strength. However, as shown in Figure 3 and 4, changes in the coating process and process parameters can result in varying degree of porosity within the coating microstructure.

In some cases, it is desirable to have a controlled amount of porosity within the coating material, for example, in hydroxyapatite coatings for biomedical implants to allow blood vessels to grow within the coating microstructure and[13] in solid oxide fuel cell materials to increase the apparent area of interaction with the
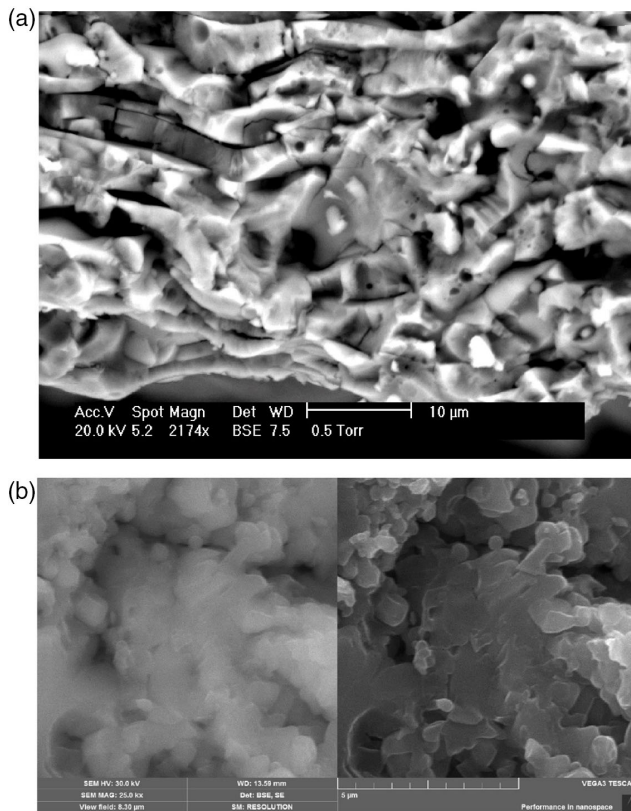
ADVANCED
SCIENCE NEWS

www.advancedsciencenews.com

ADVANCED
ENGINEERING
MATERIALS

www.aem-journal.com

Figure 3. a) Cryogenic-fractured alumina coating to reveal coating microstructure deposited by the plasma spray process. Reproduced with permission.[17] Copyright 2011, Springer Nature. b) Cryogenic-fractured nanostructured alumina coating to reveal coating of the scanning electron microscopic structure deposited by the suspension spray process (back-scattered electron/BSE (left) and secondary electron/SE (right) images, authors image).
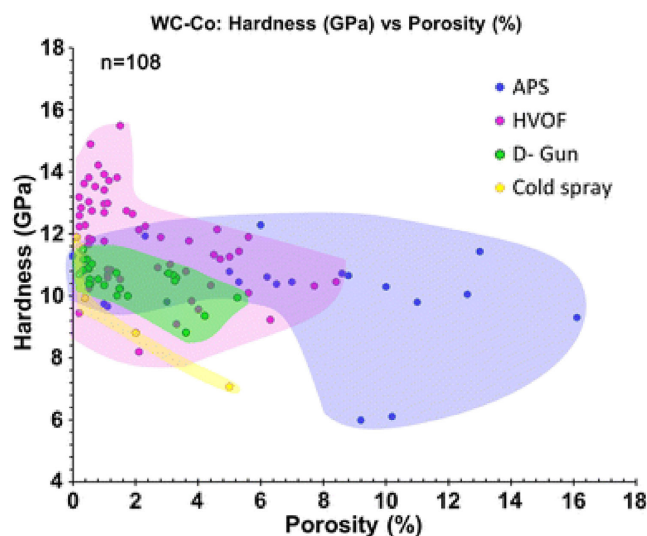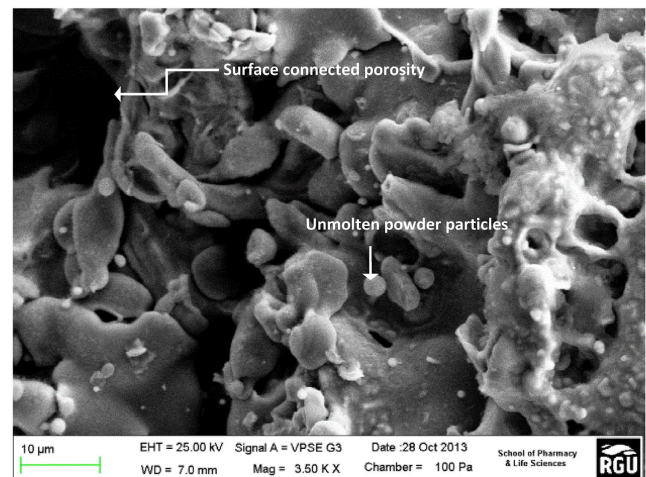

Figure 5. Scanning electron microscope (SEM) images of APS-coated anode layer surfaces showing surface-connected porosities and unmolten powder particles (Mo–Mo$_2$C/ZrO$_2$). Reproduced with permission.[31] Copyright 2015, Springer Nature.

electrochemical fuel cell environment,[31] as shown in **Figure 5**, where a 17% porosity was intentionally designed in the Mo–Mo$_2$C/ZrO$_2$ coating microstructure. Numerical and mathematical modeling can also be used to predict the evolution of coating microstructure and structure–property relationship, for example, residual stress and porosity.[32–34] This can be advantageous in the application of EM materials where the coating porosity and hence the coating architecture can be purposefully built in during coating deposition. The investigation by Wang and Zhao (2015)[35] has demonstrated this design aspect in the EM evaluation of YSZ coatings, where a porosity of 15% has been reported. In summary, thermal spray coating processes combined with the choice of coating material(s) and spray parameters provide a cost-effective design tool as a manufacturing route of EM materials.

3. EM Waves and Their Interaction with Materials

This section presents an overview on EM waves, their interaction with solid state and porous materials, as well as EM interference (EMI) shielding.

3.1. EM Waves

EM waves (ionizing or nonionizing) are forms of waves consisting of two components (i.e., an electric field, E, and a magnetic field, H).[3] EM waves are generated when charged particles are accelerated, which generates a changing electric field and magnetic field, and their vector directions of the fields and the direction of propagation are at 90° to each other. They can be characterized by speed c, wavelength λ, and frequency ν. Such waves may consist of a continuous range of wavelengths (or frequencies), which refers to the waves of the EM fields, propagating through space and carrying EM-radiant energy. The relationship among the previous quantities can be characterized as $c = \lambda\nu$. The EM waves travelling in free space have speed

Figure 4. Hardness–porosity map of thermal spray tungsten carbide–cobalt coatings. Reproduced with permission.[14] Copyright 2013, Springer Nature.

equivalent to that of speed of light, $c = \frac{1}{\sqrt{\mu_0 \varepsilon_0}} = 2.998 \times 10^8 \mathrm{m\,s^{-1}}$, where μ_0 represents free space permeability ($\approx 4\pi \times 10^{-7}\mathrm{H\,m^{-1}}$) and ε_0 refers to free space permittivity ($\approx 8.85 \times 10^{-12}\mathrm{F\,m^{-1}}$).[8,36]

As shown in **Figure 6** and listed in **Table 1**, the EM spectrum (ionizing or nonionizing) includes a broad range of frequencies (i.e., radio waves, microwaves, infrared, visible light, ultraviolet rays, X-rays, and gamma rays). EM waves can be transmitted in vacuum, air, and other media, and during the wave travel, the energy will be reflected, absorbed, transmitted, or may excite SEWs.[37] EM wave radiation is emitted and absorbed discretely by one quantum after another, each of which is called a photon (not exactly a massless, indivisible, stable particle, with no electric charge) and has an energy, E_n. A photon may be generated by the transition of charged particles through different energy levels. When a charged particle transitions from a higher energy level to a lower energy level, it sends out a photon, and the energy of a photon is given by Planck–Einstein's equation, $E_n = h\nu = \frac{hc}{\lambda}$, where $h = 6.62606979(30) \times 10^{-34}\mathrm{Js} = 4.135667662(25) \times 10^{-15}\mathrm{eVs}$ is the Planck constant, and c is the speed of light.[38,39]

3.2. Dielectric Properties

Permeability (μ) is the measure of the ability of a material to support the formation of a magnetic field within itself, measured in Henries per meter (H/m). Permittivity (ε) describes the amount of charge needed to generate one unit of electric flux in a medium, measured in Farads per meter (F/m), and thus represents the polarity of material's molecules in an electric field. The formulae that relates electric permittivity (ε) and magnetic permeability (μ) of an EM wave in a specific medium are $\varepsilon = \varepsilon' - j\varepsilon'' = \varepsilon_0 \varepsilon_r$ and $\mu = \mu_0 \mu_r$, where ε' is real part of permittivity or dielectric constant (a measure of the amount of energy from external electrical field stored in the material), ε'' is imaginary part of permittivity or dielectric loss or loss factor (is zero for lossless material, and it is a measure of the amount of energy loss in the material due to an external field), and $\varepsilon_r = \frac{\varepsilon}{\varepsilon_0}$ and $\mu_r = \frac{\mu}{\mu_0}$ are relative electric permittivity and relative magnetic permeability of the specific medium, respectively.[8,36] The complex permeability (μ) which is applicable to magnetic materials only also consists of a real part representing the amount of energy from an external magnetic field stored in the material, whereas the imaginary part represents the amount of energy dissipated due to the magnetic field. As most of the materials are nonmagnetic, their permeability is very near to the permeability of free space. Another term associated with complex permittivity is "loss tangent" or $\tan(\delta)$ that represents the ratio of the imaginary part to the real part of complex permittivity.

Dielectric properties can be measured in time or frequency domain with single or multiport (i.e., 2 or 4) systems of the measuring instruments. The methods to measure the complex permittivity and permeability can be transmission-line (or reflection-line) method, an open-ended coaxial probe method, free-space method, or resonant method. Typically, network analyzer instruments (current manufacturers such as AEA Technology, Anritsu, AWA Global, Copper Mountain Technologies, GSI, Keysight Technologies, Pico Technology, MegiQ, Micran, National Instruments Corporation, Rhode & Schwarz, SIGLENT, Tektronix Inc., Teledyne LeCroy, and Transcom Instruments, etc.) are used to measure complex permittivity and permeability, that is, quantifying EM properties of dielectric and magnetic materials. Various instruments typically provide measurement from the mid-MHz to the low-THz range.[40] Standards (ASTM D150-18,[41] ASTM D2520-13[42]) provide the procedure to measure electrical permittivity (dielectric constant), standards (ASTM D150-18,[41] ASTM D924-15[43]) provide the procedure to measure dissipation factor (or dielectric loss), and standard (ASTM D149-20[44]) provides the procedure to measure dielectric strength.[45] Experimentally, the measurement procedure using network analyzer (mainly using vector
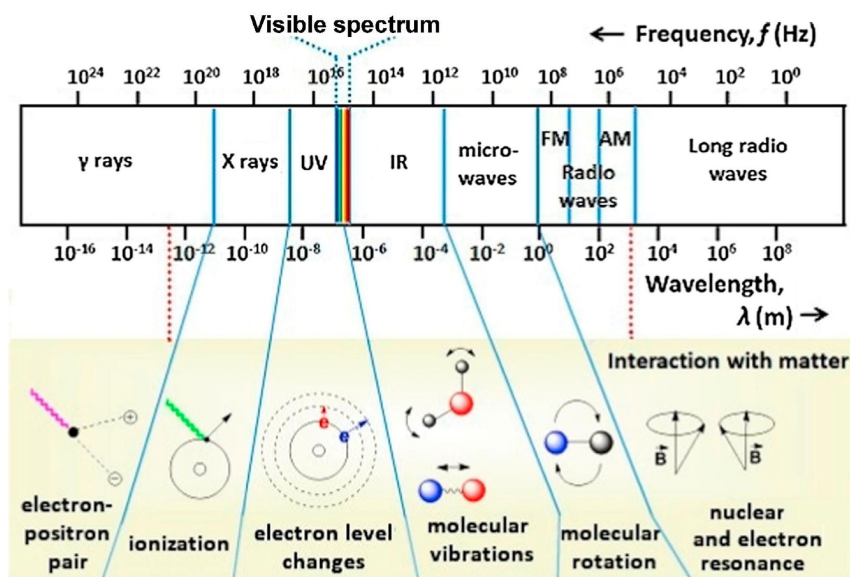

Figure 6. EM spectrum diagram for various radiation types and molecular-scale effects. Reproduced with permission.[39] Copyright 2009, Wiley.

**ADVANCED
SCIENCE NEWS**
www.advancedsciencenews.com

**ADVANCED
ENGINEERING
MATERIALS**
www.aem-journal.com

Table 1. EM wave radiation types and sources.[39,45,235]

Radiation types[a]	Spectrum region	Sources [natural, artificial]	Wavelength	Frequency	Photon energy
Ionizing (hard gamma to X-Ray and far ultraviolet)	Hard gamma	Fission in nuclear reactors, nuclear explosion, lightning, radioactive decay	1×10^{-9} nm	3×10^{26} Hz	1.2×10^{12} eV
	Gamma		1×10^{-6} nm	3×10^{23} Hz	1.2 GeV
	Gamma/X-Ray		0.001 nm	3×10^{19} Hz	12 MeV
	X-Ray	Radon gas, radioactive elements in the Earth, and cosmic rays that hit the Earth from outer space, accelerating electrons through a potential difference onto a target (e.g., tungsten)	1 nm	3×10^{17} Hz	120 keV
Nonionizing (near ultraviolet to radio waves)	X-Ray/Ultraviolet	Sunlight, tanning beds	10 nm	3×10^{16} Hz	12 keV
	Ultraviolet		100 nm	3×10^{15} Hz	1.2 keV
	Visible (blue)	Sunlight, fire, light-emitting diodes, light bulbs, lasers	400 nm	7.5×10^{14} Hz	3.1 eV
	Visible (red)		700 nm	4.3×10^{14} Hz	1.8 eV
	Infrared	Sunlight, thermal radiation, incandescent light bulbs, lasers, remote controls	10 μm	3×10^{13} Hz	0.12 eV
	Microwave	Mobile phones, microwave ovens, masers, cordless phones, millimeter waves, airport millimeter scanners, circuits, motion detectors, telecommunication transmission towers, radar, wireless fidelity (Wi-Fi)	1 cm	30 GHz	1.2×10^{-4} eV
	Microwave/Radio	Mobile phones, television, frequency modulation, amplitude modulation, shortwave, cordless phones, satellite, radar, lightning, astronomical phenomena	10 cm	3 GHz	1.2×10^{-5} eV
	Radio		100 m	3 MHz	1.2×10^{-8} eV
	Radio		100 km	3 kHz	1.2×10^{-11} eV

[a]photon energies less than 10 eV are considered nonionizing.

types which measure both amplitude and phase properties) includes setting the frequency range and number of points in the network analyzer, for the material under investigation, determining sample holder parameters (i.e., sample length, sample thickness, sample-to-holder distance, cutoff frequencies of sample holder), air gap data of material under investigation, sample holder dimension, calibration of the system, placing material under investigation on fixture, and eventually extracting scattering (S)-parameters using functions in the network analyzer and then performing the conversion of S-parameter to dielectric properties using an appropriate method and finally obtaining electric permittivity (ε) and magnetic permeability (μ).

3.3. Interaction with Solid-State Material

Photon energy is very important to study the movement of electrons in an atomic shell of a material. As listed in Table 1, an EM wave which has sufficient energy only for excitation purpose (i.e., which leads to movement of an electron to a higher energy state) is of a nonionizing radiation type. In solid-state materials, a bandgap, also called an energy gap, is an energy range in a solid where no electron states can exist. The bandgap generally refers to the energy difference (in electron volts, eV) required to promote a valence electron bound to an atom to become a conduction electron (i.e., an electron which is free to move within the "crystal lattice" and serve as a charge carrier to conduct electric current). Semiconductor materials are nominally small-bandgap materials, and most common semiconductor materials are crystalline inorganic solids.[46,47]

As mentioned earlier, the band gap refers to the energy difference between the top of the valence band and the bottom of the conduction band. Electrons can jump from one band to another, if a specific minimum amount of energy for the transition is provided. Energy required for electrons to jump from one band to another changes from material to material.[47] Electrons can gain enough energy to jump to the conduction band by absorbing either a phonon (heat) or a photon (light). When a wave with a single frequency strikes an object, several things could happen to the wave, for example, absorption, reflection, or transmission. As an example, for metal oxide semiconductors (e.g., ZnO, bandgap of 3.1 eV), photons with energy equal or slightly higher than 3.1 eV are absorbed, and this can cause electrons to pass from the valence band to the conduction band.[7] As the energy of 3.1 eV corresponds roughly to the wavelength of $\lambda = 0.3$ μm, ZnO is absorbed in the ultraviolet region of the spectrum. A perfect crystal is expected to be transparent, for example, for the visible and near-infrared wavelength light, but the presence of lattice defects and grain boundaries introduces electron states within the bandgap and causes such light to be diffused and partially absorbed. If the wave is absorbed by the object, its energy is converted to heat. When a wave with that same natural frequency impinges upon an atom, then the electrons of that atom will be set into vibrational motion. If a wave of a given frequency strikes a material with electrons having the same vibrational frequencies, then those electrons will absorb the energy of the wave and transform it into vibrational motion. During its vibration, the electrons interact with neighboring atoms in such a manner as to convert its vibrational energy into thermal energy. Subsequently, the wave with that given
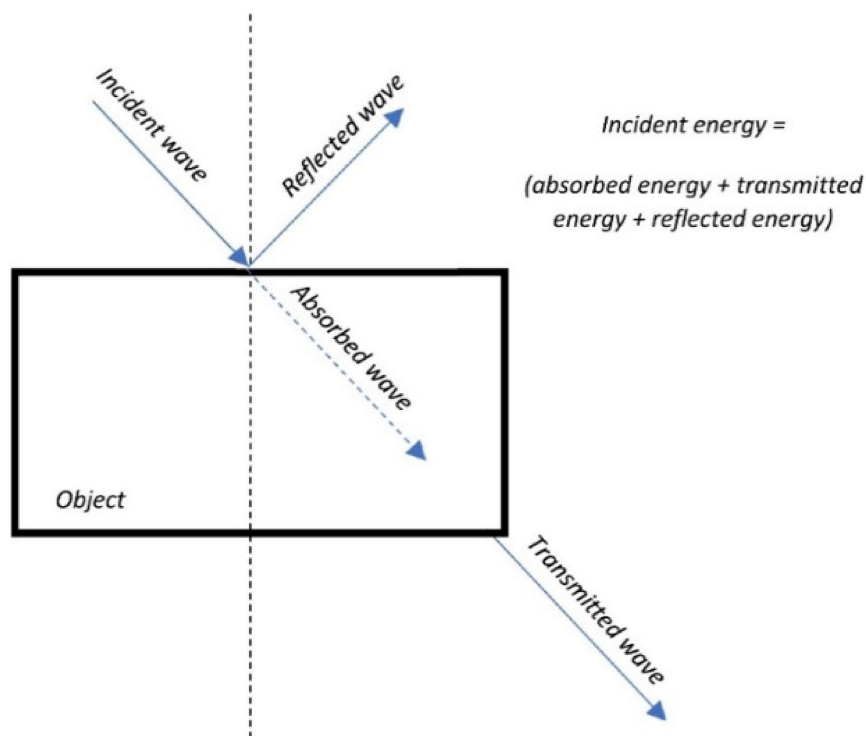
ADVANCED
SCIENCE NEWS
www.advancedsciencenews.com

ADVANCED
ENGINEERING
MATERIALS
www.aem-journal.com

Figure 7. EM wave reflection, absorption, and transmission.

frequency is absorbed by the object and its energy transformed. So, the selective absorption of wave by a material occurs because the selected frequency of the wave matches the frequency at which electrons in the atoms of that material vibrate. As different atoms and molecules have different natural frequencies of vibration, they will selectively absorb waves of different frequencies.

Figure 7 shows simplified scheme of incident EM wave reflection, absorption, and transmission in a material. Reflection and transmission of waves occur because the material impedance is different. When waves of these frequencies strike an object, the electrons in the atoms of the object begin vibrating. However, instead of vibrating in resonance at a large amplitude, the electrons vibrate for brief periods of time with small amplitudes of vibration; then, the energy is re-emitted as a wave. If the object is transparent, then the vibrations of the electrons are passed on to neighboring atoms through the bulk of the material and re-emitted on the opposite side of the object. Such frequencies of waves are said to be transmitted. If the object is opaque, then the vibrations of the electrons are not passed from atom to atom through the bulk of the material. Rather the electrons of atoms on the material's surface vibrate for short periods of time and then re-emit the energy as a reflected wave. Further details about EM wave propagation, radiation, and scattering can be found in other studies.[1,3]

3.4. Interaction with Porous Materials

Thermally sprayed coating structures can be complex systems involving elastic structures, cavities, porosities, voids, cracks, and varied specific surfaces. The absorbing properties of materials can be improved with such porous structures.[48] Considering heterogenous materials, the scattering and absorption of EM waves are impossible to find. However, the specimen can be approximated or simplified as a combination of a single layer (substrate), two-layer (coating substrate), or a number of hollow spheres (porosity in coating), as shown in **Figure 8**.

In layered and hollow sphere systems, the incident wave would be attenuated by the complex refraction and scattering as well as the dielectric losses when it propagates in the specimen. Analytically, to prepare an excellent absorber, a suppressive reflection loss, RL, is the prerequisite, which is bound up with the input impedance Z_{in} and expressed as[49]

$RL(dB) = 20\log_{10}\left|\frac{Z_{in}-Z_o}{Z_{in}+Z_o}\right|$, where $Z_0 = \sqrt{\frac{\mu_0}{\varepsilon_0}}$ and $Z_{in} = Z_0\sqrt{\frac{\mu_r}{\varepsilon_r}}\tanh\left(j\frac{2\pi\nu d}{c}\sqrt{\mu_r\varepsilon_r}\right)$ where d is the thickness of the EM wave absorbing layer (coating in current context), ν is the frequency of the incident EM wave, c is the velocity of light in free space, Z_o is the characteristic impedance of free space ($= 120\pi$), μ_0 and ε_0 are permeability and permittivity of free space, and μ_r and ε_r are the relative permeability and permittivity of the absorber, respectively. For a perfect wave absorber, RL should be infinitesimal, namely, the absorber should have ε equal to μ (to match the impedance of free space) with both being as large as possible. The scattering and absorption of the EM wave by heterogeneous materials is complex and the exact solution is impossible to find.[50,51] In thermally sprayed coatings, a number of conditions can be assumed leading to varied EM wave interactions of incident waves. Such coatings can attenuate EM waves merely by the dielectric losses resulting from coating properties. Considering thermal spray coatings, the reflection could
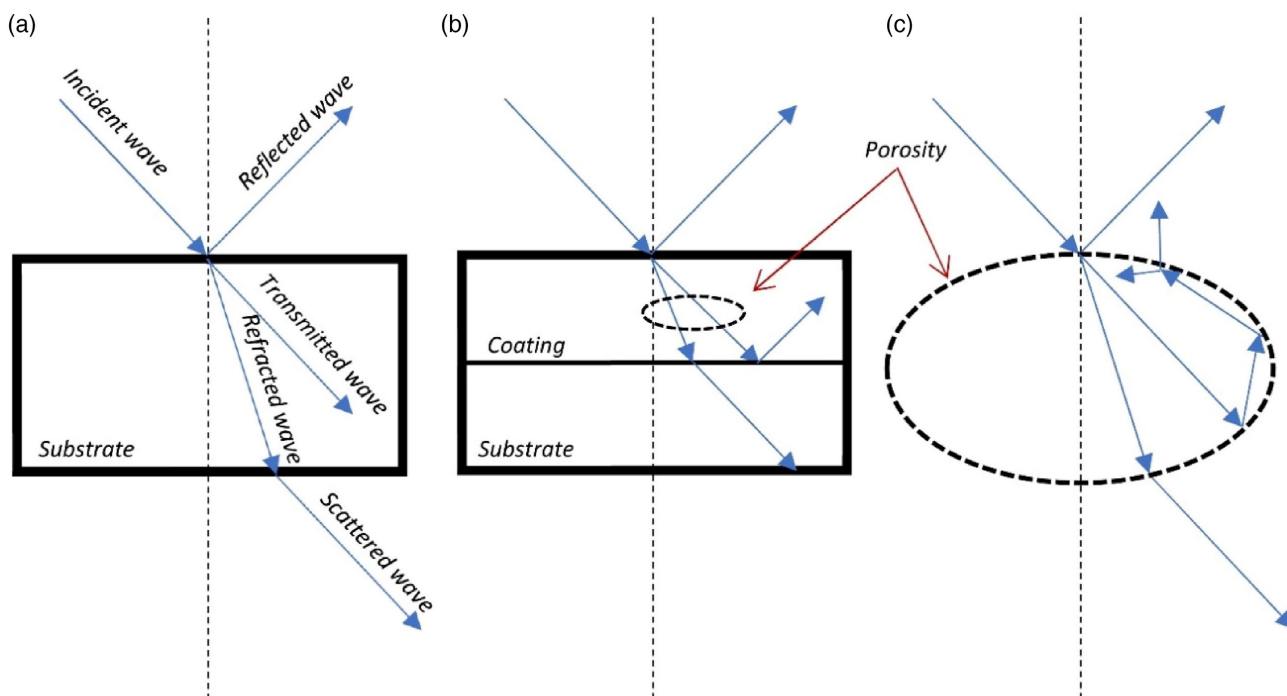
Figure 8. Sketch of the propagation of EM wave: a) single layer (substrate), b) two layer (coating substrate), and c) single hollow sphere representing porosity in coating (note: (c) figure adapted and reproduced with permission).[48] Copyright 2011, Elsevier.

potentially be reduced by fabricating or adding a dielectric material layer over the absorbing coating or by tailoring the $\sqrt{\frac{\mu}{\varepsilon}}$ ratio of the absorbing cover.

3.5. Electromagnetic Interference (EMI) Shielding Mechanism

EMI shielding is a phenomenon that involves the process of reflection and/or absorption of EM waves by a material, that acts as a shield (comprising either conductive or magnetic-based materials) in preventing the penetration of the harmful EM radiations into the electronic devices.[52] There are two shielding mechanisms of EMI, that is, reflection and absorption.[53–55] The reflection which accounts for a reduction of EMI incidence is caused by impedance discontinuity of the air/shield (or shield/air) boundary.[56,57] As an EM wave attempts to penetrate a shield medium, two reflection processes can occur:[56] 1) incident energy encounters the surface of the shield and 2) the reflection process occurs at the opposite face of the shield, and some of the energy is reflected into the shield, known as multiple reflections. While in the absorption mechanism, EM energy turns into thermal energy when an EM wave passes through a medium.

Most common EMI shielding materials are nevertheless based on metal sheets, screens, or foams made of steel, copper, nickel, or aluminum alloys (including some expensive materials such as silver or gold), owing to their combination of high electrical conductivity and dielectric constant.[52] However, as noted by Abbasi et al. (2019),[58] metal-based protective systems display important drawbacks that limit their applications: high density, poor resistance to corrosion, cost processing, and an EMI-shielding

mechanism based on reflection, preventing their use in applications where for instance the EMI absorption is dominant, such as in stealth technology, or affecting the functionality and even causing damage to other electronic circuits or components. As the metallic materials can be bulky, therefore, thermal, or CS composite coatings on polymeric or graphite-like substrates with high tribological properties of coatings (i.e., low wear, scratch resistance, enhanced bonding) can be alternative structures for EMI-shielding applications. Much details on metallic coatings (using thermal or CS techniques) over polymeric substrates have been discussed in the study by Gonzalez et al[59] However, such thermal or CS composite coatings can bring in additional functionalities; graphite substrates for such coating can be preferred as it has exceptionally high electrical and thermal conductivities, including a high specific surface area, with effectiveness for shielding up to 130 dB at 1 GHz.[52]

The EMI shielding effectiveness or efficiency (EMI SE) of a material is determined by the algebraic summation of reflection (R), absorption (A), and multiple reflection (B), in units of dB.[54,56] EMI SE is generally expressed in terms of S (or scattering) parameters, implying the way current/voltages travel in a transmission line and encountering a discontinuity caused by differing impedance between air and obstruction or in dielectric media.[54,56,57] The S parameters calculations can be done using the equation $S_{ij}(dB) = 20 \times \log(\sqrt{\alpha^2 + \beta^2})$, where α and β are the real and imaginary part of the complex S numbers.[60] As the absorption loss is found to be directly proportionate to the thickness of the shielding material, in the current context, thermally sprayed coating thickness design estimate can be of particular interest to enhance the absorption loss. The skin depth

(δ) at which the EM field reduces to $\frac{1}{e}$ (or 37%) of its initial value, represented as $\delta = \frac{1}{\sqrt{\pi\nu\mu\sigma}}$ (in meters), means that the skin depth (δ) decreases with the increase in ν, μ, or σ.[36] Therefore, an estimate of coating thickness design is possible while considering skin depth (δ) at which the EM field reduces.

As summarized by Anderson et al. (2021)[61] and well known in the sector, shielding effectiveness or efficiency classifications are as follows: <20 dB is considered small, average if between 20 and 80 dB, exceptional if between 80 and 120 dB, and attainable if >120 dB (with cost-effective methods and using potentially sensitive equipment). Including analytical derivation of Maxwell's equations for EMI analysis, a range of numerical methods in the modeling of EM waves ,[61] standard methods (ASTM D4935-18[62]), further details, and strategies about EMI shielding can be seen in the study by Shukla et al.[63]

4. Electromagnetic Wave Propagation Characteristics of Thermal Spray Coatings

This section presents relevant literature and examples where thermally sprayed coatings are developed to characterize various EM wave (i.e., microwave, millimeter wave, solar selective, photocatalytic, EMI, and thermal barrier [heat, emissivity]) interactions with materials. In all the studies, the context is largely about enhancing the absorption of various EM waves

4.1. Microwave Absorption Performance

Microwave waves are typically defined to cover the 1–1000 GHz frequency range (wavelengths approximately in the range from 30 cm to 300 μm). Within these spectra, the communication systems' applications include ground and airborne radar, electronic warfare including guided weapons, satellite communications, microwave radar (for police, small boats, intruder alarms, and door openers), direct broadcast satellites (12 GHz), and mobile (1–3 GHz band) as well as cellular ($\approx$1 GHz) communications.[64] Microwave-absorbing materials (MAMs) are types of

functional materials which dissipate EM waves by converting it into thermal energy. Considering radar (or radio detection and ranging) which is a detection system that uses radio waves to detect distance, angle, or velocity of objects,[65] there are materials which can absorb radar signals (called radar-absorbing materials or structures or RAM/RAS) which make it harder to detect or track objects (e.g., aircraft, ships, tanks, and other mobile objects, as well as human exposure mitigations).[66,67] It is important to note that RAMs neither absorb all received EM (radar) energy and nor are efficient within the absorbed frequency bands but are considered as supplementary means in reducing radar cross section (RCS) when other techniques (e.g., shaping) cannot be applied.[66]

The microwave absorption capacity is mainly determined by the relative permittivity (ε_r), the relative permeability (μ_r), the EM impedance match, and the microstructure of the absorber.[66–69] When an EM beam irradiates the surface of an absorber, a good matching condition of the EM impedance can enable almost zero reflectivity of the incident microwave, and then, the transmitted microwave can be dissipated by dielectric loss and magnetic loss.[68,69] The desirable properties for MAMs include light weight, low thickness, high chemical stability, a wide absorption frequency range, as well as high absorption performance.[69]

There are numerous examples where thermally sprayed coatings were used to absorb radar for stealth and camouflage, that is, reducing RCS. In a work by Bartuli, Cipri, and Valente (2008),[70] a range of complex ceramic-based composite coatings with an average thickness of about 3 mm ($Cr_2O_3 + BaTiO_3$ 40 wt%, $Cr_2O_3 + SrTiO_3$ 40 wt%, $Cr_2O_3 + NiO$ 40wt%, $Cr_2O_3 + ATO$ 40wt%, $Cr_2O_3 + La_{0.5}Sr_{0.5}MnO_3$ 40wt%, $Cr_2O_3 + Ni_{0.5}Zn_{0.5}Fe_2O_3$ 40 wt%, $Cr_2O_3 + Al$ 40wt%, $Cr_2O_3 + Cu$ 5wt%, $Cr_2O_3 + Cu$ 20wt% + $Ni_{0.5}Zn_{0.5}Fe_2O_3$ 20wt%, $Cr_2O_3 + Al$ 20wt% + $La_{0.5}Sr_{0.5}MnO_3$ 20wt%, $Cr_2O_3 + Co_3O_4$ 40 wt%) were fabricated by air plasma spraying to evaluate their tailored EM properties (essentially as absorbers in the microwave range [8–12 GHz]). As shown in **Figure 9**a for various coating thicknesses ($Cr_2O_3 + NiO$ 40wt%), the addition of metallic particle

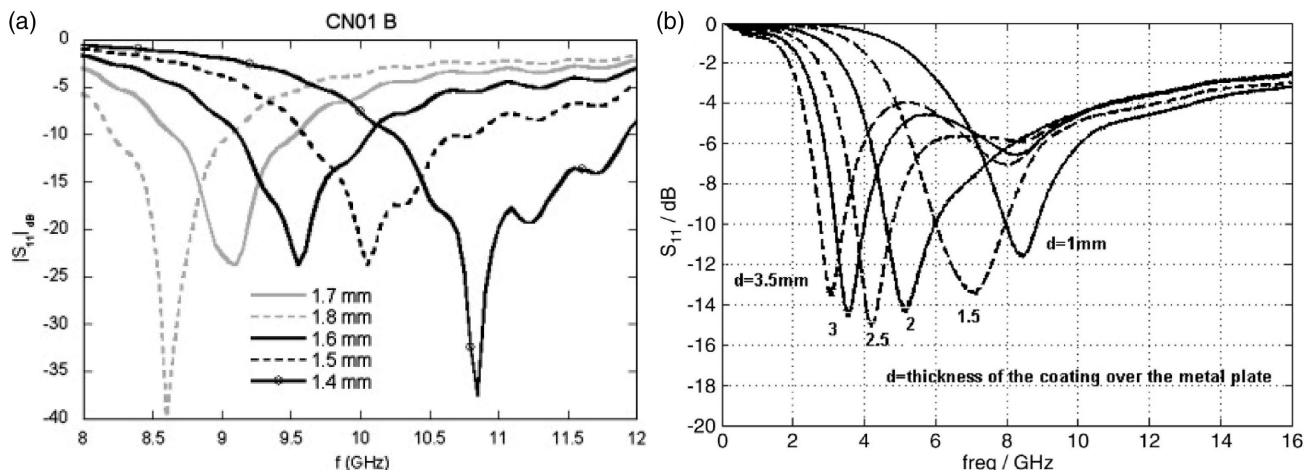**Figure 9.** a) Simulation of the RL versus frequency curve for various coating thicknesses for the sample ($Cr_2O_3 + NiO$ 40 wt%). Reproduced with permission[70] Copyright 2008, Elsevier. b) Calculated reflections from a $BaCoTiFe_{10}O_{19}$-coated metal plate versus coating thickness Reproduced with permission.[15] Copyright 2009, Elsevier.

dispersions within the dielectric ceramic matrix introduced ripples in the curves (shielding effectiveness parameter vs frequency), and the coating thickness had a direct influence on the absolute value of the measured loss parameter. The coating showed different absorbance behaviors, presenting resonance with absorbance for thickness of 1.7 mm as opposed to an absence of absorbance for higher (1.8 mm) or lower (1.4 mm) coating thickness. It is important to highlight here that plasma spraying utilizing the previously mentioned powder–liquid "hybrid" feedstock[28] could be ideally suited for depositing ceramic-based composite coatings such as those mentioned above by Bartuli, Cipri and Valente (2008).[70]

Bégard et al. (2009)[15] compared Ba–hexaferrite ($BaCoTiFe_{10}O_{19}$) coatings deposited onto nonmagnetic glass-–ceramic substrates by HVOF and air plasma spray (APS) techniques, obtaining coating layers possessing the desired structural and magnetic properties in the as-sprayed conditions, for microwave absorption applications. While the substitution of Fe^{3+} ions with Co^{2+} and Ti^{4+} reduced the ferromagnetic resonance frequency (making it suitable for microwave absorbers), to retain the crystalline hexaferrite phase, a controlled amount of unmelted agglomerates was desirable to be embedded in the coating. It was suggested that compared with HVOF spraying, APS coatings can have better magnetic properties, close to those of pure crystalline $BaCoTiFe_{10}O_{19}$. Bégard et al. (2009)[15] indicated that to achieve high and broadband absorption with a thin coating, the permeability and the magnetic losses must be high; on the other hand, using a somewhat thicker coating, the advantage of electrical losses can be exploited to increase the absorption. From calculations based on the electrical and magnetic properties of the bulk material (i.e., reflection from a metal plate coated with $BaCoTiFe_{10}O_{19}$ layers having various thicknesses), it was predicted that a thickness of 1–4 mm would therefore be optimal for microwave absorption applications (Figure 9b).

As discussed by Lisjak et al. (2011),[16] composite coatings from different volume ratios of hexaferrite ($BaFe_{12}O_{19}$ or $SrFe_{12}O_{19}$) and polyethylene were prepared, with flame spraying (**Figure 10**I, II). The hexaferrite phase (useful for high magnetic losses) retained its crystal structure and microstructure during the process, while polyethylene (useful for high dielectric losses) melted and resolidified. The coatings showed magnetic hysteresis loops with high coercivities. $BaFe_{12}O_{19}$/PE coatings with a thickness of around 1 mm absorbed 80% of EM power at 45–55 GHz and show that the composite coatings would be suitable for EM wave absorbers in the ultrawide bandwidth microwave range.

Su et al. (2014)[71] developed multiwalled carbon nanotubes (MWCNTs)/cordierite (MAS) nanocomposite coatings on to graphite substrate to a thickness about 2.5 mm via low-power APS for microwave absorption applications at the frequency of 8.2–12.4 GHz. MWCNTs/cordierite (MAS) nanocomposite coatings with different MWCNT contents (5, 7, 10, 15, 20, and 30%) were investigated. With the increase in the MWCNT content to 7%, the coating showed the highest dielectric constant and optimal microwave absorption property but further increase in MWCNT content led to severe oxidation of MWCNTs during plasma-spraying process, resulting in lower dielectric constants and poor microwave absorption properties. The sample with 2.4 mm thickness (sample thickness investigated: 1–3.5 mm) showed the best microwave absorption behavior, with minimum
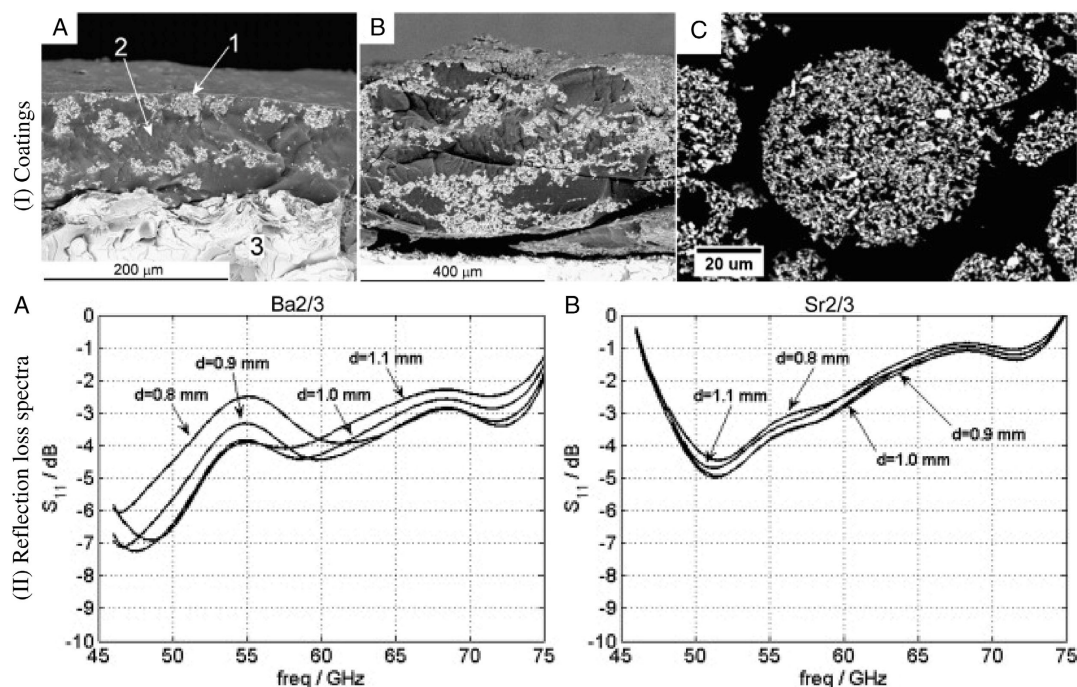
Figure 10. I) SEM images of the fracture surfaces of $SrFe_{12}O_{19}$ coatings. A) With low hexaferrite volume ratio, B) high hexaferrite volume ratio, C) images of the cross section of the as-sintered hexaferrite feedstock powder (note: label 1 = unmelted hexaferrite particles; label 2 = PE matrix; and label 3 = substrate). II) Reflection loss spectra of the A) $BaFe_{12}O_{19}$ and B) $SrFe_{12}O_{19}$ coatings, both with high hexaferrite volume ratio. Reproduced with permission.[16] Copyright 2011, Elsevier.

RL of −15.61 dB and bandwidth of 2.35 GHz. In continuation with their work, Su et al. (2015)[72] developed Ti$_3$SiC$_2$/cordierite (MAS) composite coatings on to the graphite substrate to a thickness about 2.5 mm via plasma spraying for microwave absorption applications at the frequency of 8.2–12.4 GHz. The addition of Ti$_3$SiC$_2$ significantly improved the EM shielding and complex permittivity of the coatings (due to enhanced polarization effect and electrical conductivity). With the increase in Ti$_3$SiC$_2$ content (to 30 wt%), the coating showed enhanced microwave absorption, which means that the absorption bandwidth (≤−5 dB) can be obtained across the whole measured frequency with a coating thickness of 1.8 mm (at 9.9 GHz peak frequency). Again, in a similar work, Su et al. (2015)[73] developed carbon black/cordierite composite coatings of 2.5 mm thickness on to graphite substrate using plasma spray and investigated complex permittivities of the coatings and powders with different carbon black content percentages for microwave absorption applications at the frequency of 8.2–12.4 GHz. The coating with 4.54% carbon black content and 3.0 mm thickness (analyzed thickness range: 1–3.5 mm) shows microwave absorption with a minimum RL of −23.90 dB at 10.13 GHz and RL less than −9 dB over the investigated frequency range.

To enhance the adhesion strength of MAMs, Wei et al. (2015)[74] fabricated W-type hexagonal ferrite coating by plasma spray. The feedstock of ferrite powders was synthesized by the solid-state reaction and spray-dried process. RL of the hexagonal ferrite coating is measured in the frequency of 2–18 GHz. The result shows that coating is suitable for EM wave absorbers in Ku band. It is well known that hexagonal ferrite exhibits excellent microwave absorbing behavior due to strong magnetic loss. It was observed that the simulated RL of the coating was below −5 dB in the frequency range 14.2–18 GHz with a thickness of 1.5 mm. The minimum RL is −7.2 dB at a frequency of 18 GHz. For realizing efficient microwave absorption in the wide-frequency bandwidth, the incident wave should enter the absorber as much as possible and then be fully absorbed.

Yang et al. (2016)[75] developed LaSrMnO$_3$/Al$_2$O$_3$ ceramic coatings on graphite substrates with thickness of about 2 mm using APS for the application of high-temperature microwave absorbing coating in X-band (8.2–12.4 GHz), which is an airborne interceptor and missile-seeker radar range. Al$_2$O$_3$ was chosen as insulation matrix and lanthanum strontium manganite (LSM) was chosen as a conductive filler. Microwave absorption showed that RL values exceeding −10 dB can be obtained in the frequency range of 10.5–12.4 GHz when the LSM content is 80 wt% and when the coating thickness is 1.5 mm. In a continuation to their work, Yang et al. (2016)[76,77] developed TiO$_2$/Al$_2$O$_3$ and TiAlCo ceramic coatings, respectively, onto graphite substrates with thickness of about 2 mm using APS for the application of high-temperature-microwave absorbing coating in the X-band (8.2–12.4 GHz). For both coatings (TiO$_2$/Al$_2$O$_3$ and TiAlCo), microwave absorption showed that the RL values exceeded −10 dB in the whole frequency range of X-band when the coating thickness was 2.3 mm[76] and when the coating thickness was 1.8 mm.[77]

Zhou et al. (2017)[78] investigated Cr/Al$_2$O$_3$ coatings deposited using low-power plasma spray with 3.5 mm thickness onto the graphite substrate for microwave absorption applications in the X-band (8.2–12.4 GHz). The graphite substrates were used for easy removal of coating flakes from the substrate. The coatings exhibited fully molten splat-like lamellae and partially molten/unmolten Al$_2$O$_3$ particles, surrounded by a fully molten Al$_2$O$_3$ matrix. It was observed that the content and size of Cr in the coatings played a dominant role in the formation of metallic clusters, and the coatings with higher Cr content and larger Cr particle size exhibited higher dielectric properties due to the enhanced interfacial polarization and conductance loss. In their recent work, using the same low-power plasma spraying, Zhou et al. (2019)[79] investigated the influence of NiCrAlY content on dielectric and microwave absorption properties (in the X-band) of NiCrAlY/Al$_2$O$_3$ composite coatings (3.0 mm thickness on graphite substrate). The features within the coatings indicated string or splat-like microstructures of metallic NiCrAlY. Due to interfacial polarization, relaxation loss, and conductance loss, the real and imaginary parts of complex permittivity were enhanced with the increase in NiCrAlY content. Owing to high impedance matching and the preferable attenuation coefficient, the coating with 20 wt% NiCrAlY and 2.0 mm thickness possessed an effective bandwidth (< −10 dB) 1.3 GHz in the range 8.2–9.5 GHz and minimum RL of −15.7 dB at 8.9 GHz, exhibiting enhanced microwave absorption properties.

Chen et al. (2019)[80] developed Ti$_3$SiC$_2$/NASICON coatings on a graphite substrate to a thickness about 2.5 mm via APS for high microwave absorption applications in a wide temperature range (25–500 °C) at the frequency range of 8.2–12.4 GHz (X-band). It was observed that the ionic conductivity of NASICON matrix and contact conductivity at Ti$_3$SiC$_2$/NASICON interfaces contributed to high permittivity. The permittivity increased with high temperature due to dielectric relaxation, space–charge polarization, thermal ion relaxation polarization, and conduction loss. The coating exhibited a good microwave-absorption property with a wide bandwidth (below 5 dB) with a thickness less than 2 mm when the temperature ranged from 200 to 500 °C.

Due to high conductivity loss properties of WC, Shao et al. (2020)[81] developed ceramic (WC and Al$_2$O$_3$ composite) coatings using APS on the Ni alloy substrate for microwave absorption at high temperatures in the X-band (8.2–12.4 GHz). The results showed that the absorbing bandwidth for RL below −10 dB can reach 1.5 and 2.2 GHz with the thickness of only 1.1 and 1.5 mm, respectively. In continuation with their work, Shao et al. (2020)[82] developed ceramic (20wt% Al$_2$O$_3$% and 80wt% TiC; both non-magnetic materials) coatings using APS on the Ni alloy substrate and then sprayed NiCrAlY alloy metamaterial pattern (an artificial designed structure) for the application of high-temperature metamaterial radar-absorbing coating (MRAC) in X-band at 800 °C. The metamaterial pattern using NiCrAlY alloy (replacing traditional metals) was developed to enhance relevant absorption performance (achieved EM RL below −5 dB covering the whole of X-band at 800 °C), and the coating possessed better EM-absorbing ability with a thickness of 0.96 mm. Shao et al. (2020)[83] developed plasma-sprayed coatings (combination of Al$_2$O$_3$ and TiC powder material, i.e., $(1 − x)$.wt Al$_2$O$_3$ − x wt TiC) on to a superalloy substrate at 800 °C with enhanced performance in X-band (8.2–12.4 GHz), for high-temperature absorption properties. For 80 wt% Al$_2$O$_3$–20 wt% TiC and thickness 1.6 mm, the coating exhibited

an enhanced absorption bandwidth of 3.45 GHz at 800 °C and a RL lower than −8 dB over the whole X-band.

Zhao et al. (2021)[32] investigated ultrathin high-temperature titanium diboride (TiB_2) and alumina (Al_2O_3) coatings sprayed on to a Ni-based alloy substrate using APS for high microwave absorption performance in a wide temperature range (25–800 °C). With a coating thickness of 1.4 mm, the 30wt% TiB_2–70wt% Al_2O_3 composition exhibited RL of less than −5 dB over a wide high temperature range (400 to 800 °C) in the whole X-band (8.2–12.4 GHz).

As shown through a number of examples earlier, application of thermal spray-coating methods is successful in developing microwave-absorbing composite coatings. Typical coatings thicknesses used ranged from 1 to 3 mm, which call for development of coatings with similar absorption capabilities with smaller thicknesses to ensure weight reduction, especially in some of the critical applications such as defense and stealth.

4.2. Millimeter-Wave Absorption Performance

The millimeter waves' (or mm-wave) EM radio waves typically cover the 30–300 GHz frequency range. It corresponds to a wavelength range of 10 mm at 30 GHz decreasing to 1 mm at 300 GHz,[84] and it meets the capacity requirements of the 5 G network (at 26–60 GHz) which is beyond all current cellular and Wi-Fi frequencies which are below 6 GHz. Millimeter-wave absorbing materials are important to attenuate EM pollution occurring due to rapid development of information technology and defend against radar detection for military stealth technology.[85] An ideal absorbing material should possess strong RL and a broad bandwidth.

Barium hexaferrites, well-known ferrimagnetic materials, are suitable materials for microwave and mm-wave absorber coatings, and a basic compound has a chemical composition of $BaFe_{12}O_{19}$ with a complex magneto–plumbite structure.[15] $BaFe_{12}O_{19}$ exhibits ferromagnetic resonance at around 50 GHz, making it suitable for mm-wave applications.[15] Typical commercial hexaferrite-based absorbers are ceramics or polymer composites filled with the absorbing powders. There are obvious limitations in the possibility to adjust them

to the various shapes of components requiring EM protection: these limitations can be overcome by the application of thermal spraying technologies. In a work by Bobzin et al. (2010),[86] Ba–hexaferrite coatings for EM mm-wave absorption applications were deposited by APS. A suitable powder feedstock was manufactured by blending a $BaCO_3 + Fe_2O_3$ mixture, which was then agglomerated by spray drying. The agglomerates were processed by APS without any further treatment or were heat treated and reactively sintered to stoichiometric Ba–hexaferrite prior to spraying. However, the deposition of untreated agglomerates did not result in adequate amounts of crystalline Ba–hexaferrite in the coatings, and the APS processing of reactively sintered agglomerates led to a high content of Ba–hexaferrite and similar magnetic properties to those of Ba–hexaferrite bulk materials. In another study, Bobzin et al. (2011)[87] used two different kind of feedstock powders: 1) spray-dried agglomerates of micrometric $SrFe_{12}O_{19}$ particles or 2) spray-dried agglomerates of raw materials ($SrCO_3$, Fe_2O_3), reactively sintered at 1100 °C. The high magnetic loss of crystalline $SrFe_{12}O_{19}$ plasma-sprayed coatings at about 50 GHz shows that such coatings are promising candidates for EM wave absorption applications (in mm-wave range).

Application of ceramic coatings on thick ceramic substrates can offer the benefit of preventing cryogenic delamination of the coatings, in addition to being a good antireflection coating for broadband millimeter-wave detection. Jeong et al. (2016)[88] developed plasma-sprayed antireflection coating of about 100 μm thickness with various mixtures of Al_2O_3 and microsphere powders (made of Al_2O_3 and SiO_2) on to Al_2O_3 ceramic substrate (6.35 mm thick), as shown in **Figure 11**a, for experiments with cryogenic optics, and achieved minimal dissipative loss and broad bandwidth. By mixing hollow ceramic microspheres with alumina powder as the base material and varying the plasma energy of the spray, the dielectric constants of the plasma-sprayed coatings (for controlled uniform thickness below 10 μm) were tuned between 2.7 and 7.9. By spraying low-loss ceramic materials with a tunable dielectric constant, Jeong et al. (2016)[88] were able to apply multiple layers of antireflection coating for millimeter-wave detection. At 300 K (≈27 °C), they achieved 106% fractional bandwidth over 90% transmission using a three-layer antireflection coating (see Figure 11b).
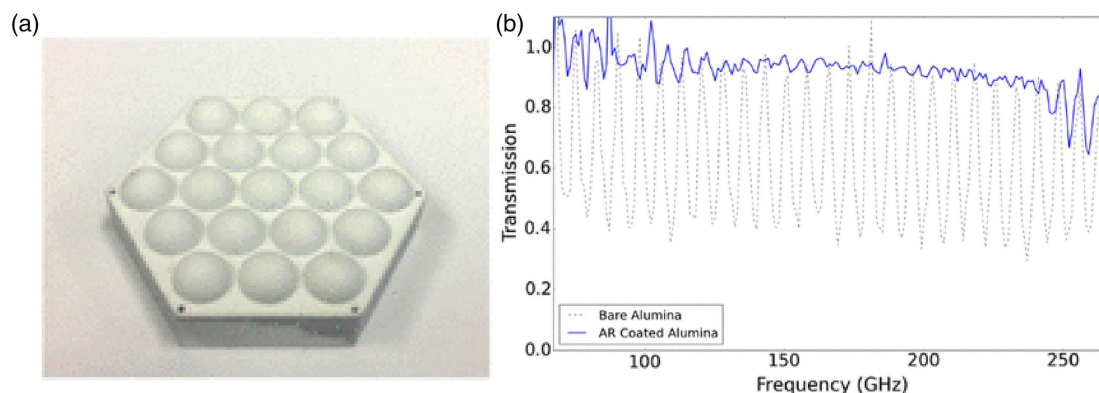

Figure 11. a) Plasma-sprayed spherical lens surfaces (or lenslet array) and b) transmission spectra of a three-layer antireflection-coated alumina disk (solid blue) and an uncoated alumina disk (dotted gray) at 300 K. Reproduced with permission.[88] Copyright 2016, Springer Nature.
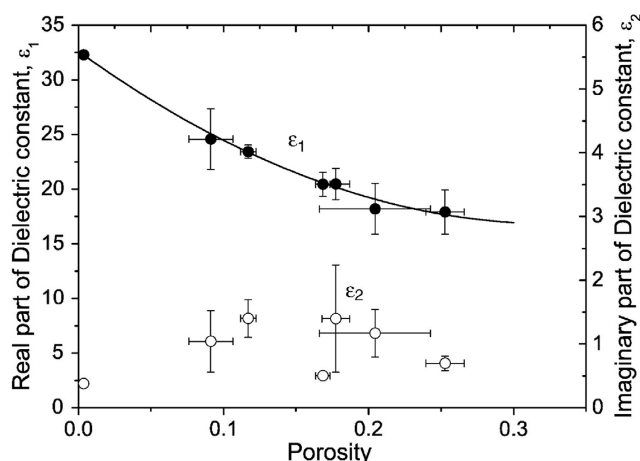
Figure 12. Dielectric constant at 0.5 THz plotted as a function of porosity of the coatings deposited with varying (200–70 mm) plasma-spray distances. Reproduced with permission.[90] Copyright 2011, Elsevier.

The submillimeter (or terahertz) EM waves typically cover the 0.3–30 THz frequency range and occupy radiation between microwaves and infrared light waves. Terahertz EMW are capable of penetrating certain nonmetals but are safer to use because they cannot disrupt molecules.[89] Their frequency range corresponds to a wavelength range of 1 mm at 0.3 THz decreasing to 10 μm at 30 THz. In the terahertz range, Watanabe et al. (2011)[90] investigated the EM wave transmittance and dielectric properties of atmospheric plasma-sprayed 146–1100 μm-thick YSZ thermal barrier coatings deposited onto a carbon steel substrate. The coated samples were produced with varied microstructures by varying spray parameters and irradiated by a pulsed 0.1–6.3 THz wave. The measurements indicated a high transmittance of 20–80% at frequencies below 0.5 THz and zero transmittance above 1.5 THz. As shown in **Figure 12**, the real part of the dielectric constant indicated strong relationship with coating's porosity, meaning, terahertz spectroscopy could be useful to nondestructively evaluate the porosity of ceramic coatings, as well as the detection of densification caused by the sintering of the coatings upon their use in high-temperature environments.

4.3. Solar-Selective Absorbing Property

The sun is a natural source of terahertz (THz) waves, and the solar emission wavelength range is 300–3000 nm or 100–1000 THz.[91] Solar energy cells can directly transfer incident light into electricity, and thermal spray has been an alternative fabrication route of absorbent coatings as it can generate submicrometer/nanocrystalline microstructures. However, as reviewed by Xu et al. (2020),[92] most of the research has been concentrated on the application of thin-film deposition techniques, namely, physical vapor deposition, ion plating, sputtering, and evaporation technique, compared with thermal spray-coating methods.

As known for thermally sprayed coatings, the existence of microstructural defects, high surface roughness, and phase contents leads to their poor optical (solar) properties, because of which it is limited to prepare solar-selective absorbers. However, with certain modification and fabrication techniques, thermally sprayed coatings can be developed for solar-absorbing properties. Vaßen et al. (2009)[93] deposited highly porous TiO_2 coatings using suspension plasma spraying on ITO-coated glass substrates for photovoltaic cells, with special emphasis on the establishment of a high volume fraction of the desired anatase phase, with the best coatings with about 90% of the anatase phase (based on the photocurrent voltage characteristic curve). In a work by Gao et al. (2015),[94] as shown in **Figure 13**, Ni–Mo- and No–Mo–Co HVOF spray coatings were deposited on 307 L stainless steel substrates, and coatings were irradiated by laser treatment with the aim of improving the solar-absorbing property for concentrating solar power applications. Changing the powder or coating morphology by laser treatment (leading to changes in phase contents before and after laser treatment) can achieve better selective EM properties of coatings (e.g., for improving the optical properties of thermal sprayed coatings, especially for concentrating solar power in the spectral range 0.3–2.5 μm). As shown in Figure 13 (for Ni–Mo coatings), the as-sprayed coating is covered by the surface-connected micropores, a useful coating feature for solar rays to penetrate the substrate and weaken the intended spectrally selective effect of the deposited coating. However, after laser treatment, as expected, the coating is denser with significantly less micropores. The reflectance curves (**Figure 14**) of laser-treated coatings compared with as-sprayed coating show suppressed reflectance, indicating
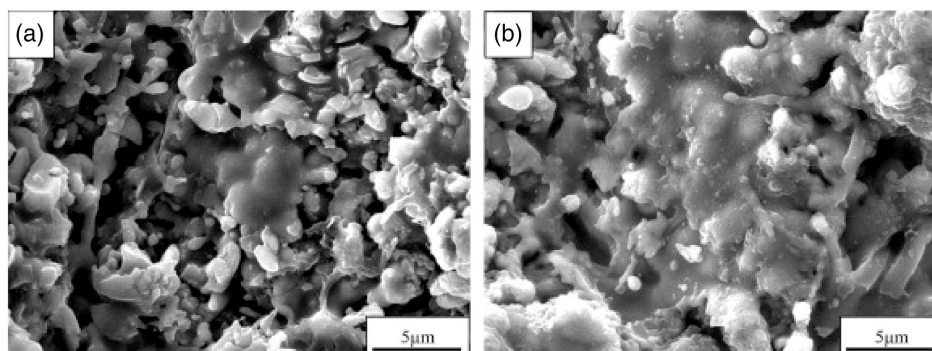

Figure 13. SEM images of the HVOF-sprayed surface: a) as-sprayed Ni–Mo coating and b) laser-treated Ni–Mo. (reproduced with permission).[94] Copyright 2015, Elsevier.
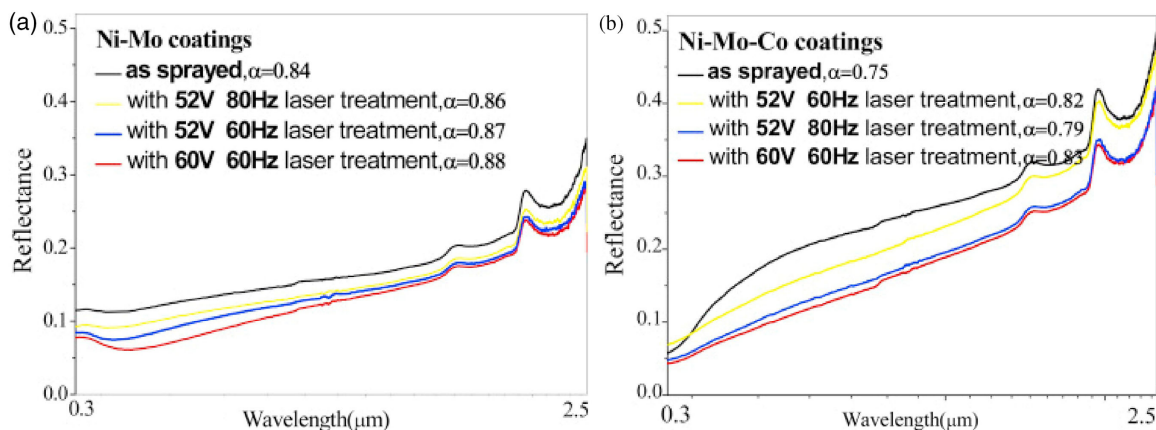
Figure 14. Reflectance curves of the HVOF-sprayed coatings (as sprayed and laser treated): a) Ni–Mo coating and b) Ni–Mo–Co coating. Reproduced with permission.[94] Copyright 2015, Elsevier.

that an enhanced solar-absorbing property is possible (i.e., absolute 10.7% increase in solar absorptance on the laser-treated coatings).

Wang et al. (2017)[95] investigated solar absorptance or solar photothermal conversion applications of HVOF-sprayed 45 μm-thick WC/Co coatings (powder comprising nanometer and submicrometer WC particles) deposited on to 1 mm-thick AISI 304 L stainless steel substrates and compared optical properties of the sprayed multimodal and conventional coatings. The multimodal WC/Co coating with coarse and fine WC particles using agglomerated feedstock powders exhibited higher solar absorptance (0.87), which was attributed to the formation of a dense coating with no decarburized phases and distributed WC particles, than what can be achieved by either coarse powders (0.80) or fine powders (0.82) alone. Similarly, in a work by Ke et al. (2018),[96] WC–Co coatings were deposited onto the stainless steel substrate by HVOF spraying, including layers of coatings (CuCoMnO$_x$, CuCoMnO$_x$–SiO$_2$, and SiO$_2$ sols) synthesized by the sol–gel method deposited successively on the coating. CuCoMnO$_x$ was used as the sealing layer to fill the larger pores and grooves on the surface; then, the composition CuCoMnO$_x$–SiO$_2$ sol was deposited as the second sealing layer to eliminate the remaining smaller pores as well as the transition layer to connect the sealing layer and the uppermost SiO$_2$ antireflective layer. For the new multilayer structure coating, the absorptance increased from 0.821 to 0.915 and the emittance decreased from 0.434 to 0.290. After being annealed in the nonvacuum environment, the absorption and emittance of the multilayered coatings' stack changed to 0.901/0.320. Using similar composite coating preparation method, Duan et al. (2017)[97] investigated solar-selective absorbing properties of duplex Co–WC–Al$_2$O$_3$ (absorbing layer using HVOF method) and Al$_2$O$_3$ (antireflection layer using sol–gel method) ceramic metal–dielectric. The coating exhibited high solar absorptance/emittance (0.908/0.145). However, after annealing the coating at 600 °C for 7 days in air, the absorptance/emittance decreased to 0.898/0.172, which indicated that the coating exhibited good thermal stability.

Within solar-selective absorptance applications, thermal absorptance represents the fraction of incident wavelength radiation that is absorbed by the material, and for objects that do not transmit energy, emissivity (= 1−reflectivity) of a surface is a measure of its ability to radiate energy in comparison with a black body. It is defined as a measure of infrared energy radiated from an object, and the ratio varies from 0 to 1.[98] Therefore, for optical emissivity in the infrared region of metal oxides, Tului et al. (2004)[7] sprayed ZnO and ZnO + (3 and 22 wt%) Al$_2$O$_3$ using plasma spray onto sand-blasted steel substrates. While measuring reflectivity, it was observed that the infrared emissivity of sprayed coatings depended on factors such as wavelength, powder chemical composition, and spraying atmosphere. As shown in **Figure 15**, coatings containing 22 wt% of Al$_2$O$_3$ showed lower emissivity in the visible range than the corresponding 3 wt% Al$_2$O$_3$-containing coatings. It is important to note that Al$_2$O$_3$ (a dielectric) is more stable and more difficult to reduce than ZnO (a semiconductor). Therefore, the plasma spray method was useful in modifying optical emissivity in infrared in the coatings doped with Al sprayed using pure ZnO. In this context, it is relevant to mention that coatings of ZnO[99] and ZnFe$_2$O$_4$[100] have also been successfully deposited by the SPPS route.

Similarly, due to high thermal and oxidation resistance of spinel (oxides), Deng et al. (2020)[101] studied plasma-sprayed vanadium tailings deposited onto the 1 mm-thick stainless steel substrate with the Ni/Al bond layer. Vanadium tailings are composed of oxides of Fe, Cr, Mn, V, Ti, and other transition metals and are byproducts of steel manufacturing. The spinel structured composite oxide coatings exhibited high absorptance (93.79%) and low-energy bandgaps, emissivity of 71% at 120 °C, and high thermal stability at 500 °C.

Therefore, in most cases, the high absorptivity, low emissivity, and the textured surfaces offered by thermal spray coatings are very well suited for selective solar absorption applications. The advent of high operating temperature concentrator solar power systems where the coating is subjected to very-high-temperature cycles for long durations means that future work on these coatings will have to be on the thermal stability of the coating systems over a high number of thermal cycles.
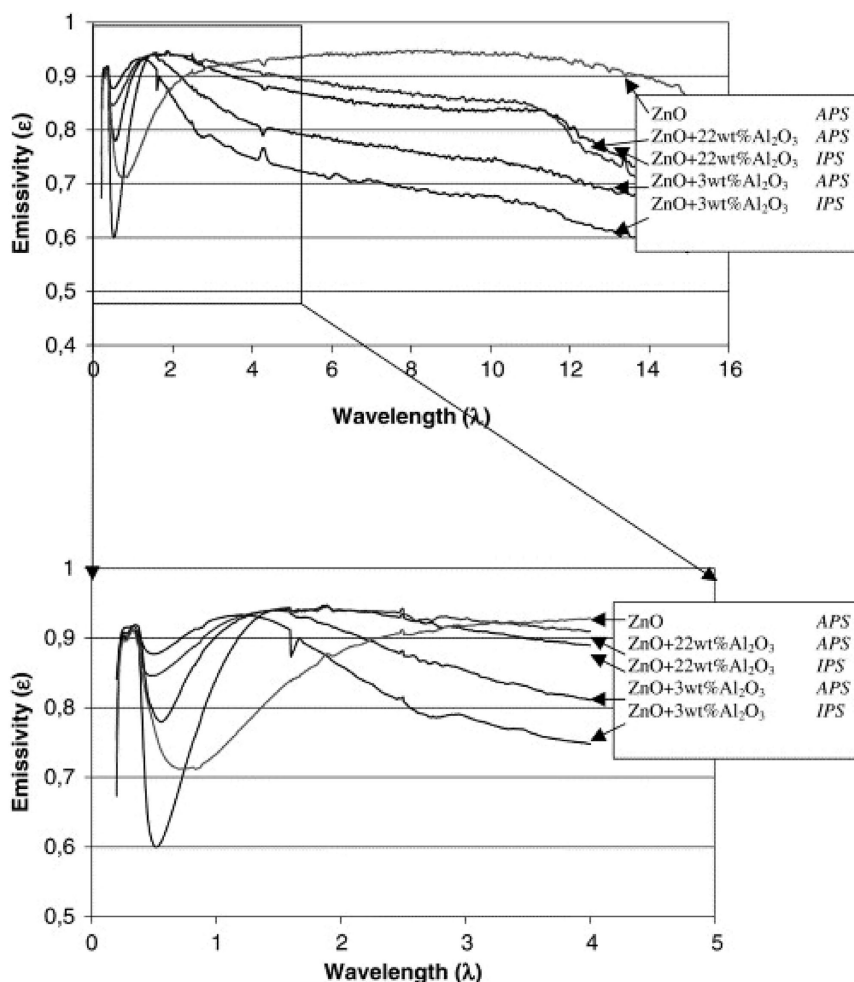
Figure 15. Emissivity of thermally sprayed coatings (ZnO, ZnO + 3 wt% Al₂O₃ and ZnO + 22 wt% Al₂O₃) using plasma spraying in air atmosphere and in inert gas atmosphere. Reproduced with permission.[7] Copyright 2004, Elsevier.

4.4. Photocatalytic (Absorption) Performance

Photocatalytic property refers to the acceleration of a chemical reaction in the presence of substances called photocatalysts, which can absorb light quanta of appropriate wavelengths depending on the band structure. Usually, semiconductors are selected as photocatalysts due to their narrow band gap, unoccupied conduction band, and occupied valence band.[102]

Light-absorbing ability of any material in the range of UV–vis–NIR is a factor which is important for improved photocatalytic property. As an example, TiO₂ (n-type semiconductor most frequently used) coating's photocatalytic property can be triggered when exposed to UV light, and there are a number of studies on such coating materials deposited using thermal-spray techniques. In all such investigations, the research has been more on enhancing the absorption capability of the material, which enhances the decomposition capability (e.g., degradation and destruction of organic pollutants,[103] or inactivation of pathogens,[104] or to mitigate the environmental impact of the textile industry by degrading dyes into water and carbon dioxide in wastewater.[105] It is also important to note that under atmospheric pressure, TiO₂ exists as amorphous, anatase, brookite, and rutile forms; however, most of the research in solar-driven applications focuses on anatase and rutile due to their stability and photoactivity.[106] Though TiO₂ material is well known largely for its absorption capabilities in the UV range, the absorption drops off in the visual range where the wavelength is higher than 387 nm. This is due to the bandgap being around 3.0–3.2 eV,[107] which means that this material cannot be used in the visual range of the radiation. However, additives are known to overcome this drawback. Ye and Ohmori (2002)[108] tested the effect of addition of Fe₂O₃ in a plasma-sprayed TiO₂ coating in comparison with TiO₂ coating without the additive. The improved absorption performance of the coating with the additive is attributed to the formation of the FeTiO₃ phase, which was shown to promote the absorption capability in the visual range. The presence of anatase phase in the pure TiO₂ coatings was also shown to improve the overall absorption performance though not as prominent.

**ADVANCED
SCIENCE NEWS**

www.advancedsciencenews.com

**ADVANCED
ENGINEERING
MATERIALS**

www.aem-journal.com

Dosta et al. (2016)[109] deposited TiO_2 coatings on Inconel alloy substrates to understand their effectiveness as photocatalytic surfaces. The feedstock powders were nanoagglomerated rutile–TiO_2, anatase–TiO_2, and TiO_{2-x} suboxides deposited through APS. The radiation absorption of these coatings has been attributed to the surface roughness and the deposition thickness. The maximum penetration depth of the radiation into the coating is directly proportional to the absorption coefficient 'α' of the coating material. 'α' is a function of the wavelength of incident light and dictates the maximum light penetration depth. The photocatalytic activity of the coatings is dictated by the crystalline phase content, which is a function of the feedstock characteristics such as particle size and morphology. These parameters also dictate the degree of melting in the coating which in turn dictates the surface roughness of the coating, which at higher values promotes better radiation absorption.

Reduced TiO_2 is known to display improved absorption in the UV–vis–NIR region in addition to improved emissivity. Wang et al. (2015)[110] used the flame spray method to produce reduced TiO_2, where a combination of ethylene and oxygen is used to produce a flame expanding through a torch. This method was chosen due to the high operational temperatures and the high quenching rates. They used commercially available rutile–TiO_2 as the feedstock. The powder was sprayed into water and later characterized to identify the phases formed. Due to the O-poor regime within the flame, the formation of oxygen (O) vacancies and titanium (Ti) interstitials leading to the formation of Ti^{3+} species was reported. This species was shown to have a lower-energy bandgap (2.32 eV) which was lower compared with that of the feedstock (3.14 eV), indicating the formation of an impure energy level. This lower bandgap was reported to have increased the absorption in the visible region. The NIR absorption was also shown to have increased with the reduced TiO_2 powder due to the impurity energy-level absorption and the free carrier absorption. The presence of oxygen vacancies leading to the presence of more holes and electrons was reported to have helped the latter.

As shown in **Figure 16**a, Mauer, Guignard, and Vaßen (2013)[111] investigated SPS TiO_2 coatings for photocatalytic applications (dye-sensitized solar cells in the visible spectrum of light), as anatase phase with specific rutile content is preferred to achieve optimum photocatalytic activity. Mauer, Guignard,

and Vaßen (2013)[111] indicated that immediately after deposition, partial transformation to rutile can take place if the substrate temperature is sufficient. As shown in Figure 16b, to improve photoactivity of TiO_2, nitrogen can be doped (by adding TiN to the thermal spray feedstock) during coating fabrication; as such, the anionic dopant can create states within the bandgap which locally reduce the energy barrier of the photoexcited electron.

Plasma spraying can be deployed to deposit thin TiO_2 coating on glass substrates for photocatalytic application along with high sunlight transmittance. Zhang et al. (2013)[112] studied the effect of porosity (8.9%, 11.2%, 17.5%) on the photocatalytic activity of plasma-sprayed TiO_2 coating on steel and FTO glass substrates. While plasma spraying, the anatase phase in starting TiO_2 powder transformed into rutile phase. While developing the optimized process parameters to obtain highest porosity, it was observed that the photocatalytic activity of TiO_2 coating (with 20-25 μm thickness) on FTO was 2.5 times better than TiO_2 coating on the steel substrate. This improvement in photocatalytic performance was due to formation of bimodal porosity (micrometer and submicrometer-sized pores, see **Figure 17**) and improved transmittance in TiO_2 coating on FTO glass. Zhang et al. (2013)[112] also observed that for TiO_2 coating's photocatalytic performance, porosity content has a dominating effect than phase type.

Robinson et al. (2015)[106] used the SPS method for the deposition of nanostructured TiO_2 coatings (of 2–15 μm thicknesses) on to AISI stainless steel substrate with predominantly anatase crystal structure. The coating exhibited granular surface, high specific surface area, along with densely packed agglomerates, interspersed with some melted material. As shown in **Figure 18**, the coatings produced demonstrated visible light absorbance (due to the creation of Ti^{3+} within the coating because of reduction by the hydrogen-containing plasma) with a significant decrease in reflectance at wavelengths >500 nm. Very recently, Khatibnezhad et al. (2021)[105] investigated the effect of oxygen deficiencies on the optical and photocatalytic activity of substoichiometric TiO_{2-x} coatings (about 100–150 μm thicknesses) deposited on to the stainless steel substrate by SPS. The coated samples were heat treated in air at four different temperatures (in the range: 400–550 °C) to vary the level
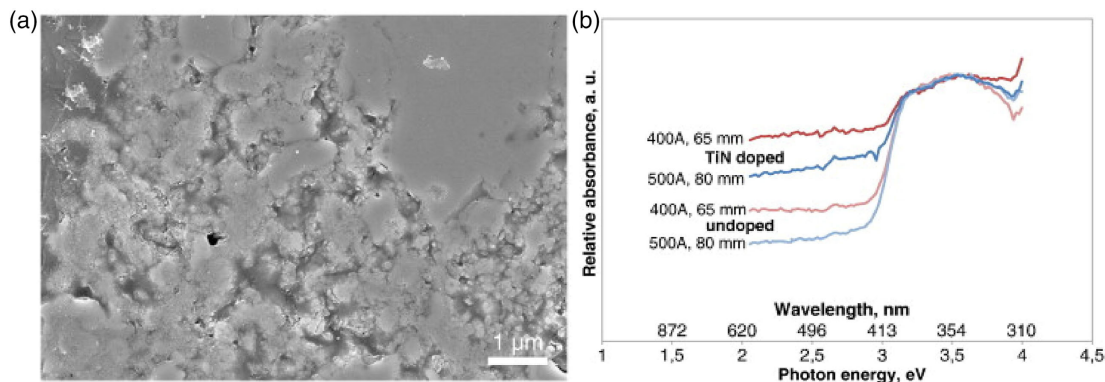

Figure 16. a) SEM images of coating (samples coated using SPS TiO_2 coatings) microstructures sprayed in hot conditions (500 A/80 mm) and b) absorption measurements by photothermal deflection spectroscopy of nitrogen-doped and undoped sprayed in hot conditions (400 A/65 mm and 500 A/80 mm). Reproduced with permission.[111] Copyright 2013, Elsevier.
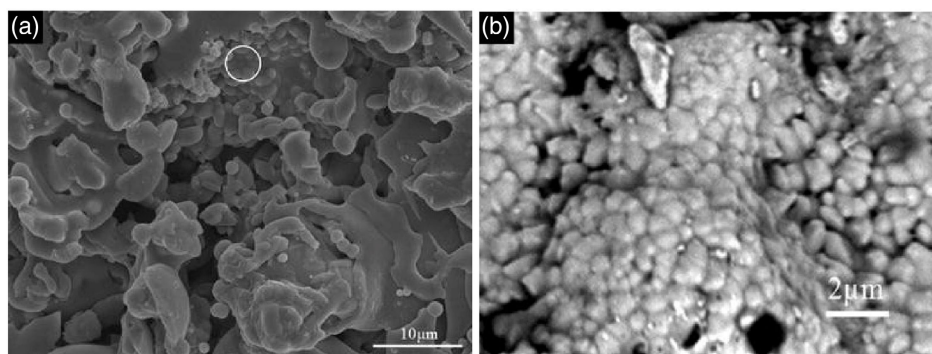
Figure 17. SEM images of micrometer-sized pores in TiO_2 coating on FTO glass: a) low magnification and b) high magnification, showing submicrometer pores in the unmelted region are marked by the circle in (a). Reproduced with permission.[112] Copyright 2013, Springer Nature.
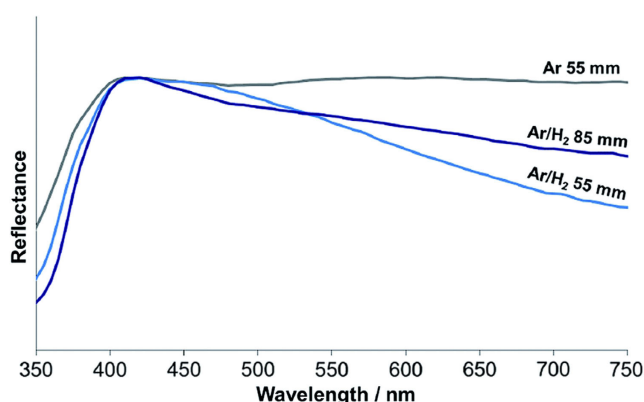
Figure 18. UV–vis reflectance spectra of TiO_2 coatings produced in the two plasma conditions. Reproduced with permission.[106] Copyright Royal Society of Chemistry.

of oxygen vacancies. The absorption spectra in the UV–vis range indicated that there was no difference in the absorption of all coatings (i.e., as-sprayed and those heat treated) in the UV range, whereas as-sprayed coating showed the highest absorption (and smallest indirect bandgap), and the absorption increased with the decrease in oxygen content in the visible light range. Considering the photocatalytic performance, analysis showed that oxygen vacancy positively affected the photocatalytic activity of TiO_{2-x} by introducing some energy levels into the bandgap of TiO_2. Khatibnezhad et al. (2021)[105] suggested that such energy levels can act as traps for photoexcited holes and electrons which can reduce the recombination rate of charges, leading to improvement in the photocatalytic activity under the visible light range.

The suitability of thermal spray methods for depositing TiO_2 has been demonstrated through numerous research publications. The retention of the anatase phase in TiO_2 is highly desirable due to its higher photocatalytic efficiency (as a large number of the photogenerated electron–hole pairs exist which can participate in surface reactions (Khatibnezhad et al., 2021)[105] is of high interest in thermal spray photocatalytic coating research. The use of different doping materials toward this end is likely to constitute further research in this area. Attempts

have also been made to deposit photocatalytically active TiO_2 coatings by SPPS, using materials such as titanium isopropoxide as the starting feedstock. It has been shown that significant control over the resulting microstructures can be exercised by suitably controlling the process conditions. For example, dense TiO_2 coatings have been fabricated using precursor solutions at near-saturation concentrations.[113] In contrast, porous TiO_2 coatings have also been realized by the SPPS route.[114] The phase constitution of the SPPS-deposited TiO_2 coatings has also been shown to be influenced by spray variables, most dominantly the plasma power,[114] suggesting that the possibility of controlling the anatase–rutile ratio that can influence the photoelectrical and photocatalytic properties. SPPS also provides a facile one-step process to synthesize efficient visible light-driven photocatalysts, such as cocatalyst-grafted Ti3 + self-doped rutile TiO_2, which has been found to exhibit excellent photocatalytic activity.[115]

4.5. EMI Shielding Performance

There are numerous examples where application of thermal spray coating-based fabrication of high-performing EMI shielding structures has been demonstrated. This is interesting as thermal spray methods can aid in developing coatings with varied phase compositions, microstructures, EM properties, oxidation resistance, chemical stability, and flexibility for large-scale production. Jang et al. (2020)[116] studied the EMI shielding effectiveness of Cu, Cu–Zn, and Cu–Ni coatings deposited on smooth steel substrates using arc thermal spray process, as shown in **Figure 19**. They studied the effect of the coating thickness, porosity, and degree of particle melting within the microstructure on the EMI shielding effectiveness over a frequency range from 0.1 to 1.0 GHz. For security applications, from EMI at 1.0 GHz, it required minimum 80 dB shielding value by the shielding materials, as recommended by national defense and military facilities.[117,118] Jang et al. (2020)[116] reported that the introduction of Zn into the coating increased the EMI shielding due to increase in the degree of melting, leading to an increase in the conduction loss. At lower thicknesses of the coating, around 100 μm, EM wave leakage through the high porosity present was reported to have reduced the EMI shielding. As the coating thickness increased, the coating density increased due to lower

ADVANCED
SCIENCE NEWS
www.advancedsciencenews.com

ADVANCED
ENGINEERING
MATERIALS
www.aem-journal.com
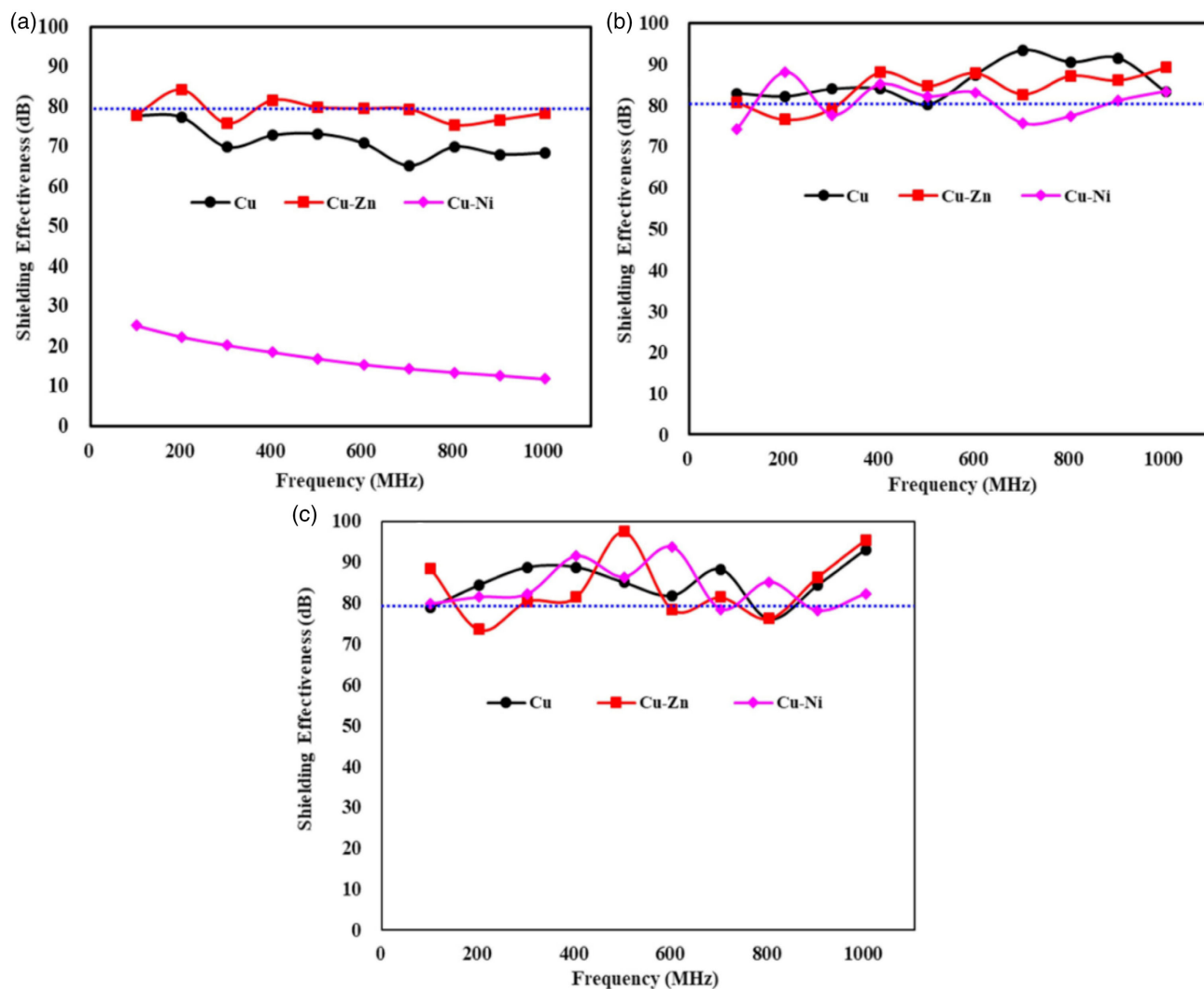
Figure 19. Shielding effectiveness value of Cu, Cu–Zn, and Cu–Ni coatings, each with thicknesses: a) 100 µm, b) 200 µm, and c) 500 µm, at different frequencies. Reproduced with permission.[116] Copyright 2020, The Authors, published by MPDI.

porosity, leading to a higher conduction loss. While the EMI shielding effectiveness values reveal that 100 µm-thick Cu–Zn coating satisfies the minimum requirement for EMI shielding, the Cu and Cu–Ni required higher thickness. In the context of metallic coatings, such as those in the Cu, Cu–Zn, and Cu–Ni category discussed earlier, the supersonic particle deposition by the CS process is particularly ideal by virtue of its ability to almost completely suppress in situ oxidation and yield dense and well-adherent coatings. CS coatings for EMI shielding using conductive or magnetic materials are considered one of the promising CS applications.[119]

Using low-power plasma spraying, Wen et al. (2016)[120] fabricated $MoSi_2$/glass composite coatings on to the graphite substrate (**Figure 20**a) with different $MoSi_2$ filler contents (20%, 22.5%, 25%, 30%) in the glass matrix, to investigate the EMI shielding effectiveness. As shown in Figure 20b, the fabricated coatings showed that $MoSi_2$ flakes aligned in the plane direction blocked the incident EM wave through the shielding materials via reflection and absorption many times by multiple layers of parallel-flake microcapacitors. They found that the shielding effectiveness was related to the electrical conductivity and dielectric properties, attributed to the high aspect ratio of lamellar structure as well as the dispersion state of $MoSi_2$. The average value of shielding effectiveness was 24.2 dB (99.6%) in X-band (8.2–12.4 GHz) for the $MoSi_2$/glass composite coating with 30 wt% $MoSi_2$ with 1.5 mm thickness. Before this, the same investigation team led by Qing et al. (2015)[121] fabricated about 3 mm-thick FeSiAl/Al_2O_3 composite coatings onto graphite substrate with different FeSiAl contents (10%, 20%, 30%, 40%) in the Al_2O_3 matrix, to investigate the shielding effectiveness. Analysis showed that the total shielding effectiveness of 40 wt% FeSiAl powder-filled Al_2O_3 ceramics exceeded 36 dB in whole X-band with a thickness of 2.0 mm, indicating high EM attenuation properties. Similarly, Zhou et al. (2011)[122] investigated Al_2O_3/Nb composite coatings sprayed on graphite substrates by low-power atmospheric plasma spraying.
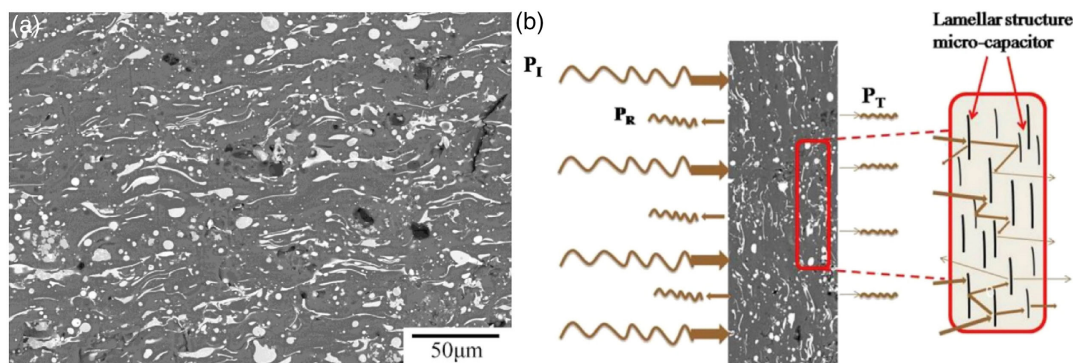
Figure 20. a) SEM image of the as-sprayed composite coating with 30% MoSi$_2$ filler content in glass matrix and b) schematic of EM wave interaction with as-sprayed MoSi$_2$/glass coating. Reproduced with permission.[120] Copyright 2016, Elsevier.

Analysis showed that for the microwave absorption as a single-layer absorber, with 10 wt% Nb content coating when the coating thickness is 1.5 mm, the RL values exceeding −10 dB can be obtained in the frequency range from 10.0 to 11.8 GHz.

Due to high EM shielding characteristics of aluminum (Al) and tantalum (Ta) materials, Hung (2019)[123] fabricated Ta–Al coating (using sputtering technique) onto glass substrate to review the shielding characteristics (at frequency range: from 50 to 3000 MHz) but investigated the coating structure and interface properties of plasma-sprayed Ta–Al coating (Al (100 μm), Ta (200, 400, and 600 μm)) onto a 1 mm-thick 304 stainless steel substrate. It was observed that after the annealing heat treatment process, the Ta–Al coatings' (onto stainless steel substrate) structural characteristics were excellent and suitable for shielding effects at different temperatures and humidity. Hung (2019)[123] concluded that increasing the Ta thickness (as well as with the increase in temperature) can improve the shielding characteristics at low- and middle-frequency conditions, while annealing also had a significant positive effect at the high-frequency condition.

Qing et al. (2021)[124] investigated EMI properties in the X-band (8.2–12.4 GHz) of 1.2 mm-thick plasma-sprayed ZrB$_2$/Al$_2$O$_3$ coatings (ZrB$_2$ is a semiconductor and Al$_2$O$_3$ is insulator). It was observed that the total EMI shielding efficiency (EMI SE) of 30 wt% ZrB$_2$-filled Al$_2$O$_3$ ceramics was greater than 31 dB at 25 °C and 44 dB at 600 °C, along with long-term life at high temperature (600 °C for 300 h). Qing et al. (2021)[124] indicated that the target value for the EMI SE needed for commercial applications is near 20 dB, meaning that ZrB$_2$/Al$_2$O$_3$ coatings can be regarded highly efficient EMI absorbing and shielding materials. Very frequently, it has been advised[61,124–126] that for enhanced EMI properties, the frequency dependence of the complex permittivity and the EMI SE can be optimized by introducing highly conductive carbon nanomaterials (carbon fibers, CNTs, graphene) and MXenes.[127] MXenes are those materials which contain novel transition metal carbides, nitrides, or carbonitrides, represented as $M_{n+1}AX_n$ ($n = 1$, 2 or 3), where M is transition metal (Sc, Ti, Zr, Hf, V, Nb, Ta, Cr, Mo, etc.), A is a group 12–16 element (Cd, Al, Ga, In, Tl, Si, Ge, Sn, Pb, P, As, etc), and X is carbon and/or nitrogen, respectively, and it is possible to thermally spray MXenes phase materials, as demonstrated in one of the rare works by Zhang et al. (2018)[128] who used kerosene-fueled HVOF spray of Ti$_2$AlC MAX-phase powders.

From the above literature, in most of the thermally sprayed coating systems, the existence of a conductive network of splats/lamellae (large interface area, along with large surface area due to porosity), along with reasonably high coating thicknesses (as the absorption loss is found to be directly proportionate to the thickness of the shielding material)[36] is crucial for the EMI shielding performance. The existence of these networks results in the formation of microcapacitors that lead to energy loss within the coating. In most systems, the conductive component exhibits a percolation (meaning to filter or trickle through) threshold beyond which the coating conduction losses dominate the energy loss mechanism and lead to high EMI shielding performance. The formation of the microcapacitor networks leads to an increase in the overall complex permittivity of the coating. The increase in the wt% of the conductive component of the composite coatings leads to an increase in its interfacial area with the matrix, leading also to an increase in the dielectric constant of the coating. All these different phenomena lead to an increase in the EMI shielding.[52]

4.6. Thermal Barrier (Heat, Emissivity) Performance

As per Kirchoff's law of thermal radiation, a body at a given temperature radiates EM energy.[129] The law of such thermal radiation suggests wavelength-specific radiative emission and absorption by a material, in thermodynamic equilibrium, including radiative exchange equilibrium. Thermal emitter materials are other types of EM wave absorbers, and due to Kirchhoff's law, a perfect emitter is equivalent to a perfect absorber.[2]

Thermal barrier coatings (TBCs) are common porous materials coating the surface of devices operating under high temperatures and are essentially designed for heat insulation purposes. There are a number of recent reviews summarizing the design aspects of TBCs[130,131] but not much has been reported about their EM wave propagation characteristics. Though some studies present a comprehensive investigation on the microstructural effect on the radiative scattering coefficient and asymmetry factor of anisotropic TBCs,[35,132,133] TBCs usually consist of bond coat

**ADVANCED
SCIENCE NEWS**

www.advancedsciencenews.com

**ADVANCED
ENGINEERING
MATERIALS**

www.aem-journal.com

(metal alloys) and topcoat (ceramics) containing 6–8 wt% yttrium-stabilized zirconia (or YSZ), and APS and electron beam physical vapor deposition (EB-PVD) are the two main approaches to fabricate TBCs. However, APS is mostly used considering its wide application, high production efficient, and low cost in fabrication. During the fabrication process, defects like pores and cracks are formed in TBCs and play an important role in heat transfer. YSZ TBCs are intrinsically semitransparent to the wavelength ranging from 0.3 to 8 μm where over 80% of thermal radiation is emitted by objects from 1700 K (1427 °C) to 2000 K (1727 °C).

Considering EM wave propagation characteristics of TBCs, Zhang, Wang, and Zhao (2014)[132] have shown that the plasma-sprayed 8YSZ TBC is semitransparent (weakly absorbing material) in the wavelength range between 0.4 and 6 μm, as shown in **Figure 21**. It was noticed that in transmittance data there is a peak at 3 μm. This was due to the reason that in the APS process of making TBCs, the iron OH– is formed, and it has a strong absorption at wavelength of 3 μm. In a work by Wang and Zhao (2015)[35] on APS 8YSZ TBCs, the optical measurements included reflectance, transmittance, and absorptance of TBC slabs with different thicknesses. It was observed that the material (8YSZ) is inapplicable in the semitransparent spectral region of TBCs, especially between around 3.2 and 5.6 μm. According to Chen, Zhao, and Wang (2018),[133] among the wavelength range from 1 to 6 μm, the microstructure does have a significant influence on the anisotropic distribution of radiation scattering in TBCs. Compared with spherical shape, irregular anisotropic pore shape reduces the forward scattering peak. For the first time, Chen, Zhao, and Wang (2018)[133] verified that the absorption coefficient of TBCs is mainly associated with the refractive index, porosity, and the wavelength. Within the range of wavelength from 0.3 to 8 μm, YSZ is semitransparent to radiation and has a quite small absorption coefficient, which was associated with porosity that increased porosity lowers absorption coefficient.

Thermal spray coatings usually exhibit microstructure-dependent absorption of EM wave energy, and numerous investigations have shown that the orientation of porosity and cracks affects the transmission of the EM wave across the coating thickness.[35,132,133] Moreover, a random arrangement of these microstructural features is shown to have a positive effect on the performance of the coating as a thermal barrier. The existence of pores with dimensions comparable with the wavelength of
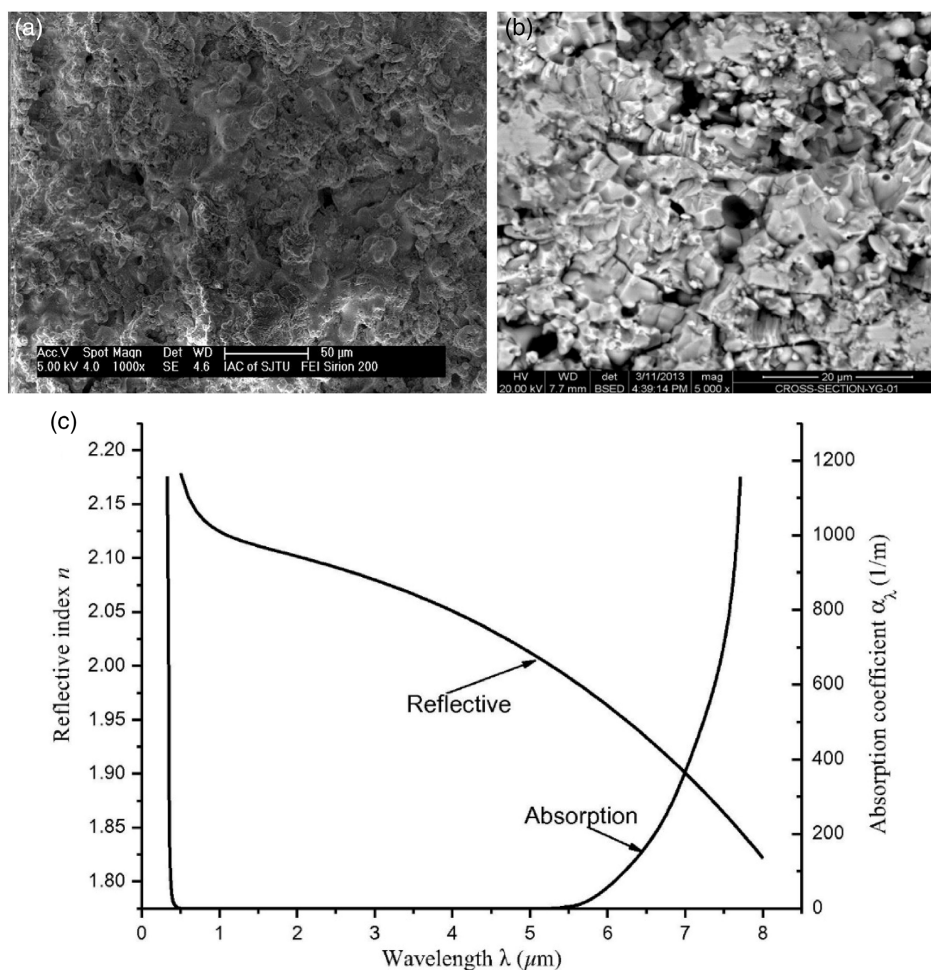

Figure 21. Plasma-sprayed YSZ coating: a) top surface view and b) cross section and (c) spectral dependence of optical constants of YSZ. Reproduced with permission.[132] Copyright 2014, Elsevier.

2200171 (21 of 46)

thermal radiation has been reported[35,132,133] as the source for radiation scattering within the coating. Further on, the liquid feedstock-based thermal spray processes involving the use of suspensions and solution precursors (SPS, SPPS) are particularly well suited for depositing a wide array of ceramic coatings, including depositing YSZ coatings. The primary focus of SPS research has been on TBCs and the technique has been shown to be capable of depositing YSZ coatings with tailored microstructures such as porous columnar, dense vertically cracked,[134] as well as alumina coatings with refined microstructures.[135] Extensive effort has also been devoted to exploring new ceramic TBC materials such as pyrochlores, perovskites, hexa-aluminates, etc., as alternatives to YSZ.[136] Among these, the two pyrochlores gadolinium zirconate ($Gd_2Zr_2O_7$) and lanthanum zirconate ($La_2Zr_2O_7$) have been most widely studied.[137] Such materials have been deposited by the SPS route,[138] with multilayer coatings involving the zirconates as well as YSZ also being investigated.[139] Although relatively less studied compared with SPS, development of the SPPS technique has also been mainly driven by the interest in exploiting it for TBC applications.[140] The SPPS deposited YSZ coatings are characterized by interesting features like fine grains, vertical cracks, fine distributed porosity, reduced interspat boundary sizes between the lamellae, etc.[141] As in the case of SPS, the precursor approach has also been demonstrated to be extended to deposit zirconates and multilayers.[142] In the context of YSZ coatings, such as those discussed above, the use of suspensions and solution precursors (SPS, SPPS) can be suitable for depositing coatings with microstructure dimensions comparable with the wavelength of thermal radiation.

To summarize, and as seen through the number of examples earlier (listed in Table 2), when EM waves hit a matter or material, its dielectric properties (i.e., electric permittivity, magnetic permeability, and electrical conductivity) determine their interaction behavior. Table 3 presents other potential materials which could be considered thermal spraying to enhance EM wave propagation characteristics for various applications identified in the current context. **Figure 22** shows the thermally sprayed feedstock materials used for various EM wave ranges, whereas **Figure 23** shows potential feedstock materials (that can be thermally sprayed) for enhanced functional and EM wave properties.

5. Special Considerations for Enhanced EM Wave Propagation Characteristics

5.1. Feedstock Material Selection and Postprocessing

As seen from examples, the feedstock materials when thermally sprayed can help achieve materials' microstructures and properties which can help absorb or shield the specific wavelengths. The selection of suitable feedstock materials requires understanding of the EM wavelength-range applications and requirements. Furthermore, the feedstock materials and its size should be appropriate (sprayable/flowable) for the specific thermal spray technique (it is important to note that all powder materials are not always or easily thermally sprayable/flowable but possible by agglomeration or use of suspension/solution thermal spray system).[143] In the current context, feedstock and substrate

material selection and deposit thickness can be based on high permeability, magnetic, and electrical conductivity losses to increase the absorption, including high thermomechanical performance.

Overall assessment of feedstock material selection also shows that that much effort by researchers has been deployed in developing composite materials along with fillers and doping, their content, and size to have a desirable EM wave propagation characteristic. Manufacturing of coatings influences the feedstock material characteristic such as morphology, size distribution, and apparent density.[103] The most important feedstock (powder) manufacturing processes has been atomization (gas or water), fusion, or sintering followed by crushing, agglomeration by spray drying, cladding, and mechanical alloying.[103,143] Considering the feedstock material requirements for desirable EM wave propagation characteristics (i.e., high permeability, magnetic and electrical conductivity losses, including high thermomechanical performance), the earlier manufacturing processes for feedstock material or a combination of those can help develop materials with complimentary properties.

Considering pre-/postprocessing of materials which leads to changes in phase contents (among other changes) before and after processing, there are examples[94] where changing the powder or coating morphology by laser treatment has been deployed to help achieve better EM (solar-selective absorption) properties of the Ni–Mo and No–Mo–Co coatings. Changing the powder morphology by laser treatment (to achieve better selective EM properties of the coatings) is not common but thermal post-treatment of sprayed coatings to refine microstructure and potentially enhance properties has been explored in the past. It is well known that the conventional furnace heat treatment of coated components presents several challenges, including influence on the substrate characteristics, possible distortion, etc. Furthermore, the dimensions of components that can be so treated are also limited by the furnace size. Post spraying laser irradiation of coatings has been investigated to overcome the above concerns. A significant advantage of this approach is the localization of heat input and elimination of constraints on part dimensions. The recent advent of compact, small-footprint high-power diode lasers capable of delivering controlled and uniform radiation over large areas also makes this route viable for industrial implementation.[144] Laser post-treatment of plasma- and HVOF-sprayed hard coatings has been reported[145,146] and has been found to result in the increase in other properties, such as erosion[145] and dry sliding wear[146] resistance. Laser glazing of ceramic coatings has also been widely studied and demonstrated to yield a completely solidified, dense top layer with segmented cracks.[147] This has potential to enhance properties such as thermal shock behavior and wear performance, as shown in case of TBCs,[148,149] including enhanced EM wave absorption properties.

Considering additional strategies for feedstock material selection for other applications (EM wave "absorbing" properties at high temperature), it has been argued that the feedstock powder materials should not react or oxidize when coating is formed or at high-temperature applications.[81–83] As an example,[83] a material like TiC can be selected for high-temperature applications as it normally does not react with Al_2O_3 and TiC does easily get oxidized when the coating is formed or at high-temperature

Table 2. Manufacturing of thermal spray coatings with EM wave characteristics.

Coating materials	Coating thickness [analyzed or optimal]	Substrate	Thermal spray process	Remarks: EM wave characteristics	References
Microwave absorption					
Cr_2O_3 (chromia-based formulations): $Cr_2O_3 + BaTiO_3$ 40 wt%; $Cr_2O_3 + SrTiO_3$ 40 wt%.; $Cr_2O_3 + NiO$ 40 wt%; $Cr_2O_3 + ATO$ 40 wt%; $Cr_2O_3 + La0.5Sr_{0.5}MnO_3$ 40 wt%; $Cr_2O_3 + Ni0.5Zn_{0.5}Fe_2O_3$ 40 wt%; $Cr_2O_3 + Al$ 40 wt%; $Cr_2O_3 + Cu$ 5 wt%; $Cr_2O_3 + Cu$ 20 wt% $+ Ni0.5Zn_{0.5}Fe_2O_3$ 20 wt%; $Cr_2O_3 + Al$ 20 wt% $+ La0.5Sr_{0.5}MnO_3$ 20 wt%; $Cr_2O_3 + Co_3O_4$ 40 wt%	2–5.5 mm	Stainless steel	APS	X-band (8–12 GHz). With chromia material (high permittivity), it was possible to identify an adsorbance frequency in the X-band by varying coating thickness in a relatively restricted range.	[70]
Co,Ti-substituted Ba–hexaferrite $(BaCoTiFe_{10}O_{19})$	1-4 mm	Glass–ceramic (with nonmagnetic properties)	APS, HVOF	Adjustment of the processing conditions enabled the deposition of a coating retaining enough hexaferrite phase, whose magnetic properties, are close to bulk $BaCoTiFe_{10}O_{19}$ (very promising for EM wave absorption).	[15]
Hexaferrite $(BaFe_{12}O_{19}$ or $SrFe_{12}O_{19})$ and polyethylene	1 mm	Glass	Flame spraying	Suitable for EM wave absorbers in the U-band. BaFe12O19/PE coatings with a thickness around 1 mm absorbed 80% of EM power at 45–55 GHz (note: polymer can have high dielectric losses; ferrite can have high magnetic losses).	[16]
MWCNTs/cordierite (MAS) nanocomposite coatings with MWCNT contents (5, 7, 10, 15, 20, and 30%)	1-3.5 mm	Graphite	APS	X-band (8.2–12.4 GHz). Sample with 2.4 mm thickness showed the microwave absorption property, with minimum RL of −15.61 dB and bandwidth of 2.35 GHz	[71]
Ti_3SiC_2/cordierite (MAS)	2.5 mm	Graphite	APS	X-band (8.2–12.4 GHz); Ti_3SiC_2 improved the EM shielding and complex permittivity of the coatings (due to enhanced polarization effect and electrical conductivity); absorption bandwidth ($\leq$−5 dB) can be obtained across the whole measured frequency with a coating thickness of 1.8 mm	[72]
Carbon black/cordierite	1–3.5 mm	Graphite	APS	Absorption with a minimum RL of −23.90 dB at 10.13 GHz and RL less than −9 dB over the whole investigated frequency	[73]
W-type hexagonal ferrite	1.5 mm	–	APS	2–18 GHz; coating is suitable for EM wave absorbers in Ku-band; simulated RL of the coating below −5 dB is in frequency of 14.2–18 GHz at thickness of 1.5 mm. The minimum RL is −7.2 dB at frequency of 18 GHz	[74]
$LaSrMnO_3/Al_2O_3$	2 mm	Graphite	APS	X-band (8.2–12.4 GHz); RL values exceeding −10 dB can be obtained in the frequency range of 10.5–12.4 GHz when the LSM content is 80 wt% and when the coating thickness is 1.5 mm	[75]
TiO_2/Al_2O_3	2 mm	Graphite	APS	X-band (8.2–12.4 GHz); RL values of TiO_2/Al_2O_3 coatings exceeding −10 dB (larger than 90% absorption) can be obtained in the whole frequency range of X-band with 17 wt% TiO_2 content when the coating thickness is 2.3 mm	[76]
TiAlCo (formed using mixture of powders TiO_2, Co_3O_4, and Al_2O_3)	1.8 mm	Graphite, metal	APS	X-band (8.2–12.4 GHz); RL values of TiAlCo coatings exceeding −10 dB in the whole frequency range of X-band when the coating thickness is 1.8 mm	[77]
Cr/Al_2O_3	3.5 mm	Graphite	Low-power plasma spray	Higher Cr content and larger Cr particle size exhibited higher dielectric properties due to the enhanced interfacial polarization and conductance loss	[78]

Table 2. Continued.

Coating materials	Coating thickness [analyzed or optimal]	Substrate	Thermal spray process	Remarks: EM wave characteristics	References
$NiCrAlY/Al_2O_3$	3 mm	Graphite	Low-power plasma spray	X-band (8.2– 12.4 GHz); 20 wt% NiCrAlY and 2.0 mm thickness possessed effective bandwidth ($<$-10 dB) 1.3 GHz in 8.2– 9.5 GHz and minimum RL -15.7 dB at 8.9 GHz, exhibiting enhanced microwave absorption properties	[79]
$Ti_3SiC_2/NASICON$	2.5 mm	Graphite	APS	X-band (8.2–12.4 GHz); absorption applications in a wide temperature range (25 °C– 500 °C); microwave-absorption property with a wide bandwidth (below 5 dB) with a thickness less than 2 mm when the temperature ranged from 200 to 500 °C	[80]
WC and Al_2O_3	1.1 and 1.5 mm	Ni alloy	APS	X-band (8.2–12.4 GHz); absorbing bandwidth for RL below −10 dB can reach 1.5 and 2.2 GHz with the thickness of only 1.1 and 1.5 mm	[81]
20 wt% Al_2O_3% and 80 wt% TiC and then sprayed NiCrAlY alloy metamaterial pattern	0.96 mm	Ni alloy	APS	X-band (8.2–12.4 GHz); achieved EM RL below −5 dB covering the whole of X-band at 800 °C; and the coating possessed better EM absorbing ability with a thickness of 0.96 mm	[82]
Al_2O_3 and TiC	1.6 mm	Ni alloy	APS	X-band (8.2–12.4 GHz); For 80 wt.% Al_2O_3–20 wt.% TiC and thickness 1.6 mm, the coating exhibited an enhanced absorption bandwidth of 3.45 GHz at 800 °C, and a RL lower than −8 dB in whole X-band	[83]
TiB_2 and Al_2O_3	1.4 mm	Ni alloy	APS	X-band (8.2–12.4 GHz); With a coating thickness of 1.4 mm, the 30wt%. TiB_2–70wt%. Al_2O_3 material exhibited a RL of less than −5 dB over a wide high temperature range (400–800 °C) in the whole X-band.	[32]
Millimeter-wave absorption					
Ba–hexaferrite [$(BaFe_{12}O_{19})$] using mixture of $(BaCO_3 + Fe_2O_3)$	24 to 107 μm	–	APS	–	[86]
Hexaferrite $SrFe_{12}O_{19}$		Glass–ceramic (nonmagnetic properties)	APS	The high magnetic loss of crystalline $SrFe_{12}O_{19}$ coatings at about 50 GHz shows that such coatings are promising candidates for EM wave absorption applications (in mm-wave range).	[87]
YSZ	146 to 1100 μm	carbon steel	APS	High transmittance of 20%–80% at frequencies below 0.5 THz and zero transmittance above 1.5 THz	[90]
Mixtures of Al_2O_3 and microsphere powders (made of Al_2O_3 and SiO_2)	100 μm	Al_2O_3	APS	At 300 K ($\approx$27 °C), they achieved a fractional bandwidth of 106 over 90% transmission using a three-layer antireflection coating	[88]
Solar-selective absorbing					
ZnO and ZnO + (3 and 22 wt%) Al_2O_3	–	Sand-blasted steel	APS	Coatings containing 22 wt% of Al_2O_3 showed lower emissivity in the visible range than the corresponding 3 wt% Al_2O_3-containing coatings.	[7]
TiO_2	–	ITO-coated glass substrates	Suspension plasma spray (SPS)	Best coatings of about 90% of anatase phase (based on photocurrent voltage characteristic curve)	[93]
Ni–Mo and No–Mo–Co	30 μm	307 L stainless steel	HVOF	Nd:YAG laser treatment showed increment on solar absorptance as the Ni–Mo sample increased from 0.84 to 0.88 and Ni–Mo–Co sample from 0.75 to 0.83.	[94]

Table 2. Continued.

Coating materials	Coating thickness [analyzed or optimal]	Substrate	Thermal spray process	Remarks: EM wave characteristics	References
WC–Co	45 μm	AISI 304 L stainless steel	HVOF	Higher solar absorptance (0.87) was attributed to the formation of a dense coating with no decarburized phases and distributed WC particles than what can be achieved by either coarse powders (0.80) or fine powders (0.82) alone	[95]
Co–WC–Al$_2$O$_3$	–	–	HVOF	Absorptance/emittance (0.908/0.145), however, after annealing the coating at 600 °C for 7 days in air, the absorptance/emittance decreased to 0.898/0.172.	[97]
WC–Co (powders composed of 80% Co + 10% sub-micrometer WC + 10% nano-meter WC)	–	Stainless steel	HVOF	Other top coatings (CuCoMnO$_x$, CuCoMnO$_x$-SiO$_2$, and SiO$_2$ sols) synthesized by sol–gel method. Absorptance (0.915) and emittance (0.29), followed by annealing under nonvacuum environment, led to further changes in absorption and emittance.	[96]
Vanadium tailings (oxides of Fe, Cr, Mn, V, Ti and other transition metals)	–	Stainless-steel substrate with Ni/Al bond layer	APS	Absorptance ($\approx$94%), emissivity of 71% at 120 °C, and high thermal stability at 500 °C.	[101]
Photocatalytic absorption					
Fe$_2$O$_3$ + TiO$_2$	–	–	APS	Improved absorption performance of the coating attributed to the formation of FeTiO$_3$ phase	[108]
TiO$_2$, nitrogen-doped TiO$_2$ (by adding TiN to the thermal spray feedstock)	–	–	Suspension plasma spray (SPS)	Anatase phase with specific rutile content is preferred to achieve optimum photocatalytic activity. Dopants create states within the bandgap which reduce the energy barrier of the photoexited electron.	[111]
TiO$_2$	–	Steel, FTO glass	APS	Anatase phase in starting TiO$_2$ powder transformed into rutile phase. Photocatalytic activity of TiO$_2$ coating (with 20–25 μm thickness) on FTO was 2.5 times better than TiO$_2$ coating on the steel substrate.	[112]
TiO$_2$ (anatase)	–	AISI stainless steel	Suspension plasma spray (SPS)	Visible light absorbance (due to the creation of Ti^{3+} within the coating because of reduction by the hydrogen containing plasma) with a significant decrease in reflectance at wavelengths >500 nm.	[106]
TiO$_2$ (rutile)	–	–	Flame spray	Formation of Ti^{3+} species showed a lower-energy bandgap (2.32 eV) which is lower compared with that of the TiO$_2$ feedstock (3.14 eV). Improved absorption in the UV–vis–NIR region in addition to improved emissivity	[110]
TiO$_2$ (rutile, anatase) and TiO$_{2-x}$	–	Inconel	APS	Absorption attributed to the surface roughness and deposition thickness. Photocatalytic activity of the coatings dictated by the crystalline phase content.	[109]
TiO$_{2-x}$	100–150 μm	Stainless steel	Suspension plasma spray (SPS)	Oxygen vacancy positively affected the photocatalytic activity of TiO$_{2-x}$ by introducing some energy levels into the bandgap of TiO$_2$, leading to improvement in the photocatalytic activity under the visible light range.	[105]
EMI shielding					
Al$_2$O$_3$/Nb	1.5 mm	Graphite	APS (low power)	With 10 wt% Nb content coating (1.5 mm coating thickness), the RL values exceeding −10 dB can be obtained in the frequency range from 10.0 to 11.8 GHz	[122]
FeSiAl/Al$_2$O$_3$ (with 10%, 20%, 30%, 40% FeSiAl in Al$_2$O$_3$ matrix)	3 mm	Graphite	APS	Shielding effectiveness of 40 wt% FeSiAl powder-filled Al$_2$O$_3$ ceramics exceeded 36 dB in whole X-band with a thickness of 2 mm.	[121]

ADVANCED
SCIENCE NEWS
www.advancedsciencenews.com

ADVANCED
ENGINEERING
MATERIALS
www.aem-journal.com

Table 2. Continued.

Coating materials	Coating thickness [analyzed or optimal]	Substrate	Thermal spray process	Remarks: EM wave characteristics	References
MoSi$_2$/glass (with 20%, 22.5%, 25%, 30% MoSi$_2$ filler in glass matrix)	1.5 mm	Graphite	APS	Shielding effectiveness was 24.2 dB (99.6%) in X-band (8.2–12.4 GHz) for the MoSi$_2$/glass composite coating with 30 wt.% MoSi$_2$ in 1.5 mm thickness	[120]
Ta–Al	Al (100 µm), Ta (200, 400, and 600 µm)	304 stainless steel	APS	Increasing Ta thickness (and temperature) can improve the shielding characteristics at low- and middle-frequency conditions (range: from 50 to 3000 MHz)	[123]
Cu, Cu–Zn, and Cu–Ni	100 µm	Steel	Arc thermal spray	Zn increased the EMI shielding due to increase in the degree of melting, leading to an increase in the conduction loss.	[116]
ZrB$_2$/Al$_2$O$_3$	1.2 mm	–	APS	EMI SE of 30 wt% ZrB$_2$-filled Al$_2$O$_3$ ceramics was greater than 31 dB at 25 °C and 44 dB at 600 °C, along with long-term life at high temperature (600 °C for 300 h)	[124]
Thermal barrier (heat, emissivity)					
8YSZ/TBC	200 µm, 15% porosity	–	APS	8YSZ is semitransparent (weakly absorbing material) in wavelength range between 0.4 and 6 µm	[132]
8YSZ/TBC	50, 100, 200, 300 µm; 15% porosity	–	APS	Reflectance, transmittance, and absorptance measured. Inapplicable in the semitransparent spectral region of TBCs, especially between around 3.2 and 5.6 µm.	[35]
Metamaterial					
Aluminum patches onto TiAlCo	–	Metal	APS	X-band (8.2–12.4 GHz); RL values of TiAlCo coatings exceeding −10 dB in the whole frequency range of X-band when the coating thickness is 1.8 mm. Proposed absorbers insensitive to polarized EM waves because of the symmetric structure of the frequency-selective surface. TiAlCo coating can be used to design microwave absorber for wide incidence angle application.	[77]
Periodic metamaterial structural unit (of (NiCrAlY) coated on top of plasma-sprayed 80%TiC/20%Al$_2$O$_3$ coating was designed i.e., (metamaterial radar absorbing coatings)	0.96 mm	Nickel alloy	APS	0.96 mm-thick sample achieved EM RL below −5 dB at 800 °C over the whole X band	[82]
Periodic metamaterial structural unit (of (Pt, MoSi$_2$, TiB$_2$, and glass powder) coated on top of plasma-sprayed Al$_2$O$_3$ coating was designed using screen printing (i.e., metamaterial radar absorbing coatings)	1.5 mm	Superalloy	APS, screen printing (200-mesh screen printing)	EM wave absorption performance in the 8–18 GHz band at 800 °C with a thickness of 1.5 mm.	[32]
Cr$_2$O$_3$, TiO$_2$	124–755 nm; 12–17 µm	Steel, glass, ITO-coated glass, aluminum	Suspension-HVOF, APS	EM wave absorption (in the solar spectrum between 250 to 2500 nm, that is., scan range is from UV–vis–NIR light).	[218]

applications. In this example by Shao et al. (2020),[83] TiC with high ε' (real part of permittivity) and ε'' (imaginary part of permittivity) was used as the absorbent which gets dispersed in Al$_2$O$_3$ (a matrix material with low ε' and ε''). Mixture of such feedstock powders can be coupled with each other via thermal spraying, which can then help in obtaining desirable ε' and ε'', creating an enhanced EM impedance matching. As mentioned by Zikidis, Skondras, and Tokas (2014),[66] due to operational reasons, potentially using iron-based compounds (e.g., nanoparticles) as magnetic absorbers mixed can be useful

Table 3. Other potential feedstock materials to manufacture thermal spray coating with EM wave characteristics (note: for potential deposit material in the first column, the references are listed in second column, while the third and fourth column remarks are by proposed by authors).

Potential deposit materials [to enhance EM wave characteristics]	References	Remarks: EM wave characteristics	Remarks: Thermal spray processes [deployed or possible]
Semiconducting oxides (e.g., ZnO, SnO$_2$) doped with other oxides (e.g., Fe$_2$O$_3$, CeO$_2$)	[103]	Such materials can be doped with other oxides for modified photocatalytic activity (possible due to change in bandgap of the intermediate phases)	Various thermal spray (deployed)
TiO$_2$–Cu, TiO$_2$–SrCO$_3$, TiO$_2$–HA–rGO, TiO$_2$–Hβ Zeolite, TiO$_2$–HA, TiO$_2$–Fe$_3$O$_4$, ZnO	[104]	Photocatalytic materials for biocidal applications (solar light, fluorescent lamp, Xe lamp, UV lamp, simulated sunlight, white light)	Various thermal spray (deployed)
TiO$_2$ with CNTs	[150]	Such materials can also be considered to enhance photocatalytic activity	APS (deployed)
TiO$_2$ with ethylene chlorotrifluoroethylene polymer	[151]	Such materials can also be considered to enhance photocatalytic activity	Low pressure cold spraying (deployed)
TiO$_2$ with hydroxyapatite/reduced graphene	[152]	Such materials can also be considered to enhance photocatalytic activity	Flame spraying (deployed)
REEs consist of 17 elements (i.e., Scandium/Sc, Yttrium/Y, Lanthanum/La, Cerium/Ce, Praseodymium/Pr, Neodymium/Nd, Promethium/Pm, Samarium/Sm, Europium/Eu, Gadolinium/Gd, Terbium/Tb, Dysprosium/Dy, Holmium/Ho, Erbium/Er, Thulium/, Ytterbium/Yb, Lutetium/Lu)).	[155]	Doping certain REEs with known feedstock materials can improve the magnetic loss of materials and enhance the absorption of EM waves	Various thermal spray (possible)
Lanthanum/La REE (e.g., Cr$_2$O$_3$ + La$_{0.5}$Sr$_{0.5}$MnO$_3$ 40 wt%, Cr$_2$O$_3$ + Al 20 wt% + La$_{0.5}$Sr$_{0.5}$MnO$_3$ 20 wt%)	[70]	Can act as absorbers in microwave range (8–12 GHz)	APS (deployed)
An REE and a group 2 element is not oxygen, which is at least one element selected, for example, from titanium, zirconium, hafnium, vanadium, niobium, tantalum, zinc, boron, aluminum, gallium, silicon, molybdenum, tungsten, manganese, germanium, and phosphorus	[159]	Thermal spray powder that contains REE	Various thermal spray (possible)
Silver, copper, gold, aluminum, brass, bronze, tin, lead, nickel, stainless steel, mumetal (80 % Nickel, 4.5 % Molybdenum, balance Iron)	[52]	EMI shielding application	CS (possible)
Aluminum, aluminum–12silicon, NiCrAlY, Ni-20Cr, Zn, tin, copper, titanium,	[59]	EMI shielding application (possible), substrates: Polyester fabric (thermoset), glass fiber-reinforced epoxy composite (thermoset), basalt fiber-reinforced epoxy composite (thermoset), carbon fiber-reinforced epoxy (thermoset), Polyurethane (thermoplastic), quartz fiber-reinforced polyimide (thermoset), polyurethane (thermoset), Unidirectional glass fiber-reinforced epoxy composite (thermoset), carbon fiber-reinforced PEEK (thermoplastic), commercial thermoplastic blend of polycarbonate and acrylonitrile butadiene styrene, polyamide-6 (thermoplastic), polypropylene (thermoplastic), polystyrene (thermoplastic), polyvinyl chloride (thermoplastic), HDPE (thermoplastic), nylon 6 (thermoplastic), epoxy (thermoset), polyetheretherketone (thermoplastic), polytetrafluoroethylene (thermoplastic)	Flame spray, arc spray, plasma spray, CS
Metal-reinforced polymer composites; Carbon-based polymer composites; Carbon fiber-based composites; CNT-based polymer composites; Graphite-based polymer composites; Graphene-based polymer composites; Graphene oxide-based polymer composites; Graphene nanoribbon-based polymer composites; Graphene nanoplatelets-based polymer composites	[36]	EMI shielding application: Pure polymers (insulating or conducting polymer matrix) or polymer blends such as PVA, PVDF, PP, PANI, PPy, PEDOT, PS, PU, PVA/PPy, PVA/PANI, etc. loaded with one or more conductive fillers such as metals, metal oxides, and various carbon forms such as CF, CB, graphite, graphene, GO, GNP, GNR, etc., are the best candidates suitable for EMI shielding applications, which can be mainly attributed to their lightweight, noncorrosiveness, low environmental degradation, and also, commercial feasibility.	Various thermal spray (possible, potentially using low temperature thermal spray and/or CS)

ADVANCED
SCIENCE NEWS

www.advancedsciencenews.com

ADVANCED
ENGINEERING
MATERIALS

www.aem-journal.com

Table 3. Continued.

Potential deposit materials [to enhance EM wave characteristics]	References	Remarks: EM wave characteristics	Remarks: Thermal spray processes [deployed or possible]
Iron oxides, ferric oxide, magnetite, ferrous oxides (FeO) and iron hydroxide (FeOOH); Anchoring of transition metal oxides such as ZnO, ZrO_2, MnO_2, SnO_2, $BaTiO_3$, TiO_2, SiO_2 with Fe ingredient enhance the permittivity of EMI preventing materials; Conducting polymers (CPs): Polyaniline (PANI) polymer, Polypyrrole (PPy) polymer, Poly(3,4-ethylenedioxythiophene) (PEDOT) polymer, Polythiophene (PT) polymer; Nonconducting polymers nanocomposites: Polyvinylidene fluoride (PVDF) polymer, Thermosetting polymers, Elastomeric polymers, (Others (polyvinylpyrrolidone (PVP), polyvinyl chloride (PVC), poly(*p*-phenylenevinylene) (PPV), polypropylene (PP), polyvinyl butyral (PVB), polyvinyl alcohol (PVA), polyethylenimine (PEI) and polycarbonate, along with blends (PC (polycarbonate)/SAN [poly(styrene-*co*-acrylonitrile)]) and polymer composites); Carbonaceous materials: Graphite/expanded graphite, Graphene (GO, RGO), CNTs (SWCNTs, MWCNTs, CFs)	[63]	EMI shielding application: Composites comprising carbonaceous, polymer, and dielectric materials with iron components as important constituents for the prevention of EMI by reflection as well as by absorption.	Various thermal spray (possible, potentially using low temperature thermal spray and/or CS)
Polymeric composites, conducting polymer-based materials, porous materials for EMI shields, biodegradable and bioderived materials for EMI shields, high-temperature EMI shields, ceramic and cement-based EMI shields, EMI shields based on textile materials	[125]	Conventional metallic EMI shields are nowadays not preferred owing to their corroding nature, heavy weight, and processing difficulties.	Various thermal spray (possible, potentially using low temperature thermal spray and/or CS)

to enhance EM wave absorbing properties, as well as forming composites with traditional carbon material (which is an imperfect conductor) can also help enhance the absorption.

Considering strategies for feedstock material selection for enhanced photocatalytic (absorptance in visible and UV radiation range) performance, apart from TiO_2, other semiconducting oxides (e.g., ZnO, SnO_2) can be used and be doped with other oxides (e.g., Fe_2O_3, CeO_2) for modified photocatalytic activity (possible due to change in bandgap of the intermediate phases).[103] Further on, composite feedstocks of TiO_2 with CNTs for plasma spraying,[150] with ethylene chlorotrifluoroethylene polymer for low-pressure CS and[151] with hydroxyapatite/reduced graphene for flame spraying[152] can also be considered to enhance photocatalytic activity. In all such investigations, the research has been on enhancing the absorption capability of feedstock materials, which enhances the decomposition capability (e.g., to degrade NO/NO_2 pollutants, water disinfection and air purification, benzene degradation, self-cleaning of surfaces, etc.).[103] Other than TiO_2 materials, Liu et al. (2021)[104] summarized additional categories of photocatalytic materials which can be sprayed using thermal spray techniques for pathogen inactivation (e.g., TiO_2–Cu, TiO_2–$SrCO_3$, black TiO_2, TiO_2–HA–rGO, TiO_2–Hβ zeolite, TiO_2–HA, TiO_2–Fe_2O_3, ZnO) to attain visible light-induced photocatalytic activities and not as always using ultraviolet range.

During thermal spraying, the feedstock powder materials (e.g., nanostructured particles) can undergo rapid melting for the large specific surface area while the aggregated powders were heated, but not necessarily melted. The molten nanostructured particle could fill the available pores between the softened and heated aggregates, providing a layered distribution of sprayed particles. In an example, Wang et al. (2017)[95] developed WC/Co coatings (with feedstock powder materials comprised of nanometer and sub-micrometer WC particles) and compared optical properties of the sprayed multimodal and conventional coatings and demonstrated that light trapping in such multimodal coatings (due to light reflection among the multimodal WC particles) can help enhance the solar absorptance.

5.2. Carbon/polymer-Based Feedstock Material Selection

Carbon-based materials have a dramatic, breakthrough impact on magnetic devices, for space and aircraft application. It follows that electrical conductivity is a requirement for attaining proper magnetic applications such as EMI protection or enhanced EMI shielding properties; emerging trends suggest that SE can be optimized by introducing highly conductive carbon nanomaterials (carbon fibers, CNTs, graphene) and MXenes[124,126] into feedstock materials. Considering range of absorption and

EXAMPLES OF THERMALLY SPRAYED FEEDSTOCK MATERIALS USED & ELECTROMAGNETIC WAVE RANGE MAP
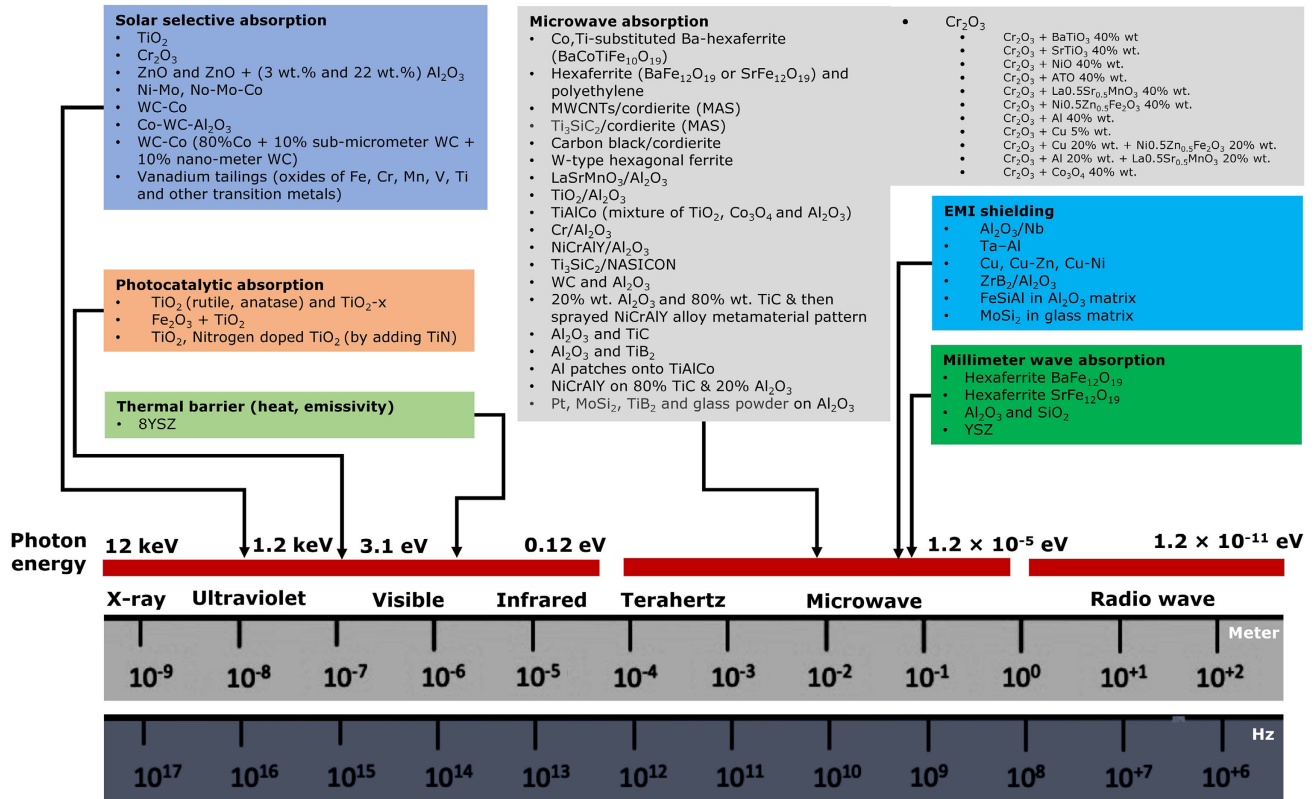
Solar selective absorption
- TiO_2
- Cr_2O_3
- ZnO and ZnO + (3 wt.% and 22 wt.%) Al_2O_3
- Ni-Mo, No-Mo-Co
- WC-Co
- Co-WC-Al_2O_3
- WC-Co (80%Co + 10% sub-micrometer WC + 10% nano-meter WC)
- Vanadium tailings (oxides of Fe, Cr, Mn, V, Ti and other transition metals)

Photocatalytic absorption
- TiO_2 (rutile, anatase) and TiO_2-x
- $Fe_2O_3 + TiO_2$
- TiO_2, Nitrogen doped TiO_2 (by adding TiN)

Thermal barrier (heat, emissivity)
- 8YSZ

Microwave absorption
- Co,Ti–substituted Ba-hexaferrite ($BaCoTiFe_{10}O_{19}$)
- Hexaferrite ($BaFe_{12}O_{19}$ or $SrFe_{12}O_{19}$) and polyethylene
- MWCNTs/cordierite (MAS)
- Ti_3SiC_2/cordierite (MAS)
- Carbon black/cordierite
- W-type hexagonal ferrite
- $LaSrMnO_3/Al_2O_3$
- TiO_2/Al_2O_3
- TiAlCo (mixture of TiO_2, Co_3O_4 and Al_2O_3)
- Cr/Al_2O_3
- $NiCrAlY/Al_2O_3$
- Ti_3SiC_2/NASICON
- WC and Al_2O_3
- 20% wt. Al_2O_3 and 80% wt. TiC & then sprayed NiCrAlY alloy metamaterial pattern
- Al_2O_3 and TiC
- Al_2O_3 and TiB_2
- Al patches onto TiAlCo
- NiCrAlY on 80% TiC & 20% Al_2O_3
- Pt, $MoSi_2$, TiB_2 and glass powder on Al_2O_3

- Cr_2O_3
  - Cr_2O_3 + $BaTiO_3$ 40% wt
  - Cr_2O_3 + $SrTiO_3$ 40% wt.
  - Cr_2O_3 + NiO 40% wt.
  - Cr_2O_3 + ATO 40% wt.
  - Cr_2O_3 + $La0.5Sr_{0.5}MnO_3$ 40% wt.
  - Cr_2O_3 + $Ni0.5Zn_{0.5}Fe_2O_4$ 40% wt.
  - Cr_2O_3 + Al 40% wt.
  - Cr_2O_3 + Cu 5% wt.
  - Cr_2O_3 + Cu 20% wt. + $Ni0.5Zn_{0.5}Fe_2O_4$ 20% wt.
  - Cr_2O_3 + Al 20% wt. + $La0.5Sr_{0.5}MnO_3$ 20% wt.
  - Cr_2O_3 + Co_3O_4 40% wt.

EMI shielding
- Al_2O_3/Nb
- Ta–Al
- Cu, Cu-Zn, Cu-Ni
- ZrB_2/Al_2O_3
- FeSiAl in Al_2O_3 matrix
- $MoSi_2$ in glass matrix

Millimeter wave absorption
- Hexaferrite $BaFe_{12}O_{19}$
- Hexaferrite $SrFe_{12}O_{19}$
- Al_2O_3 and SiO_2
- YSZ

Photon energy: 12 keV | 1.2 keV | 3.1 eV | 0.12 eV | 1.2 × 10⁻⁵ eV | 1.2 × 10⁻¹¹ eV

X-ray | Ultraviolet | Visible | Infrared | Terahertz | Microwave | Radio wave

Meter: 10^{-9} 10^{-8} 10^{-7} 10^{-6} 10^{-5} 10^{-4} 10^{-3} 10^{-2} 10^{-1} 10^{0} 10^{+1} 10^{+2}

Hz: 10^{17} 10^{16} 10^{15} 10^{14} 10^{13} 10^{12} 10^{11} 10^{10} 10^{9} 10^{8} 10^{+7} 10^{+6}

Figure 22. Mapping the thermally sprayed feedstock materials used and EM wave range.

POTENTIAL FEEDSTOCK MATERIALS FOR ENHANCED FUNCTIONAL & EMW PROPERTIES

Metal oxides, Ferrites
- Iron oxides, ferric oxide, magnetite, ferrous oxides (FeO) and iron hydroxide (FeOOH)
- Anchoring of transition metal oxides such as ZnO, ZrO_2, MnO_2, SnO_2, $BaTiO_3$, TiO_2, SiO_2 with Fe.
- Other metal oxides

Metals & metal alloys
- Al, Co, Fe, Mo, Ni, Zn, Sn, Ti, Ag, Cu, Au, Pb, Ni
- Al-12Si, MCrAlY (composed of Ni or Co or both), Ni-20Cr, brass, bronze, stainless steel, mumetal (80% Ni, 4.5% Mo, balance Iron)
- High entropy alloys ($FeCoNiCrAl$, $FeCoNiCrCuAl_{0.3}$, $FeCoNiSi_xAl_{0.4}$, $FeCoNiCrAl_{0.8}$, $FeCoNi(Si_{0.6}Al_{0.2}B_{0.2}$, Ni-NiO)
- Other metals & metal alloys

Rare earth elements
- Rare earth elements consist of 17 elements (i.e., Scandium/Sc, Yttrium/Y, Lanthanum/La, Cerium/Ce, Praseodymium/Pr, Neodymium/Nd, Promethium/Pm, Samarium/Sm, Europium/Eu, Gadolinium/Gd, Terbium/Tb, Dysprosium/Dy, Holmium/Ho, Erbium/Er, Thulium/Tm, Ytterbium/Yb, Lutetium/Lu)
- A rare earth element and a group 2 element and is not oxygen, which is at least one element, for example, from titanium, zirconium, hafnium, vanadium, niobium, tantalum, zinc, boron, aluminum, gallium, silicon, molybdenum, tungsten, manganese, germanium, and phosphorus
- Lanthanum/La rare earth element (e.g., $Cr_2O_3 + La_{0.5}Sr_{0.5}MnO_3$ 40% wt., Cr_2O_3 + Al 20% wt. + $La_{0.5}Sr_{0.5}MnO_3$ 20% wt.)
- Other material mixed with rare earth elements

Such materials can enable magnetic loss, dielectric loss, and electrical conductivity for EMI shielding application

Introduction of rare earth elements in thermally sprayed coatings can improve the magnetic loss of materials and enhance the absorption of electromagnetic waves

Anchoring of transition metal oxides with Fe ingredient can enhance the permittivity of EMI preventing materials

Semiconducting oxides materials can be doped with other oxides for modified photocatalytic activity (possible due to change in band gap of the intermediate phases)

Feedstock materials & key functions

Semiconducting oxides
- ZnO, SnO_2 doped with other oxides (e.g., Fe_2O_3, CeO_2)
- TiO_2-Cu, TiO_2-$SrCO_3$, TiO_2-HA-rGO, TiO_2-Hβ Zeolite, TiO_2-HA, TiO_2-Fe_3O_4, ZnO
- TiO_2 with carbon nanotubes
- TiO_2 with ethylene chlorotrifluoroethylene polymer
- TiO_2 with hydroxyapatite/reduced graphene
- Other semiconducting oxides

Carbides can provide higher elastic modulus, lower thermal expansion coefficient, hardness stability over wide temperature range

Ceramics can provide high hardness, high melting temperature, corrosion resistance, low density, availability

Shielding efficiency can be optimised by introducing high conductive carbon nanomaterials.

Polymeric composite has advantages (low density, noncorrosive, commercial viability) and can be reinforced with fillers such as metals, metal oxide, nanoparticles, different types of carbon materials.

Composites comprising carbonaceous, polymer and dielectric materials with iron components for the prevention of EMI by reflection as well as by absorption.

Carbon based polymers & polymeric composites
- Carbonaceous materials: Graphite/expanded graphite, Graphene (GO, RGO), CNT's (SWCNTs, MWCNTs, CFs), Graphene nanoribbon, Graphene nanoplatelets
- Metal reinforced polymer composites
- Conducting polymers (CPs): Polyaniline (PANI) polymer, Polypyrrole (PPy) polymer, Poly(3,4-ethylenedioxythiophene) (PEDOT) polymer, Polythiophene (PT) polymer
- Nonconducting polymers nanocomposites: Thermosetting polymers, Elastomeric polymers, Polyvinylidene fluoride (PVDF) polymer, Others (polyvinylpyrrolidone (PVP), polyvinyl chloride (PVC), poly(p-phenylenevinylene) (PPV), polypropylene (PP), polyvinyl butyral (PVB), polyvinyl alcohol (PVA), polyethylenimine (PEI) and polycarbonate, along with blends (PC (polycarbonate)/SAN [poly(styrene-co-acrylonitrile)]) and polymer composites)
- Carbon fiber based composites
- Other polymeric composites

Ceramics
- Aluminium oxide
- Chromium oxide
- Yttrium oxide
- Zirconium oxide

Carbides
- Chromium carbide
- Tungsten carbide
- Titanium carbide
- Other carbides

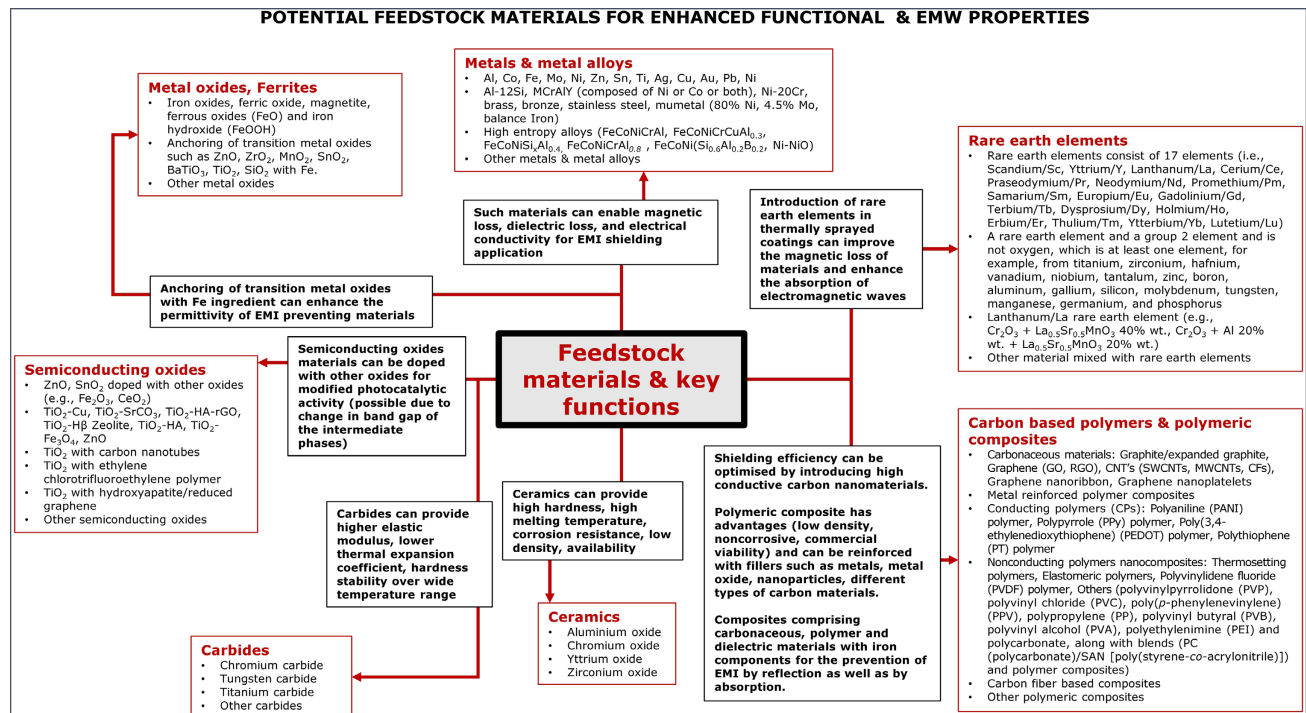**Figure 23.** Mapping potential feedstock materials (thermally sprayed) for enhanced functional and EM wave properties.

ADVANCED
SCIENCE NEWS

www.advancedsciencenews.com

ADVANCED
ENGINEERING
MATERIALS

www.aem-journal.com

shielding properties, the advantage of using WC/Co feedstock materials during thermal spraying (e.g., higher elastic modulus, lower thermal expansion coefficient, hardness stability over wide temperature range) and addition of CNTs as nanofillers (demonstrated by Venturi et al. (2021)[153]) can bring in new functionalities for future EM applications.

Basic electronic properties of semiconducting with CNT change when placed in a magnetic field. Nanotubes bandgaps are comparable with silicon and gallium arsenide which are currently the mainstays of the computer industry because their narrow bandgaps correspond with how much electricity it takes to flip a transistor from "on to off." Both doping the SWNT with cesium (Cs), potassium (K), or rubidium (Rb) and packing small bucky balls inside the SWNT produce superconductivity. With the possibility of CNTs' bandgap disappearing all together in the presence of stronger magnetic fields, they could take over the roles of silicon and gallium arsenide potentially revolutionizing the computer industry. If either the superconductivity promises of current densities of 106 A cm^{-2} or higher or the greatly improved strength of a composite material based on CNTs fibers is achieved, it can result in significant weight reduction in magnets. Therefore, the most urgent need to pursue this technology is to determine the superconducting properties of possible CNTs. That is, we need to know the feasible current density as a function of temperature, magnetic field, and strain. For example, the conduction of electricity through coiled nanotubes will generate an inductive magnetic field, an indication that coiled nanotubes, unlike straight nanotubes, are of use as EM nanotransformers or nanoswitches.

Alternative coatings solutions are polyhedral oligomeric silsesquioxanes (POSS).[154] It has been found that propargyl groups reacted in preference to methacrylate groups in Pt-catalyzed hydrosilylation, as modeled using triethylsilane. Further, tetramethacrylate cubes can be photochemically curable using visible light and free-radical initiators. For example, the cubes, when mixed with camphorquinone, cure almost instantaneously in the presence of visible light (450 nm), forming clear, hard, crosslinked materials insoluble in common solvents. In addition, both compounds cured at 100 °C without initiators to produce clear, abrasion-resistant coatings.

However, it should be noted that the presence of nanoparticles may cause agglomerates in the polymer matrix that causes an uneven material heating in response to the applied stimulus, as the region with agglomerated particles will quickly absorb much of the stimulus energy and will melt the surrounding polymer excessively or undergo pyrolysis. Therefore, mechanical and chemical dispersion techniques can be used to achieve uniform heating of the polymer in nanocomposites. To improve the nanoparticles' dispersion efficacy, it is critical to adjust the level of interaction and bonding strength between the nanoparticles and the surrounding polymer matrix. All such strategies could be considered for future generation carbon-based thermally sprayed feedstock materials for enhanced EM wave characteristics.

As summarized by Wilson, George, and Joseph (2020),[125] pure carbon-based shields are not preferred as EMI shields because of their restraint in mechanical flexibility. This opens opportunity for other categories of materials, which is typically flexible (e.g., polymeric composites) as EMI shields. Polymeric

composites have advantages, such as low density, being noncorrosive, and commercial viability. Such materials can be reinforced with one or more conductive fillers such as metals, metal oxide, nanoparticles, different types of carbon materials (carbon black, graphite, graphene, CNT, etc.), etc. While the incorporation of metallic/carbon-based materials into polymeric systems is possible in EMI shielding applications, the practical issue remains, such as a high percolation threshold and lower aspect ratios of polymers which require further research, including improvement in the dispersion state of carbon fillers in polymeric matrices and adding them at higher concentrations.

5.3. Materials Doped with Rare Earth Elements

Rare earth elements (or REEs) consist of 17 elements (i.e., Scandium/Sc, Yttrium/Y, Lanthanum/La, Cerium/Ce, Praseodymium/Pr, Neodymium/Nd, Promethium/Pm, Samarium/Sm, Europium/Eu, Gadolinium/Gd, Terbium/Tb, Dysprosium/Dy, Holmium/Ho, Erbium/Er, Thulium/, Ytterbium/Yb, Lutetium/Lu).[155] Considering EM properties of these earth elements, they can be characterized by good paramagnetism (where materials are weakly attracted by an externally applied magnetic field), saturation magnetization (i.e., an increase in applied external magnetic field H cannot increase the magnetization of the material further), large magnetocrystalline anisotropy (i.e., if it takes more energy to magnetize it in certain directions than in others), and magnetostriction (i.e., property of ferromagnetic materials which causes them to expand or contract in response to a magnetic field) because of the unique outer electronic structures.[156,157]

The introduction of REEs in thermally sprayed coatings can improve the magnetic loss of materials and enhance the absorption of EM waves. It is possible to develop feedstock thermal spray materials containing REEs (patents such as EP1167565A2;[158] WO2013047589A1;[159] US9670099B2;[160] EP1642994B8[161]). The role of REEs in thermal spray coatings has been investigated to understand the chemical, physical, mechanical, and tribological properties of coatings.[162–165] However, further enhancement in the range of properties depends on elements used in coating powder.[166]

While there are numerous examples where material has been doped with REEs using techniques other than thermal spray to improve EM wave propagation characteristics, such as chemical coprecipitation[167] or hydrothermal synthesis,[156] it is also possible that doping certain REEs during thermally sprayed coatings could also help improve the EM propagation wave characteristics of materials. In an example, Bartuli, Cipri and Valente (2008)[70] used a range of complex ceramic-based composite coatings, which included lanthanum/La REE (e.g., Cr_2O_3 + $La_{0.5}Sr_{0.5}MnO_3$ 40wt%, Cr_2O_3 + Al 20 wt% + $La_{0.5}Sr_{0.5}MnO_3$ 20wt%) fabricated by air plasma spraying to evaluate their tailored EM properties (essentially as absorbers in the microwave range (8–12 GHz)). However, thermal spraying can make REEs prone to oxidation during processing and operation, and oxidation can lead to brittle coatings and deterioration of magnetic properties.[163] Therefore, with certain microstructure formation limitations, spraying performed within a vacuum

chamber to minimize oxidation,[168] as well as application of CS, can be a way forward.[169]

5.4. Application of Suspension, Solution, or Hybrid Thermally Sprayed Coatings

As identified and proposed in various sections above, with the advancement in deposition of finely grained coatings, the powder-based thermal spraying of coatings is possible by preagglomeration of fine particles into microstructured powders.[103] This can then be followed by managing the process parameters of thermal spray to melt (or partially melt) the powder particles and preserve its fine-grained structures or use liquid feedstock (suspension, solution) to change the interaction between hot gases and feedstock in the way to enable obtaining finely grained coatings.[6,24,103,170–172] Considering some examples where suspension-based plasma spray coating has been developed by Vaßen et al. (2009),[93] Mauer, Guignard and Vaßen (2013),[111] Robinson et al. (2015),[106] and Khatibnezhad et al. (2021),[105] for photocatalytic (absorption) applications, future work may be promising in the current context, where suspension or solution spraying (SPS, SPPS) can allow convenient deposition of range of coatings to yield desirable EM wave propagation properties.

Considering the need to spray different feedstocks simultaneously, hybrid spraying is possible, where the combinations of powder with suspension, powder with solution, and suspension with solution can be deployed[24,103,173] to have desirable composite coatings and tunable EM wave propagation characteristics. The hybrid spraying can allow coarse-grade powder (from 10 to 100 μm in size) or fine powders (from 100 nm to 2 μm in size) already suspended in a suitable medium or generated in situ from a solution precursor.[24,174] Among many possibilities, hybrid spraying can offer sequential injection of powder and liquid feedstock-layered coatings (in either order) with each involving the feature of distinct length scales. This can enable fabricating layers, composite, or functionally graded coatings with a complex mix of dielectric properties (i.e., electric permittivity, magnetic permeability, and electrical conductivity), including lightweight high-performing thermomechanical properties.

5.5. Integrating Thermally Sprayed Coatings with Multicomponent Alloys

Thermal spray coatings have good inherent advantages, such as, low production cost, automated operation, high reliability and stability, and high production efficiency. Nevertheless, deficiencies in the thermally sprayed coatings include microstructure flaws, larger surface roughness, and some indiscernible reasons lead to their poor selective EM properties. Future generation components with EM interference shielding and absorption characteristics should investigate improving their EM wave propagation characteristics by fabricating composite structures while integrating thermally sprayed coatings with multicomponent alloys.

The new materials such as high-entropy alloys (HEAs) hold higher potentials to be used as EM wave shielding coating due to flexibility in tuning the composition and their elemental proportions. The multicomponent single-phase alloys, known as HEAs have five or more elements, and each element concentration is more than 5 at% and less than 35 at%.[175,176] The atomically mixed five elements show exceptional properties compared with conventional alloys due to their four core effects: 1) severe lattice distortion, 2) cocktail effect, 3) high entropy effect, and 4) sluggish diffusion effect. The high entropy and sluggish diffusion restrict the HEAs to decompose into multiphase.[176,177] However, the severe lattice distortion and cocktail impart exceptional properties. The origin of severe lattice distortion comes from the different atomic sizes of their constituent elements, and exposure to EM radiation over HEAs can change their properties. Two types of change may occur by EM radiation (i.e., high-energy particles like displacement of atoms [kinetic damage] and thermal spike due to energy deposition).[178]

As mentioned above, in the case of EM shielding, there are two phenomena required as absorption and reflection. The incident radiation can be absorbed by materials if magnetic and electric dipole interacts with the incident EM wave vectors. In the case of multielement or HEAs, materials were tested for the EM wave absorption properties.[179,180] Yang et al. (2016)[181] studied the FeCoNiCrAl alloy EM radiation absorption efficiency in the frequency range 2–18 GHz. The ball-milled prepared high-entropy-alloy materials introduced many defects during processing, and these defects act as a polarized center. This is the cause of an additional dielectric loss due to more energy required to alternate the EM field in the damaged lattice.[181] The high-entropy-alloy FeCoNiCrAl shows very less RL with different thicknesses in a wide range (2-18 GHz), as shown in **Figure 24**.

On the other hand, the special microstructure over the surface of materials enhances the absorption of the EM waves due to the enhanced surface area.[182] Lan et al. (2020)[182] described the high-entropy-alloy (FeCoNiCrCuAl$_{0.3}$) EM wave absorption phenomena on a special microstructured surface. The solid ball or particles of HEAs do not allow to enter the EM wave and maximum percentage back reflected, but the creating microstructure over the surface trapped the EM waves. The complex permittivity and permeability of each element in the alloys are close to each other, and we can tune it by adjusting the content, which allows the impedance matching. Similarly, the different magnetic and nonmagnetic contents in high-entropy-alloy materials enable it to have certain magnetic loss and dielectric loss. These phenomena make the materials for EM absorbance. The incoming wave and reflected wave can be superposed and cancel each other and this effect enhances the dissipation of the EM energy, as shown in Figure 24.[182]

Similarly, another research group examined EM wave shielding in epoxy composite with high–entropy-alloy (AlCoCrFeNi) materials and found maximum 20 dB maximum shield from microwaves.[183] There is an advantage in multicomponent that the multielement can be used to tune the properties like it can contain magnetic elements (Fe, Co, Ni) and nonmagnetic metallic elements, where strong ferroresonance materials imparting impedance mismatching leads to narrow absorption bandwidth. However, nonmagnetic materials can be used to enhance the corrosion resistance as well as impedance matching like chromium for corrosion resistance, aluminum for adjusting the impedance, and copper for the appropriate dielectric loss.
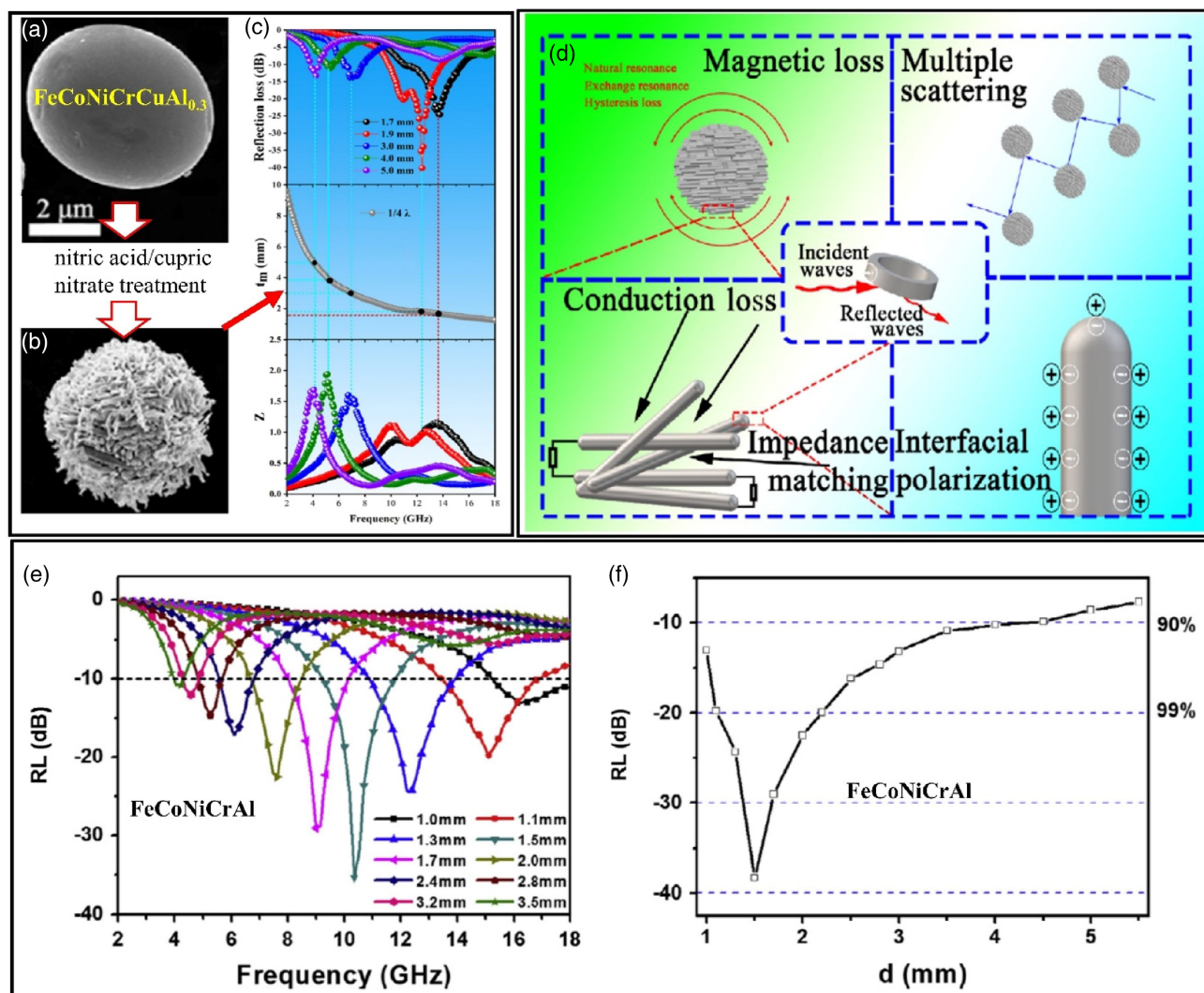
Figure 24. a) As-prepared HEA particle. b) Surface-treated HEA alloy FeCoNiCrCuAl$_{0.3}$. c) RL, thickness matching () with frequency (l/4 wavelength theory), and impedance with frequency variation. d) Mechanism of different losses on EM wave interaction with multielement alloy, (a–d) Reproduced with permission,[182] Copyright 2020, Elsevier. e) RL in FeCoNiCrAl alloy with frequency variation. f) RL at different thicknesses, (e,f) Reproduced with permission.[181] Copyright 2016, Elsevier.

Zhang et al. (2019)[184] prepared the HEA (FeCoNiSi$_x$Al$_{0.4}$) by tunning the Si atom concentration in the materials and studied the variation on microwave absorption characteristics. The addition of Si alters the crystal structure of the materials, which directly impacts the EM wave interaction behavior. The sample prepared by ball milling found that the as-cast dry-milling method is most suitable for microwave absorption because this method provides a large aspect ratio and less defect particles and dual-phase nanocrystalline and nanoglass (DPNCG). The crystalline powder behaves better for the absorption of EM waves compared with the amorphous phase powder, as shown in **Figure 25**a, b. The crystalline FeCoNiCrAl$_{0.8}$ powder of 5–15 mm exhibited minimum RL of −41.8 dB at 11.9 GHz with the thickness 2.3 mm.[185] The amorphous role has been studied by designing an HEA material FeCoNi(Si$_{0.6}$Al$_{0.2}$B$_{0.2}$) synthesized by melt-spun and subsequently ball milling. The obtained

powder looked flaky and has particle size of 2.5–32 mm (average size 14.7 mm) after 50 h of ball milling consisting of body-centred cubic and amorphous phase.[186] The longer ball milling process kept decreasing the particle size and increasing the aspect ratio. The decreasing particle size enhanced the surface area; as a result, the interfacial polarization enhanced, which is the cause of increasing complex permittivity in microwave frequency region.[180,186]

Wu et al. (2019)[187] prepared core–shell particles of HEAs as core (FeCoNiCrCuAl$_{0.3}$) and the shell as metal–oxide (Ni–NiO) for studying the dual loss. The HEA material plays a crucial role in magnetic loss and Ni–NiO shell for dielectric loss and impedance matching, as shown in Figure 25S1-S3. The HEAs as EM wave shielding materials are in the preliminary phase. Only a few articles are available and are focused on different composition studies to achieve the higher EM wave's shielding HEA materials
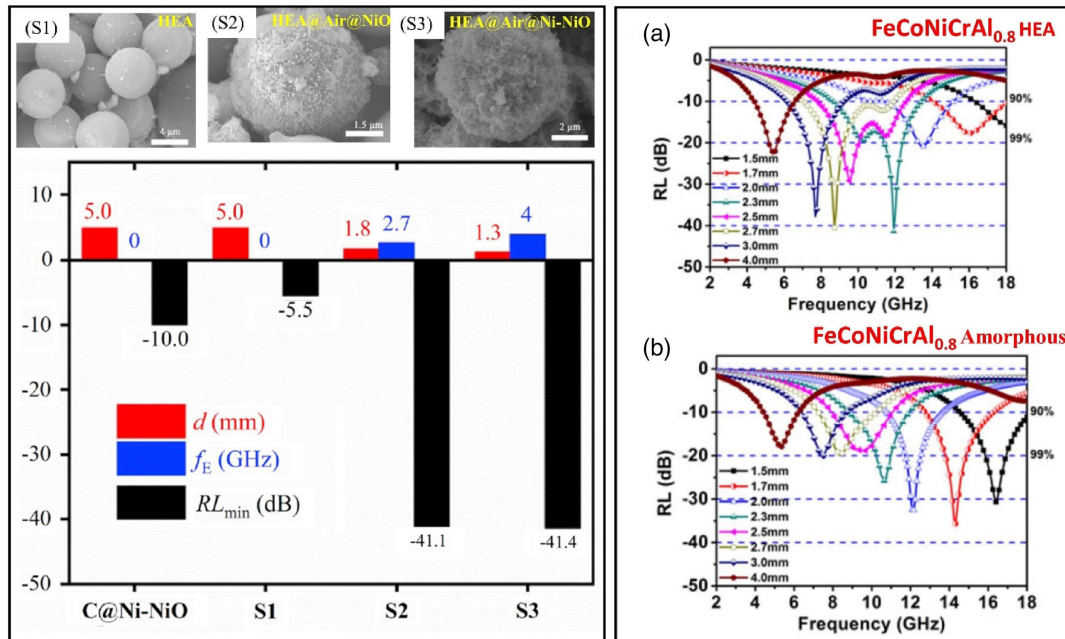
Figure 25. SEM image (S1) HEA, (S2) HEA@Air@NiO, (S3) HEA@Air@Ni-NiO; EM wave absorption by different materials (d: thickness, f_E: absorption bandwidth, RL$_{min}$: RL minimum). Reproduced with permission.[187] Copyright 2019, Elsevier, (a) and (b) RL against frequency for FeCoNiCrAl$_{0.8}$. Reproduced with permission.[185] Copyright 2016, Springer Nature.

development. The HEAs can easily be scalable to a large surface by thermal spray coating and have drawn tremendous attention by the scientific community to prepare thermal spray coating on large panels for different applications.[188]

5.6. Modeling Needs in Layered and Composite Structures

For a device with tailored EM wave propagation characteristics, modeling approach (analytical, numerical, computational) can help demonstrate or benchmark various functionalities from the predetermined properties of materials or to validate the experimental findings. Maxwell's equations can provide analytical solutions to EM wave propagation,[189] which allows us to calculate the electric field (E) and magnetic field (H) within a volume of interest, if the permeability, permittivity, and electrical conductivity of medium is known at a given angular frequency of the field. However, the range of numerical methods (e.g., finite element method [FEM], finite volume method [FVM], finite difference time domain [FDTD], and finite integration technique [FIT]) can be useful to establish EM properties from the predetermined properties of materials.[61]

As thermal spraying (on to a substrate, as shown in **Figure 26**a) is a layered structure as well as heterogenous composite layer (void, pore, microcrack), which consists of domains of multiple distinct materials or phases, analytical, numerical, and computational modeling approaches may be a cumbersome task. Such layered and heterogenous structures can have different mechanical, thermal, electrical, and dielectric properties. However, considering the possibility to control and manipulate EM wave propagations in an idealized thermal spray coating–substrate system at will opens new research areas that can lead
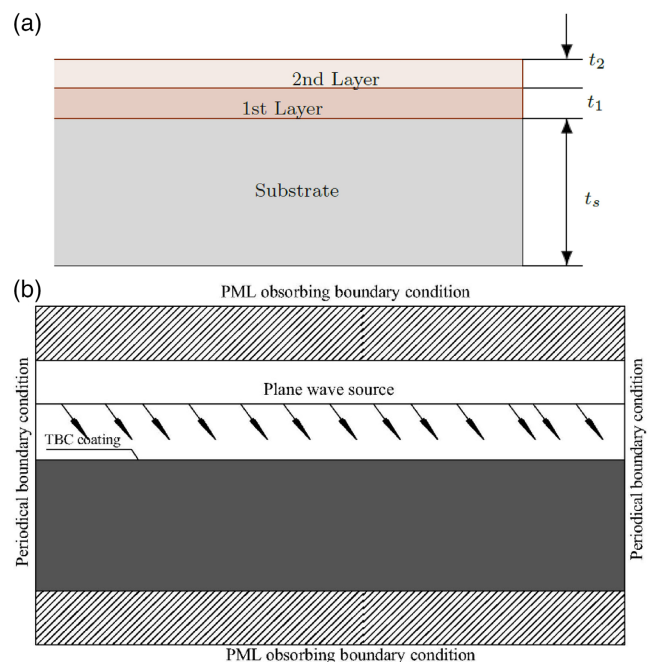
Figure 26. Thermally sprayed coating-substrate system: a) idealized multilayer structure and b) computational domain and boundary conditions used in the FDTD approach [PML: perfectly matched layer, TBC: thermal barrier coating], (b) Reproduced with permission.[132] Copyright 2014, Elsevier.

to novel applications, and this can be well understood using a modeling approach, for example, work by Zhang, Wang, and

**ADVANCED
SCIENCE NEWS**

www.advancedsciencenews.com

**ADVANCED
ENGINEERING
MATERIALS**

www.aem-journal.com

Zhao (2014),[132] where the FDTD approach was used to simulate the radiative heat transfer behaviors of TBCs with different microstructure types (Figure 26b). In such cases, simplification of the microstructures can be considered by idealizing the defects to be spherical and elliptical pores, and the porosity can be modeled by changing the number of the pores, whereas the size and shape of microstructures can be modeled by changing the ratios of the pore. While the FDTD procedure can help obtain the EM fields (H, E), the transmission/reflectance of the EM wave can be calculated, including the radiative properties of the material at various microstructure parameters (such as defect size, shape coefficient, porosity, and orientation angle).

The layered structures, as suggested by Jaber and Miehé-Brendlé (2009),[190] can be classified in different categories depending on the type of the layer: 1) neutral layers, 2) negatively charged layers with compensating cations in the interlayer space, and 3) positively charged layers with compensating anions in the interlayer space, the most common of which are the anionic clays. In the field of EMs, layered structure modeling has an important role in the study of EM wave scattering in layered media. The control of emission, propagation, and detection of the EM wave would help the design of new EM devices. The importance of the role of layered structure modeling for these different applications has created an increased use and focus on the analytical methods used to evaluate scattering in layered media in the past decades.[191–193] There are different techniques and methods for modelling the propagation of EM waves in layered structures. However, the clear understanding and modelling of the wave scattering in layered structures remain a great theoretical challenge.

The formulation of the simulation problem could be achieved with different methods and strategies using different techniques. These strategies can be classified in two main groups: direct and inverse approaches. Direct modelling methods can generally be categorized in analytical and numerical methods. They are used for different applications such as optics, radiowave propagation, and radar imaging. As an example of application, the concept of plasma–graphene-based multilayer composites was developed by Rahmanzadeh et al. (2017)[194] to design ultrabroadband radar absorbing structures. The schematic of this type of absorber including several layers is illustrated in **Figure 27**, showing the proposed graphene-plasma absorber and geometry of the multilayer structure when illuminated by oblique incidence.[194] For the direct modelling method, Lord Rayleigh originally proposed for the first time at the end of 19th century, that is, small perturbations method (SPM), for the description of wave scattering from a surface separating two media. This method was studied and enhanced in different studies.[195–197] A second approach called the "Kirchhoff approximation (KA)" was used to compute the tangential fields at the interfaces of layered structures. Bass and Fuks (1979)[196] presented an extensive discussion of this approach. The method is based on replacing the surface its tangent plane at any surface points.[198,199] It is worth mentioning that there is another analytical approach proposed by Voronovich (1994, 1999).[199,200] The method is called the small-slope approximation (SSA). It bridges the gap between two classical approaches to the problem: the method of small perturbations and KA.
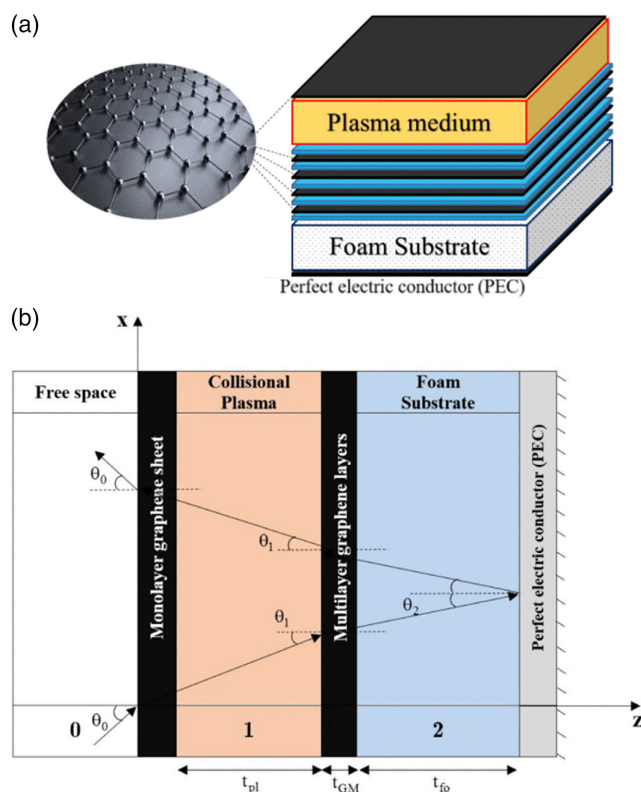

Figure 27. a) Schematic of the proposed graphene–plasma absorber and b) geometry of the multilayer structure when illuminated by an oblique incidence. Reproduced with permission.[194] Copyright 2017, IEEE.

There are also several numerical methods used to simulate the scattering of EM wave in layered structures. One of the numerical methods known by its simplicity is the method of moments (MOM). It involves equating sample moments with theoretical moments and assumes that conductors are infinitely thin and only surface currents need be modeled. The integral equation to be solved for this method and its solution can be obtained from other studies.[201,202] The main disadvantage of the MOM is the high computational cost. This can be decreased by using iterative methods. The iterative methods can be classified in two categories: 1) nonstationary methods and 2) stationary methods. The iterative methods are called nonstationary if the linear functions adaptively change at each iteration. They are called stationary in the opposite case. For the stationary methods, we can mention symmetric successive overrelaxation (SSOR)[203] and for stationary the Jacobi (or simple iteration) method.[204]

Different nonstationary methods have been applied to the rough interface scattering problem, namely, the conjugate gradient squared (CGS), biconjugate gradient-stable (BICGSTAB), quasiminimum residual (QMR), general minimal residual (GMRES), and conjugate gradient-normal equation (CGNR).[205,206] The nonstationary methods proved an ability to converge for a wider range of roughness conditions. On the other hand, it is easier to predict interface roughness conditions under which they rapidly converge with the stationary methods.

For a range of applications and to facilitate multifunctional material design, Kim and Torquato (2020)[207] established microstructure-dependent crossproperty relations for composite materials that link effective elastic and EM wave propagation characteristics to one another, including effective wave speeds and attenuation coefficients, whereas Yang et al. (2015)[208] established design and reflectivity of high-temperature wave-absorbing coatings with circular periodic structures. While there is lack of such modeling, that is, microstructure-dependent crossproperty relations for thermal spray coatings and substrate systems, similar approaches can be useful to establish crossproperty relationships in designing multifunctional thermally sprayed coatings with desirable attenuation properties for EM waves.

5.7. Low-Observable, Metamaterial, and Energy Conversion Functions of Thermal Spray Coatings

As seen throughout this review, numerous works have been done to enhance absorption and shielding of EM waves, in most cases, leading to development of low-observable (stealth) coatings. Therefore, advancement in thermal spray feedstock materials and coating processes can be critical for future generation of enhanced low-observable technology as well as solar energy conversion, photocatalytic, heat, and emissivity applications. While the specially structured coatings on to the underlying body (substrate) or using special composites or materials in underlying structures has been proven, from literature, it was observed that it is not possible to become completely stealthy but delaying the detection to lessen an opponent's ability to track the target after detection provides a major advantage to low-observable users.[209] While the material selections and coating can also increase the weight, cost, and the maintenance requirements, applications of simple coating materials can usually be effective only in narrowband and in limited spatial regions. There have also been suggestions for developing environmentally compliant low-observable coating materials that can facilitate rapid material removal, repair, and biodegradability, including avoiding any legal scrutiny with improved stealth capability and durability.[210,211]

Meanwhile, thermal spraying onto polymer-based flexible structures is possible.[59] However, future directions could be looking into modelling of EM wave propagation and developing an absorbing material that can not only dissipate EM energy but
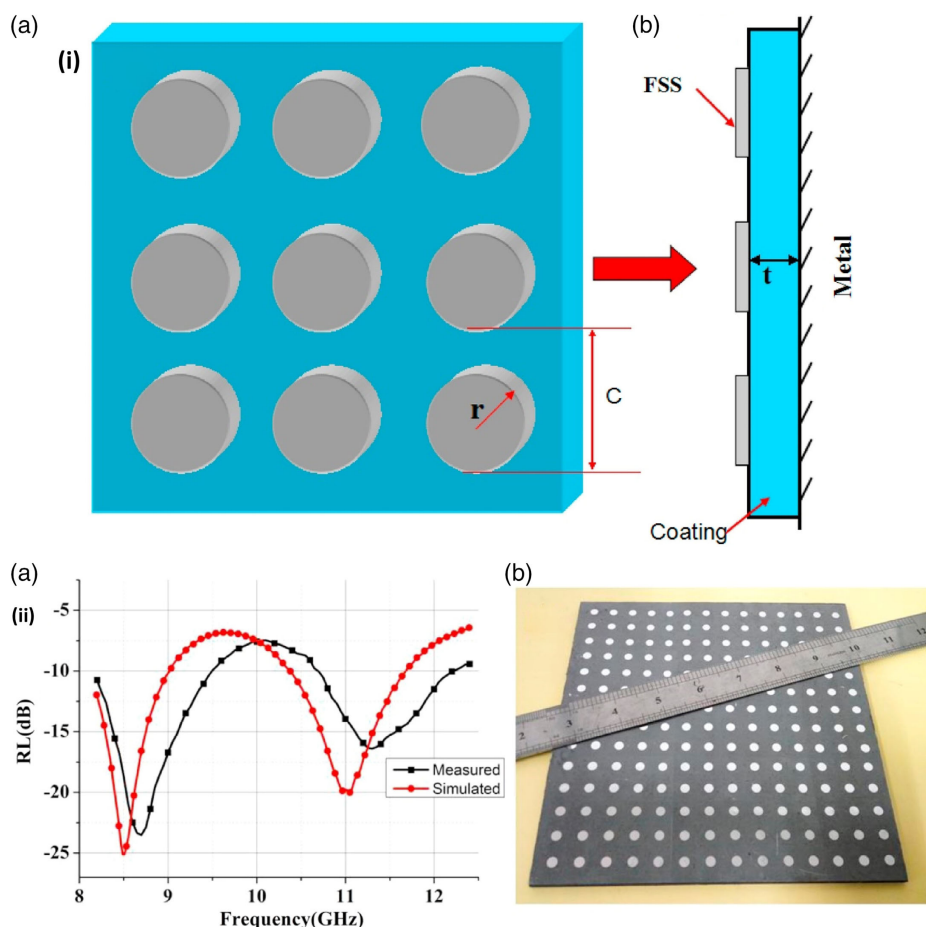

Figure 28. Metamaterial: i) a,b) Structure of radar-absorbing material showing top and side view which includes circular aluminum patches, where *c* is the period of the absorber, *a* is the radius of the patch unit, *t* is the APS-sprayed TiAlCo coating onto metal substrate. ii) (a,b) Measured and simulated reflectivity versus frequency and sample. Reproduced with permission.[77] Copyright 2016, Elsevier.

ADVANCED
SCIENCE NEWS
www.advancedsciencenews.com

ADVANCED
ENGINEERING
MATERIALS
www.aem-journal.com

also convert the generated heat into electricity to realize a self-powering function,[212] as well as artificially periodic structured digital and programmable smart metamaterials to obtain unusual negative refraction, perfect lensing, and superlensing.[213] Such coatings can be attractive for applications, such as controlling the antenna radiation beams and reducing the scattering features of targets, in the range of frequencies. As shown in **Figure 28**, metamaterials are artificial materials that are tailored to exhibit unique properties such as negative refractive index which are not readily available in the naturally available materials.[2,214,215] Negative-index metamaterials (NIMs)[214] were first demonstrated by Veselago (1968)[216] for microwave frequencies, but since then it has been challenging to design NIMs for other frequencies (e.g., optical) and they have so far been limited to optically thin samples because of significant fabrication challenges and strong energy dissipation in metals.[217] However, metamaterials fabrication using thermal spray techniques are poised to make a huge impact primarily because they can shape EM radiations in ways like other materials and methods or better, as demonstrated in some of the pioneering work.[77,82,218,219] The thermal spray coating technique can be

a viable method to design surface structures to synthesize newer category of metamaterials. It may be noted that metamaterials gain their properties not from their composition, but from engineered and designed artificial structures.[220] Structural building blocks (particle shape, geometry, size, orientation, and arrangement) during thermal spraying of a chosen metamaterial can affect the EM waves in an unconventional manner, thereby creating material (surface) properties which are unachievable using conventional processes. It is anticipated that thermally sprayed metamaterial coating layers can achieve desired effects by incorporating structural elements of subwavelength sizes, that is, features that are smaller than the wavelength of the waves they affect.

EM wave energy conversion is important in many applications, such as energy harvesting, signal detection, nonlinear optics, etc., and with the application of the energy conversion adapter, it can achieve signal transfer between EM energy into various forms of energy, such as, thermal, DC electric, or higher harmonic EM wave energy.[221] **Figure 29** shows the schematic of the conceptual coating design with functional layers and structures, which can be considered for related applications. EM wave
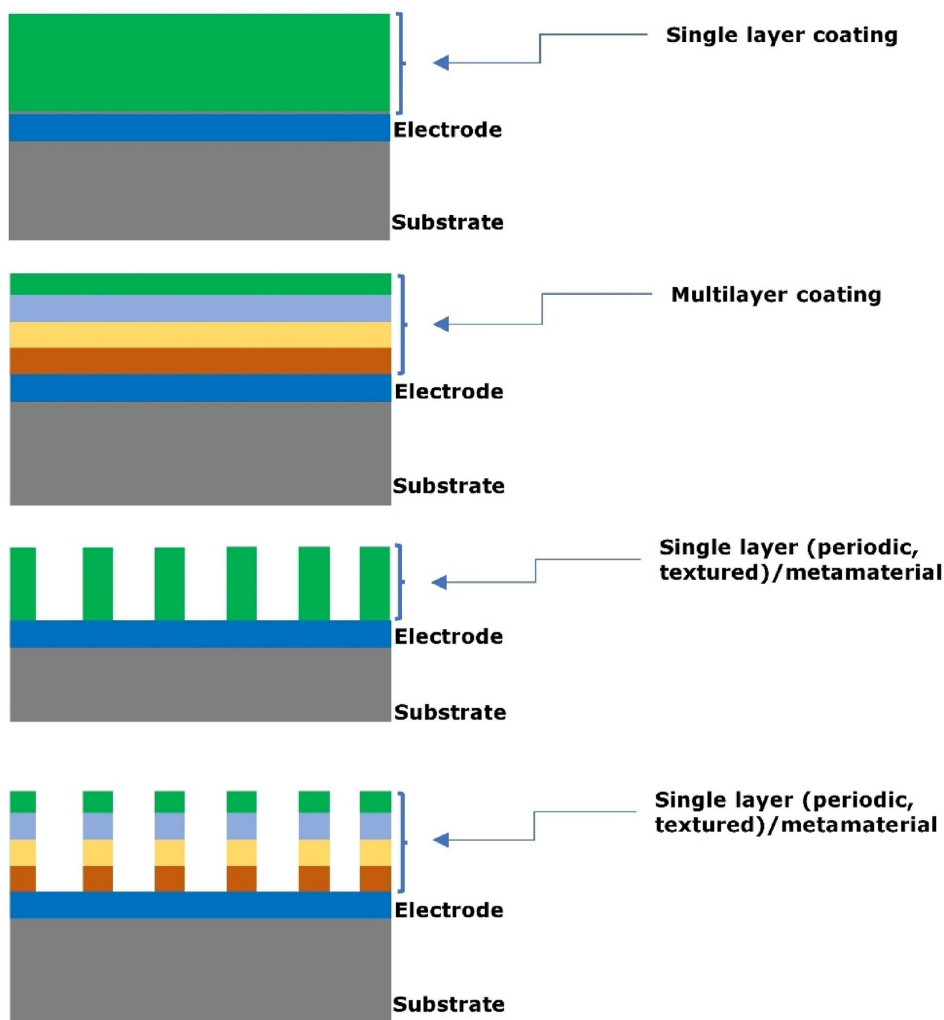

Figure 29. Schematic of the coating design with functional layers and structures.

absorption can bring energy into a coating–substrate system due to their fields within their waves, and smart coating design with functional layers and structures can be an area of interest. Through absorption of the EM wave (dissipated by dielectric loss and magnetic loss[68,69] by the coating–substrate system), we can consider that the energy contained in the coating (of an optimal thickness and cross-sectional area that passes through the cross-sectional plane in time interval) can help determine calculating the energy flux (i.e., energy per unit area per unit time). The energy flux can as well depend on the orientation of the coated surface with the incident EM wave. With the variation in frequency of the EM wave, the energy flux quantity can rapidly vary. Potentially, designing the coatings as metamaterial absorber and confining EM wave within subwavelength structures (of optimal geometry and materials) can help demonstrate enhancing energy conversion from the coating–substrate system.

Despite the potential benefits that thermal spray processing can offer in low-observable, metamaterial, and energy conversion technology, significant challenges remain in the development of thermal spray processing in comparison with other methods. The thermal spray processing must be controlled to ensure that the deposited phases have the desired crystalline structure, avoiding delamination, amorphous structure, and impurities' contamination during thermal spray processing. Typical in-plane splat orientation, although beneficial for some applications, optimized control of substrate heating, and cooling can minimize the effect of thermal stresses during the deposition process. While cost and performance coatings remain major barriers to their widespread use, thermal spray processing has the potential to drastically reduce these barriers by rapidly increasing production rates and reducing capital equipment, materials, and overall system cost. It also offers the potential to increase performance using graded composition and microstructures. Nanostructured composite powders (e.g., hollow and yolk-shelled nanostructures)[222] can also be of considerable interest for use in such applications due to their potential to increase the surface area, thereby improving the desirable EM wave propagation performance. As an example, some hollow and yolk-shelled nanostructures as feedstock materials could enhance absorption performances compared with the solid counterparts. Enhanced absorption performances of yolk-shelled structures are possible as additional free space in the interior compared with their corresponding solid ones could lead to their better impedance matching characteristics. With low mass density and larger specific surface area, the yolk-shelled structures could reduce filler ratio in the matrix and facilitate construction of lightweight coating as absorbers. It could also possess rich interfaces, which can increase the interfacial polarization loss. Various hollow and yolk-shelled nanostructures have been reported for EM absorption (e.g., Fe_3O_4/hollow carbon microspheres, CoO@Co yolk-shelled NPs on graphene sheets, Fe_3O_4/C nanorings, Fe@air@Co, nitrogen-doped CNTs using $Ni(OH)_2$@SiO_2 core-shelled spheres).[222–226]

5.8. Dielectric Properties Measurements

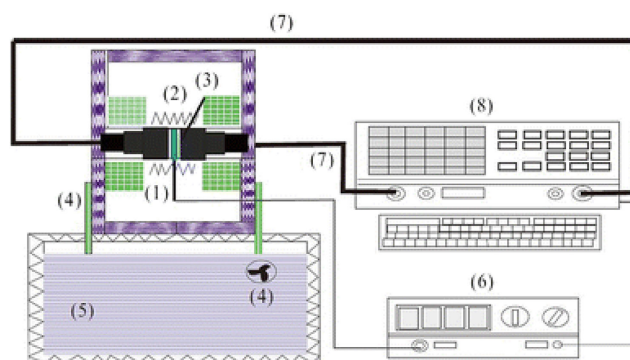For thermally sprayed coating–substrate systems, investigation of EM properties (i.e., electric permittivity, magnetic

Figure 30. Schematic of apparatus to measure the complex permittivity coatings from 25 to 700 °C temperature using coaxial line method in the frequency range of 8.2–12.4 GHz. Reproduced with permission.[227] Copyright 2015, Springer Nature. 1) thermocouple, 2) heater, 3) sample, 4) circulating water cooling system, 5) flume tank, 6) temperature controller, 7) coaxial cable, 8) vector network analyzer).

permeability) of the coating layer require special consideration unlike bulk materials. This means that coating needs to be detached from the substrate so that standalone coating properties can be investigated. Due to high strain rate during impact of sprayed particles during thermal spraying, the splats can form a strong mechanical bond at the interface with the substrate. Removal of such coatings from the substrate can be a challenge. Therefore, to mitigate this, as listed in Table 2, most investigators used graphite as substrate material (as it can be easy to remove from the thick coatings) to overlay the thermally sprayed layer but mainly for microwave absorption applications[73–75,77,82] and EM interference application.[120–122] As an example (shown in **Figure 30**), the dielectric parameters of plasma sprayed Ti_3SiC_2/cordierite coatings can be determined by network analyzer (e.g., using Agilent Technologies E8362B) using coaxial line method measured at this temperature (at 25–700 °C) test setup.[227] In this example, the Ti_3SiC_2/cordierite coating was sprayed on a graphite substrate and then mechanically removed from the substrate to carry dielectric measurements. For other applications (mainly solar-selective absorption, photocatalytic absorption, thermal barrier (heat, emissivity)), the substrate selection such as metals, alloys, ceramic, or glass, etc. (depending upon various requirements) may be appropriate as the EM wave propagation, namely, absorption, reflection, or transmission can be investigated using optical spectroscopy techniques without removal of substrate. The selections of measuring equipment and sample holder design (an important aspect) depend upon the dielectric materials to be measured, and for thermally sprayed coating, special considerations may be needed if testing is needed under various environmental conditions (e.g., effect of temperature, debris, water droplets, ice, etc.). However, in all cases, the dielectric properties' measurement needs to be accurate, repeatable, reliable, and verifiable, as such materials are finding increasing application for use in various applications and industries.[228]

5.9. Environmental and Economic Factors in Absorbing EM Waves

While the demand for thermally sprayed coatings is growing, energy consumption for large-scale coating production (leading

**ADVANCED
SCIENCE NEWS**
www.advancedsciencenews.com

**ADVANCED
ENGINEERING
MATERIALS**
www.aem-journal.com

to carbon emission and environmental impact) must be a concern for all parties.

As mentioned above, the global market size for thermal spray coating is projected to reach 10.7 billion USD with a CAGR of 6.4% expected in the next 2-year time.[229] The market segment covers mainly applications in sectors such as gas turbines, aerospace, automotive, energy and power, healthcare devices, electronics, oil and gas, and forestry.[230] There is no further segmentation or market share data available for EM wave tapping applications using thermally sprayed materials (e.g., absorption, solar, photocatalytic, heat, emissivity, interference shielding, etc.), but it is expected to grow, considering a similar sector-wise trend over the next many years.

Despite many researchers arguing that thermal spray coating is a cost-effective manufacturing technique,,[70,231,232] broadly, it is still quite a challenge for this technology to compete with the other cheaper techniques available in the market[233] mainly due to sophisticated devices involved in thermal spray techniques. This view is also shared by Wijewardane (2015)[234] who indicated that there is still a challenge in producing a cost-effective plasma thermal spray coating, for example, for photovoltaic applications. Fauchais (2015)[233] however argued that the cost could be further reduced in the future through the advancement of the overall thermal spray sector (i.e., simple, less sophisticated, cost-effective, low maintenance, no special treatment or storage, and robust technologies). Ke et al. (2018)[96] already indicated that thermal spray offers a much lower cost solar thermal system than the conventional ones.

As can be seen through the samples of literature on the application of thermal spray coatings for specialized EM wave propagation characteristics (e.g., absorption, solar, photocatalytic, heat, emissivity, interference shielding, etc.), the methods and protocols are well in place and established for research and commercial use. While such coatings can also help shield environmental EM wave pollutions, the usage of harmful feedstock materials during fabrication and long exposure to such materials might raise some issue, as it can be health hazard and damage the environment during the manufacturing and disposal of materials. For future success, the application of such techniques must also be cost-effective, with minimal or no carbon emission, potentially with little or zero pollution. As seen above, many improvements in efficiency of coated structures have been made (in absorption, solar, photocatalytic, heat, emissivity, interference shielding) and further considerations are still necessary to quantify their socioeconomic benefits for specific markets and applications.

6. Concluding Remarks and Future Directions

This review indicates that range of specialized feedstock materials and thermal/CS coating techniques can play a key role in providing a scalable route to current- and next-generation surface manufacturing of EM devices. Noteworthy, unlike other deposition techniques, thermal spray techniques may not suffer from limited build volume, low throughput speed, problems in scalability, and high manufacturing cost. While thermal spray deposition techniques have their limitations, the choice of fabrication method can be a critical choice that dictates the resolution,

material, and working frequency of the resultant materials or structures. Also, to meet the specifications of current and future EM devices, improved or new components based on selected dielectric materials and new surface designs are required. Looking into the feedstock materials used, potential feedstock materials not used but can be easily used, and other category of materials that is wide open to use (from metals, metal alloys, metal oxides and ferrites, semiconducting oxides, carbides, ceramics, cermets, REE, carbon-based polymers, polymeric composites, etc., including their doped design with hollow and yolk-shelled nanostructure types) can also be of considerable interest for use in such applications due to their potential to increase in the surface area, thereby improving the desirable EM wave propagation performance. The possibilities to have very diverse and broad EM properties of future-generation devices in this domain is immense. What is needed is a mix of fabrication resources (including thermal spray techniques) to manufacture artificial surface structures (e.g., full coating or periodic/textured coating, leading to the formation of metamaterial). This can be necessary as different materials need different processing techniques and processing conditions to engineer the surface.

In this article, various thermal spray techniques and fabrication strategies to develop coatings with nonionizing EM wave propagation characteristics (i.e., absorption, solar, photocatalytic, heat, emissivity, and interference shielding) have been critically reviewed. This review presents fabrication of thermally sprayed coatings (single or multiple layers, planar structures), which can change propagation characteristics of EM waves. Selections of feedstock, substrate materials, and deposition techniques have led to the identification of numerous (most suitable) class of materials to be used to produce coatings. The current ability of thermal spray techniques to utilize feedstock in the form of powders, suspensions, or solution precursors makes it immensely versatile, not only to deposit a wide array of material chemistries but also to create unique microstructures. Consequently, the technology has considerable potential to be successful in modifying the absorption, reflection, and transmission of EM waves, and it is assessed that such coatings with certain EM wave propagation characteristics depend on the wavelength in the spectrum that may be useful in many applications.

The fabricated coating microstructures can make changes to EM waves using the functionalities that arise from such artificial surface structures (e.g., full coating or periodic/textured coating leading to the formation of metamaterials), potentially as shields from radiofrequency and EM fields, reducing radar signatures to be opaque to hostile radar, absorbing solar radiation to convert to electricity, enhancing decomposition of organic pollutants or to mitigate the environmental impact, as thermal barrier to turbine components, and to induce semitransparency at optical frequencies, as well as protecting heat-sensitive substrates or antennas. Focus was given to materials' microstructural features in coatings produced using conventional thermal spray techniques as well as those produced using modern techniques (e.g., suspension and solution precursor) and how high entropy alloying can easily be scalable to a large surface by thermal spray coating.

Considerable research is needed to analyze (to enhance) the EM wave propagation characteristics of materials to respond to wide-frequency ranges. This could require multiple materials'

fabrication approach to block EM radiations at different broad frequency ranges. Further advances in the application of thermal spray coating techniques could be surged by considering the usage of the range of feedstock composite and hybrid materials to achieve EM distinctiveness of materials. Additionally, the fabrication of coatings with functionally gradient and hybrid properties is quite possible to tune to certain EM wave propagation characteristics. The substrates to deposit thermally sprayed coatings varied for EM wave propagation applications (such as metals, alloys, glass, ceramics, and graphite, etc.). However, the previous approach did not consider the advantage of thermoplastic or polymer science to have a lightweight substrate structure. It is expected that the selection of lightweight substrates can potentially become future norms in the thermal spray industry with some degree of limitations.

Most applications for nonionizing EM wave interference (e.g., protection of electronic equipment, scientific and medical devices, etc. against EM noise) require metallic substrates, and thermal spray coatings are typically sprayed on metallic substrates. As presented above, layered system fabrication using thermal spray techniques can be advantageous in the application of EM materials where the coating priority and hence the coating architecture can be purposefully built in during coating deposition. These cannot be easily possible when deploying other techniques (e.g., tape casting, doctor blade, sol gel, or physical or chemical vapor deposition). Hence thermal spray coating processes combined with the choice of coating material(s) and spray parameters provide higher deposition rate and a cost-effective design tool as a large-scale manufacturing route to EM materials and metamaterials.

The most crucial point is that the thermal spray coating method is industrially viable, which makes it promising to be applied to the large-scale as well as large length-scale applications. Such strategies could also help fabrication of components with key attributes such as high strength, high flexibility, lightweight, noncorrosiveness, high thermal and electrical conductivity, low environmental degradation, and cost-effective commercial feasibility. Along with microstructural features, pore surface area and size, composition, spray particle size, and bandgap energies, further experimental, modeling, as well as data-driven (machine learning) work would be required to analyze the range of dielectric constant, magnetic permeability, and electrical conductivity of coating materials, to prove if (and how) the electromagnetic wave propagation characteristics are governed by dielectric loss or the magnetic loss.

Conflict of Interest

The authors declare no conflict of interest.

[1] C. Van Der Wyck, *Nature* **1936**, *137*, 1072.
[2] C. M. Watts, X. Liu, W. J. Padilla, *Adv. Mater.* **2012**, *24*, OP98-OP120.
[3] A. Ishimaru, in *Electromagnetic Wave Propagation, Radiation, and Scattering: From Fundamentals to Applications*, Wiley, Hoboken, NJ **2017**.
[4] L. Pawlowski, in *The Science and Engineering of Thermal Spray Coatings*, Wiley, Chichester, England **1995**.
[5] D. Tejero-Martin, M. Rezvani Rad, A. McDonald, T. Hussain, *J. Therm. Spray Technol.* **2019**, *28*, 598.
[6] M. Aghasibeig, F. Tarasi, R. S. Lima, A. Dolatabadi, C. Moreau, *J. Therm. Spray Technol.* **2019**, *28*, 1579.
[7] M. Tului, F. Arezzo, L. Pawlowski, *Surf. Coat. Technol.* **2004**, *179*, 47.
[8] S. Geetha, K. K. S. Kumar, C. R. Rao, M. Vijayan, D. C. Trivedi, *J. Appl. Polym. Sci.* **2009**, *112*, 2073.
[9] R. Ahmed, O. Ali, C. C. Berndt, A. Fardan, *J. Therm. Spray Technol.* **2021**, *30*, 800.
[10] K. Bobzin, W. Wietheger, M. A. Knoch, *J. Therm. Spray Technol.* **2021**, *30*, 157.
[11] A. S. M. Ang, C. C. Berndt, *Int. Mater. Rev.* **2014**, *59*, 179.
[12] R. Ahmed, N. H. Faisal, A. M. Paradowska, M. E. Fitzpatrick, K. A. Khor, *J. Mech. Behav. Biomed. Mater.* **2011**, *4*, 2043.
[13] R. B. Heimann, *J. Therm. Spray Technol.* **2016**, *25*, 827.
[14] A. S. M. Ang, N. Sanpo, M. L. Sesso, S. Y. Kim, C. C. Berndt, *J. Therm. Spray Technol.* **2013**, *22*, 1170.
[15] M. Bégard, K. Bobzin, G. Bolelli, A. Hujanen, P. Lintunen, D. Lisjak, S. Gyergyek, L. Lusvarghi, M. Pasquale, K. Richardt, T. Schläfer, T. Varis, *Surf. Coat. Technol.* **2009**, *203*, 3312.
[16] D. Lisjak, P. Lintunen, A. Hujanen, T. Varis, G. Bolelli, L. Lusvarghi, M. Jagodič, M. Drofenik, *Mater. Lett.* **2011**, *65*, 534.
[17] R. Ahmed, N. H. Faisal, A. M. Paradowska, M. Fitzpatrick, *J. Therm. Spray Technol.* **2012**, *21*, 23.
[18] P. Fauchais, R. Etchart-Salas, V. Rat, J. F. Coudert, N. Caron, K. Wittmann-Ténèze, *J. Therm. Spray Technol.* **2008**, *17*, 31.
[19] J. Karthikeyan, C. C. Berndt, S. Reddy, J.-Y. Wang, A. H. King, H. Herman, *J. Am. Ceram. Soc.* **2005**, *81*, 121.
[20] L. Pawlowski, *Surf. Coat. Technol.* **2009**, *203*, 2807.
[21] Y. Qiao, T. E. Fischer, A. Dent, *Surf. Coat. Technol.* **2003**, *172*, 24.
[22] R. S. Lima, B. R. Marple, *J. Therm. Spray Technol.* **2007**, *16*, 40.
[23] P. Fauchais, A. Joulia, S. Goutier, C. Chazelas, M. Vardelle, A. Vardelle, S. Rossignol, *J. Phys. D: Appl. Phys.* **2013**, *46*, 224015.

[24] S. Joshi, N. Markocsan, P. Nylén, G. Sivakumar, in *Handbook of Advanced Ceramics and Composites* (Eds: Y. Mahajan, J. Roy), Springer, Cham **2020**, pp. 1–42.

[25] S. Govindarajan, R. O. Dusane, S. V. Joshi, *J. Eur. Ceram. Soc.* **2011**, *94*, 4191.

[26] A. Ganvir, R. Filomena, N. Markocsan, N. Curry, S. Joshi, *J. Eur. Ceram. Soc.* **2019**, *39* 470.

[27] S. Mahade, K. Narayan, S. Govindarajan, S. Björklund, N. Curry, S. Joshi, *Materials* **2019**, *12*, 2344.

[28] S. Björklund, S. Goel, S. Joshi, *Mater. Des.* **2018**, *142*, 56.

[29] S. Sampath, *J. Therm. Spray Technol.* **2010**, *19*, 921.

[30] H. Herman, S. Sampath, in *Metallurgical and Ceramic Protective Coatings* (Ed: K. H. Stern), Springer, Dordrecht **1996**, pp. 261–289.

[31] N. H. Faisal, R. Ahmed, S. P. Katikaneni, S. Souentie, M. F. A. Goosen, *J. Therm. Spray Technol.* **2015**, *24*, 1415.

[32] S. Zhao, H. Ma, T. Shao, J. Wang, L. Zhang, S. Sui, M. Feng, J. Wang, S. Qu, *Ceram. Int.* **2021**, *47*, 17337.

[33] A. Fardan, C. C. Berndt, R. Ahmed, *Surf. Coat. Technol.* **2021**, *409*, 126835.

[34] K. Bobzin, N. Bagcivan, D. Parkot, I. Petković, *J. Therm. Spray Technol.* **2009**, *18*, 975.

[35] B. X. Wang, C. Y. Zhao, *Int. J. Heat Mass Transfer* **2015**, *89*, 920.

[36] S. Sankaran, K. Deshmukh, M. B. Ahamed, S. K. K. Pasha, *Composit. Part A: Appl. Sci. Manufact.* **2018**, *114*, 49.

[37] C. M. Watts, X. L. Liu, W. J. Padilla, *Adv. Mater.* **2012**, *24*, OP98-OP120.

[38] S. Schlamminger, D. Haddad, F. Seifert, L. S. Chao, D. B. Newell, R. Liu, R. L. Steiner, J. R. Pratt, *Metrologia* **2014**, *51*, S15.

[39] T. H. Wendell in *Applied Physics*, Wiley-VCH, Hoboken, NJ **2003**.

[40] Keysight Technologies, *Featured Resources for N1500A Materials Measurement Suite*, https://www.keysight.com/gb/en/support/N1500A/materials-measurement-suite.html (accessed: June 2021).

[41] *ASTM D150-18, Standard Test Methods for AC Loss Characteristics and Permittivity (Dielectric Constant) of Solid Electrical Insulation*, ASTM International, West Conshohocken, PA **2018**.

[42] *ASTM D2520-13, Standard Test Methods for Complex Permittivity (Dielectric Constant) of Solid Electrical Insulating Materials at Microwave Frequencies and Temperatures to 1650°C*, ASTM International, West Conshohocken, PA **2013**.

[43] *ASTM D924-15, Standard Test Method for Dissipation Factor (or Power Factor) and Relative Permittivity (Dielectric Constant) of Electrical Insulating Liquids*, ASTM International, West Conshohocken, PA **2015**.

[44] *ASTM D149-20, Standard Test Method for Dielectric Breakdown Voltage and Dielectric Strength of Solid Electrical Insulating Materials at Commercial Power Frequencies*, ASTM International, West Conshohocken, PA **2020**.

[45] C. O. Mgbemena, D. Li, M.-F. Lin, P. D. Liddel, K. B. Katnam, V. K. Thakur, H. Y. Nezhad, *Composit. Part A: Appl. Sci. Manufact.* **2018**, *115*, 88.

[46] R. H. Bube, R. H. Bube, in *Electrons in Solids* 3rd ed., Academic Press, Cambridge, MA **1992**, pp. 107–130, Ch. 7.

[47] F. Casula, G. Mula, *Encyclopedia of Condensed Matter Physics* (Eds: F. Bassani, G. L. Liedl, P. Wyder), Elsevier, Amsterdam **2005**, pp. 374–380.

[48] L. Baoyi, D. Yuping, Z. Yuefang, L. Shunhua, *Mater. Des.* **2011**, *32*, 3017.

[49] S. M. Abbas, A. K. Dixit, R. Chatterjee, T. C. Goel, *Mater. Sci. Eng. B* **2005**, *123*, 167.

[50] A. Alexopoulos, *Phys. Lett. A* **2009**, *373*, 3190.

[51] G. Videen, P. Chylek, *Opt. Commun.* **1998**, *158*, 1.

[52] D. D. L. Chung, *J. Mater. Eng. Perform.* **2000**, *9*, 350.

[53] P. C. Kim, D. G. Lee, *Compos. Struct.* **2009**, *87*, 161.

[54] I. W. Nam, H. K. Lee, J. H. Jang, *Compos. Part A: Appl. Sci. Manufact.* **2011**, *42*, 1110.

[55] A. K. Singh, A. Shishkin, T. Koppel, N. Gupta, *Compos. Part B: Eng.* **2018**, *149*, 188.

[56] L. H. Hemming, Institute of Electrical and Electronics Engineers, New York **1992**.

[57] D. M. Pozar, in *Microwave Engineering*, John Wiley and Sons, Inc., Danvers **2005**.

[58] L. H. Hemming, *Architectural Electromagnetic Shielding Handbook: A Design and Specification Guide*, Institute of Electrical and Electronics Engineers, New York **1992**.

[59] R. Gonzalez, H. Ashrafizadeh, A. Lopera, P. Mertiny, A. McDonald, *J. Therm. Spray Technol.* **2016**, *25*, 897.

[60] S. H. Kwon, H. K. Lee, *Comput. Mater. Contin.* **2009**, *12*, 197.

[61] L. Anderson, P. Govindaraj, A. Ang, A. Mirabedini, N. Hameed, *Carbon Trends* **2021**, 100047.

[62] *ASTM D4935-18, Standard Test Method for Measuring the Electromagnetic Shielding Effectiveness of Planar Materials*, ASTM International, West Conshohocken, PA, **2018**.

[63] V. Shukla, *Nanoscale Adv.* **2019**, *1*, 1640.

[64] M. Ohring, L. Kasprzak, in *Reliability and Failure of Electronic Materials and Devices* 2nd Ed., (Eds: M. Ohring, L. Kasprzak), Academic Press, Cambridge, MA **2015**, pp. 39–109, Ch. 2.

[65] C. Cook, in *Radar Signals: An Introduction to Theory and Application*, 1st edn., Academic Press, Cambridge, MA **1967**, p. 550.

[66] K. Zikidis, A. Skondras, C. Tokas, *J. Comput. Modell.* **2014**, *4*, 129..

[67] D. K. Setua, B. Mordina, A. K. Srivastava, D. Roy, N. E. Prasad, in *Micro and Nano Technologies, Fiber-Reinforced Nanocomposites: Fundamentals and Applications*, (Eds: B. Han, S. Sharma, T. A. Nguyen, L. Longbiao, K. S. Bhat), Elsevier, Amsterdam **2020**, pp. 395-430, Ch. 18.

[68] F. Qin, H. X. Peng, *Progr. Mater. Sci.* **2013**, *58*, 183.

[69] X. Zhao, Z. Zhang, L. Wang, K. Xi, Q. Cao, D. Wang, Y. Yang, Y. Du, *Sci. Rep.* **2013**, *3*, 3421.

[70] C. Bartuli, F. Cipri, T. Valente, *Inorg. Chim. Acta* **2008**, *361*, 4077.

[71] J. Su, W. Zhou, Y. Liu, F. Luo, D. Zhu, *J. Therm. Spray Technol.* **2014**, *23*, 1065.

[72] J. Su, W. Zhou, Y. Liu, Y. Qing, F. Luo, D. Zhu, *Surf. Coat. Technol.* **2015**, *270*, 39.

[73] J. Su, W. Zhou, Y. Liu, Y. Qing, F. Luo, D. Zhu, *J. Therm. Spray Technol.* **2015**, *24*, 826.

[74] S. Wei, Y. Liu, H. Tian, H. Tong, Y. Liu, B. Xu, *J. Magn. Magn. Mater.* **2015**, *377*, 419.

[75] Z. Yang, F. Luo, J. Xu, W. Zhou, D. Zhu, *J. Alloys Compd.* **2016**, *662*, 607.

[76] Z. Yang, F. Luo, Y. Hu, S. Duan, D. Zhu, W. Zhou, *J. Alloys Compd.* **2016**, *678*, 527.

[77] Z. Yang, F. Luo, Y. Hu, D. Zhu, W. Zhou, *Ceram. Int.* **2016**, *42*, 8525.

[78] L. Zhou, Y. Dong, Z. Wang, Y. Wang, D. Hua, *Surf. Coat. Technol.* **2017**, *313*, 374.

[79] L. Zhou, G. Su, H. Wang, J. Huang, Y. Guo, Z. Li, X. Su, *J. Alloys Compd.* **2019**, *777*, 478.

[80] D. Chen, F. Luo, W. Zhou, D. Zhu, *J. Electron. Mater.* **2019**, *48*, 1506.

[81] T. Shao, H. Ma, M. Feng, J. Wang, M. Yan, J. Wang, S. Zhao, S. Qu, *J. Alloys Compd.* **2020**, *818*, 152851.

[82] T. Shao, H. Ma, J. Wang, M. Yan, M. Feng, Z. Yang, Q. Zhou, J. Wang, Y. Meng, S. Zhao, S. Qu, *J. Alloys Compd.* **2020**, *832*, 154945.

[83] T. Shao, H. Ma, J. Wang, M. Yan, M. Feng, M. Yan, J. Wang, Z. Yang, Q. Zhou, H. Luo, S. Qu, *J. Eur. Ceram. Soc.* **2020**, *40*, 2013.

[84] T. E. Bogale, X. Wang, L. B. Le, in *mmWave Massive MIMO*, (Eds: S. Mumtaz, J. Rodriguez, L. Dai), Academic Press, Cambridge, MA **2017**, pp. 195–225, Ch. 9.

[85] W. Tian, R. Ma, J. Gu, Z. Wang, N. Ma, P. Du, *J. Mater. Chem.* **2018**, *6*, 12965.

[86] K. Bobzin, T. Schlaefer, M. Bégard, M. Bruehl, G. Bolelli, L. Lusvarghi, D. Lisjak, A. Hujanen, P. Lintunen, U. Kanerva, T. Varis, M. Pasquale, *Surf. Coat. Technol.* **2010**, *205*, 1015.

[87] K. Bobzin, G. Bolelli, M. Bruehl, A. Hujanen, P. Lintunen, D. Lisjak, S. Gyergyek, L. Lusvarghi, *J. Eur. Ceram. Soc.* **2011**, *31*, 1439.

[88] O. Jeong, A. Lee, C. Raum, A. Suzuki, *J. Low Temp. Phys.* **2016**, *184*, 621.

[89] H.-J. Song, T. Nagatsuma, in *Handbook of Terahertz Technologies Devices and Applications*, 1st Ed, Jenny Stanford Publishing, New York **2015**.

[90] M. Watanabe, S. Kuroda, H. Yamawaki, M. Shiwa, *Surf. Coat. Technol.* **2011**, *205*, 4620.

[91] I. Wilke, *Encyclopedia of Spectroscopy and Spectrometry*, 3rd edn., (Eds: J. C. Lindon, G. E. Tranter, D. W. Koppenaal), Academic Press, Cambridge, MA **2017**, pp. 427–431.

[92] K. Xu, M. Du, L. Hao, J. Mi, Q. Yu, S. Li, *J. Materiom.* **2020**, *6*, 167.

[93] R. Vaßen, Z. Yi, H. Kaßner, D. Stöver, *Surf. Coat. Technol.* **2009**, *203*, 2146.

[94] Y. Gao, J. Xiong, D. Gong, J. Li, M. Ding, *Vacuum* **2015**, *121*, 64.

[95] X. Wang, T. Ouyang, X. Duan, C. Ke, X. Zhang, J. Min, A. Li, W. Guo, X. Cheng, *Metals* **2017**, *7*, 137.

[96] C. Ke, X. Zhang, W. Guo, Y. Li, D.-Q. Gong, X. Cheng, *Vacuum* **2018**, *152*, 114.

[97] X. Duan, X. Zhang, C. Ke, S. Jiang, X. Wang, S. Li, W. Guo, X. Cheng, *Vacuum* **2017**, *145*, 209.

[98] C. Meola, S. Boccardi, G. M. Carlomagno, in *Infrared Thermography in the Evaluation of Aerospace Composite Materials*, (Eds: C. Meola, S. Boccardi, G. Carlomagno), Woodhead Publishing, Swaston, UK **2017**, pp. 57-83, Ch. 3.

[99] R. Tummala, R. K. Guduru, P. S. Mohanty, *Mater. Res. Bull.* **2011**, *46*, 1276.

[100] R. Dom, G. S. Kumar, N. Y. Hebalkar, S. V. Joshi, P. H. Borse, *RSC Adv.* **2013**, *3*, 15217.

[101] X.-Q. Deng, M.-M. Xue, Y.-L. Lv, R.-H. Li, J.-M. Tong, G.-H. Shi, Y. Yang, Y.-C. Dong, *Vacuum* **2020**, *174*, 109214.

[102] V. Etacheri, C. D. Valentin, J. Schneider, D. Bahnemann, S. C. Pillai, *J. Photochem. Photobiol. C: Photochem. Rev.* **2015**, *25*, 1.

[103] L. Łatka, L. Pawłowski, M. Winnicki, P. Sokołowski, A. Małachowska, S. Kozerski, *Appl. Sci.* **2020**, *10*, 5153.

[104] Y. Liu, J. Huang, X. Feng, H. Li, *J. Therm. Spray Technol.* **2021**, *30*, 1.

[105] H. Khatibnezhad, F. Ambriz-Vargas, F. B. Ettouil, C. Moreau, *J. Eur. Ceram. Soc.* **2021**, *41*, 544.

[106] B. W. Robinson, C. J. Tighe, R. I. Gruar, A. Mills, I. P. Parkin, A. K. Tabecki, H. L. de Villiers Lovelockc, J. A. Darr, *J. Mater. Chem. A* **2015**, *3*, 12680.

[107] M. R. A. Kumar, B. Abebe, H. P. Nagaswarupa, H. C. A. Murthy, C. R. Ravikumar, F. K. Sabir, *Sci. Rep.* **2020**, *10*, 1249.

[108] F. Ye, A. Ohmori, *Surf. Coat. Technol.* **2002**, *160*, 62.

[109] S. Dosta, M. Robotti, S. Garcia-Segura, E. Brillas, I. G. Cano, J. M. Guilemany, *Appl. Catal., B* **2016**, *189*, 151.

[110] F. Wang, X. Qian, X. Li, J. Ye, Z. Han, Y. Chen, G. Liu, J. Li, *Mater. Lett.* **2015**, *151*, 82.

[111] G. Mauer, A. Guignard, R. Vaßen, *Surf. Coat. Technol.* **2013**, *220*, 40.

[112] C. Zhang, U. Chaudhary, S. Das, A. Godavarty, A. Agarwal, *J. Therm. Spray Technol.* **2013**, *22*, 1193.

[113] D. Chen, E. H. Jordan, M. Gell, *Surf. Coat. Technol.* **2008**, *202*, 2132.

[114] D. Chen, E. H. Jordan, M. Gell, *Surf. Coat. Technol.* **2008**, *202*, 6113.

[115] R. Kumar, S. Govindarajan, K. S. K. J. Reddy, T. N. Rao, S. V. Joshi, S. Anandan, *ACS Appl. Mater. Interfaces* **2016**, *8*, 27642.

[116] J.-M. Jang, H.-S. Lee, J. K. Singh, *Materials* **2020**, *13*, 5776.

[117] *MIL-STD-188-125-1, High-Altitude Electromagnetic Pulse (HEMP) Protection for Ground-Based C4I Facilities Performing Critical, Time-Urgent Missions Part 1 Fixed Facilities*, Department of Defense Interface Standard, Alexandria, VA **1998**.

[118] IEEE Std 299., *IEEE Standard Method for Measuring the Shielding Effectiveness of ELECTROMAGNETIC Shielding Enclosures*, IEEE, Piscataway, NJ **2006**, p. 50.

[119] D. J. Helfritch, in *Woodhead Publishing Series in Metals and Surface Engineering, The Cold Spray Materials Deposition Process*, (Eds: V. K. Champagne), Woodhead Publishing, Swaston, UK **2007**, pp. 315–326, Ch. 16.

[120] Q. Wen, W. Zhou, J. Su, Y. Qing, F. Luo, D. Zhu, *J. Alloys Compd.* **2016**, *666*, 359.

[121] Y. Qing, J. Su, Q. Wen, F. Luo, D. Zhu, W. Zhou, *J. Alloys Compd.* **2015**, *651*, 259.

[122] L. Zhou, W. Zhou, M. Chen, F. Luo, D. Zhu, *Mater. Sci. Eng. B* **2011**, *176*, 1456.

[123] F.-S. Hung, *Coatings* **2019**, *9*, 495.

[124] Y. Qing, H. Yao, Y. Li, F. Luo, *J. Eur. Ceram. Soc.* **2021**, *41*, 1071.

[125] R. Wilson, G. George, K. Joseph, in *Materials for Potential EMI Shielding Applications* (Eds: K. Joseph, R. Wilson, G. George), Elsevier, Amsterdam **2020**, pp. 1–8, Ch. 1.

[126] H. Liu, S. Wu, C. You, N. Tian, Y. Li, N. Chopra, *Carbon* **2021**, *172*, 569.

[127] A. Iqbal, J. Kwon, M.-K. Kim, C. M. Koo, *Mater. Today Adv.* **2021**, *9*, 100124.

[128] Z. Zhang, S. H. Lim, J. Chai, D. M. Y. Lai, P. C. Lim, A. K. H. Cheong, S. Wang, H. Jin, J. Pan, *J. Alloys Compd.* **2018**, *735*, 377.

[129] C. Balaji, B. Srinivasan, S. Gedupudi, in *Heat Transfer Engineering*, Academic Press, **2021**, pp. 233-, Ch. 8.

[130] D. Chellaganesh, M. A. Khan, J. T. W. Jappes, *Mater. Today: Proc.* **2020**, *45*, 1529.

[131] A. Mehta, H. Vasudev, S. Singh, *Mater. Today: Proc.* **2020**, *26*, 1336.

[132] B. J. Zhang, B. X. Wang, C. Y. Zhao, *Int. J. Heat Mass Transfer* **2014**, *73*, 59.

[133] X. W. Chen, C. Y. Zhao, B. X. Wang, *J. Quant. Spectrosc. Radiat. Transfer* **2018**, *210*, 116.

[134] A. Ganvir, S. Joshi, N. Markocsan, R. Vassen, *Mater. Des.* **2018**, *144*, 192.

[135] S. Goel, S. Björklund, N. Curry, U. Wiklund, S. V. Joshi, *Surf. Coat. Technol.* **2017**, *315*, 80.

[136] A. Aygun, A. L. Vasiliev, N. P. Padture, X. Ma, *Acta Mater.* **2007**, *55*, 6734.

[137] R. Vassen, X. Cao, F. Tietz, D. Basu, D. Stöver, *J. Am. Ceram. Soc.* **2000**, *83*, 2023.

[138] S. Mahade, N. Curry, S. Björklund, N. Markocsan, P. Nylén, R. Vaßen, *J. Therm. Spray Technol.* **2017**, *26* 108.

[139] S. Mahade, D. Zhou, N. Curry, N. Markocsan, P. Nylén, R. Vaßen, *J. Mater. Process. Technol.* **2019**, *264*, 283.

[140] M. Gell, E. H. Jordan, M. Teicholz, B. M. Cetegen, N. P. Padture, L.D. XieChen , D. Chen, X. Ma, J. Roth, *J. Therm. Spray Technol.* **2008**, *17*, 124.

[141] L. Xie, D. Chen, E. H. Jordan, A. Ozturk, F. Wu, X. Ma, B. M. Cetegen, M. Gell, *Surf. Coat. Technol.* **2006**, *201* 1058.

[142] C. Jiang, E. H. Jordan, A. B. Harris, M. Gell, J. Roth, *J. Therm. Spray Technol.* **2015**, *24*, 895.

[143] P. Fauchais, G. Montavon, G. Bertrand, *J. Therm. Spray Technol.* **2010**, *19*, 56.

[144] L. Zhong, X. Ma, *Optoelectronics — Devices and Applications* (Ed: P. Predeep), InTech **2011**, pp. 325–348.

[145] B. S. Mann, V. Arya, B. K. Pant, *J. Mater. Eng. Perform.* **2013**, *22*, 1995.

[146] J. Mateos, J. M. Cuetos, E. Fernández, R. Vijande, *Wear* **2000**, *239*, 274.

[147] R. Ghasemi, R. Shoja-Razavi, R. Mozafarinia, H. Jamali, *Ceram. Int.* **2013**, *39*, 9483.

[148] D. Wang, Z. Tian, L. Shen, Z. Liu, Y. Huang, *Ceram. Int.* **2014**, *40*, 8791.

[149] P.-C. Tsai, J.-H. Lee, C.-L. Chang, *Surf. Coat. Technol.* **2007**, *202* 719.

[150] P. Daram, C. Banjongprasert, W. Thongsuwan, S. Jiansirisomboon, *Surf. Coat. Technol.* **2016**, *306*, 290.

[151] M. Robotti, S. Dosta, C. Fernandez-Rodriguez, M. J. Hernandez-Rodriguez, I. G. Cano, E. Pulido Melian, J. M. Guilemany, *Appl. Surf. Sci.* **2016**, *362*, 274.

[152] J. Huang, Y. Gong, Y. Liu, X. Suo, H. Li, *J. Eur. Ceram. Soc.* **2017**, *37*, 3705.

[153] F. Venturi, S. Kamnis, T. Hussain, *Mater. Des.* **2021**, *202*, 109566.

[154] K. Pielichowski, J. Njuguna, B. Janowski, J. Pielichowski, in *Supramolecular Polymers Polymeric Betains Oligomers. Advances in Polymer Science*, Springer, Berlin, Heidelberg **2006**, p. 201.

[155] M. Hoshino, K. Sanematsu, Y. Watanabe, in *Handbook on the Physics and Chemistry of Rare Earths*, (Eds: B. Jean-Claude, V. K. Pecharsky), Vol. 49, Elsevier, Amsterdam **2016**, pp. 129–291, Ch. 279.

[156] C. Mang, Z. Ma, J. Luo, M. Rao, X. Zhang, Z. Peng, *J. Rare Earths* **2020**, *39*, 1415.

[157] F. Wall, Rare Earth Elements, *Encyclopedia of Geology*, 2nd edn., (Eds: D. Alderton, S. A. Elias), Academic Press **2021**, pp. 680–693.

[158] EP1167565A2, **2002**. https://patents.google.com/patent/EP1167565B1.

[159] WO2013047589A1, **2013**. https://patents.google.com/patent/US9670099B2/en.

[160] US9670099B2, **2017**. https://patents.google.com/patent/US9670099B2/en.

[161] EP1642994B8, **2017**. https://patents.google.com/patent/EP1642994A2/en.

[162] S. P. Sharma, D. K. Dwivedi, P. K. Jain, *J. Eng. Tribol.* **2008**, *222*, 925.

[163] J. A. Gan, C. C. Berndt, *J. Therm. Spray Technol.* **2013**, *22*, 1069.

[164] H. Singh, S. S. Chatha, B. S. Sidhu, in *TEQIP-II Sponsored National Conf. on "Latest Developments in Materials, Manufacturing and Quality Control* February **2015**.

[165] C. Hu, S. Hou, *Coatings* **2017**, *7*, 30.

[166] M. Vishnoi, Q. Murtaza, P. Kumar, *Mater. Today: Proc.* **2020**, *44*, 4053.

[167] W. Jing, Z. Hong, B. Shuxin, C. Ke, Z. Changrui, *J. Magn. Magn. Mater.* **2007**, *312*, 310.

[168] M. Willson, S. Bauser, S. Liu, M. Huang, *J. Appl. Phys.* **2003**, *93*, 7987.

[169] P. C. King, S. H. Zahiri, M. Z. Jahedi, *J. Therm. Spray Technol.* **2008**, *17*, 221.

[170] R. Ahmed, O. Ali, N. H. Faisal, N. M. Al-Anazi, S. Al-Mutairi, F.-L. Toma, L.-M. Berger, A. Potthoff, M. F. A. Goosen, *Wear* **2015**, *322–323*, 133.

[171] W. Fan, Y. Bai, *Ceram. Int.* **2016**, *42*, 14299.

[172] A. Rincón, Z. Pala, T. Hussain, *Mater. Lett.* **2020**, *281*, 128601.

[173] S. V. Joshi, G. Sivakumar, T. Raghuveer, R. O. Dusane, *J. Therm. Spray Technol.* **2014**, *23*, 616.

[174] S. V. Joshi, G. Sivakumar, *J. Therm. Spray Technol.* **2015**, *24*, 1166.

[175] E. P. George, D. Raabe, R. O. Ritchie, *Nat. Rev. Mater.* **2019**, *4*, 515.

[176] J. W. Yeh, *Ann. de Chimie: Sci. des Mater.* **2006**, *31*, 633.

[177] M. C. Gao, J. W. Yeh, P. K. Liaw, Y. Zhang, in *High-entropy Alloys: Fundamentals and Applications*, Springer, New York **2016**.

[178] T. Egami, W. Guo, P. D. Rack, T. Nagase, *Metall. Mater. Trans. A* **2014**, *45*, 180.

[179] Z. Yingzhe, C. Yudao, Q. Qingdong, L. Wei, *J. Magn. Magn. Mater.* **2020**, *498*, 166151.

[180] Y. Duan, X. Wen, B. Zhang, G. Ma, T. Wang, *J. Magn. Magn. Mater.* **2020**, *497*, 165947.

[181] P. Yang, Y. Liu, X. Zhao, J. Cheng, H. Li, *Adv. Powder Technol.* **2016**, *27*, 1128.

[182] D. Lan, Z. Zhao, Z. Gao, K. Kou, G. Wu, H. Wu, *J. Magn. Magn. Mater.* **2020**, *512*, 167065.

[183] Y. Zhang, B. Zhang, K. Li, G.-L. Zhao, S. M. Guo, *J. Alloys Compd.* **2018**, *734*, 220.

[184] B. Zhang, Y. Duan, X. Wen, G. Ma, T. Wang, X. Dong, H. Zhang, N. Jia, Y. Zeng, *J. Alloys Compd.* **2019**, *790*, 179.

[185] P. Yang, Y. Liu, X. Zhao, J. Cheng, H. Li, *J. Mater. Res.* **2016**, *31*, 2398.

[186] Y. Li, S. Shang, W. Zhang, *AIP Adv.* **2019**, *9*, 125045.

[187] H. Wu, D. Lan, B. Li, L. Zhang, Y. Fu, Y. Zhang, H. Xing, *Composit. Part B: Eng.* **2019**, *179*, 107524.

[188] A. Meghwal, A. Anupam, B. S. Murty, C. C. Berndt, R. S. Kottada, A. S. M. Ang, *J. Therm. Spray Technol.* **2020**, *29*, 857.

[189] D. B. Avdeev, *Surv. Geophys.* **2005**, *26*, 767.

[190] M. Jaber, J. Miehé-Brendlé, in *Ordered Porous Solids*, (Eds: V. Valtchev, S. Mintova, M. Tsapatsis), Elsevier, Amsterdam **2009**, pp. 31-49, Ch. 2.

[191] A. Berrouk, R. Dusseaux, S. Afifi, *Progr. Electromagnet. Res. B* **2014**, *57*, 177.

[192] S. Perna, A. Iodice, *IEEE Trans. Antennas Propag.* **2011**, *59*, 595.

[193] H. Zamani, A. Tavakoli, M. Dehmollaian, *IEEE Trans. Antennas Propag.* **2016**, *64*, 1877.

[194] M. Rahmanzadeh, H. Rajabalipanah, A. Abdolali, *IEEE Trans. Plasma Sci.* **2017**, *45*, 945.

[195] A. Ishimaru, in *Wave Propagation and Scattering in Random Media*, Academic Press, Cambridge, MA **1978**.

[196] F. G. Bass, I. M. Fuks, in *Wave Scattering from Statistically Rough Surfaces*, Pergamon, Oxford, UK **1979**.

[197] L. Tsang, J. A. Kong, R. T. Shin, in *Theory of Microwave Remote Sensing*, John Wiley and Sons, New York **1985**.

[198] F. T. Ulaby, R. K. Moore, A. K. Fung, in *Microwave Remote Sensing: Active and Passive*, Vol. Vol. 1, Addison-Wesley, Reading **1981**, p. 456.

[199] A. G. Voronovich, in *Wave Scattering from Rough Surfaces*, edn. 2, Springer, Berlin **1999**, p. 237.

[200] A. G. Voronovich, *Waves Random Media* **1994**, *4*, 337.

[201] B. B. Mandelbrot, in *The Fractal Geometry of Nature*, W. H. Freeman and Company, New York, NY **1982**.

[202] A. J. Poggio, E. K. Miller, in *International Series of Monographs in Electrical Engineering, Computer Techniques for Electromagnetics* (Ed: R. Mittra), Pergamon, Oxford, UK **1973**, pp. 159–264, Ch. 4.

[203] A. G. Yarovoy, R. V. de Jongh, L. P. Ligthart, *Radio Sci.* **2000**, *35*, 455.

[204] K. Sarabandi, T. Chiu, *IEEE Trans. Antennas Propag.* **1997**, *45*, 1419.

[205] C. F. Smith, A. F. Peterson, R. Mittra, *IEEE Trans. Antennas Propag.* **1990**, *38*, 938.

[206] L. Zhang, G. G. Pan, J. A. Jones, *IEEE Trans. Antennas Propag.* **2017**, *65*, 2615.

[207] J. Kim, S. Torquato, *Proc. Natl. Acad. Sci.* **2020**, *117*, 8764.

[208] Z. Yang, F. Luo, M. Sun, J. Xu, W. Zhou, Y. Qing, D. Zhu, Z. Huang, *Mater. Lett.* **2015**, *151*, 109.

[209] D. V. Dranidis, *Airborne Stealth in a Nutshell-Part I*, Waypoint Magazine, 5th Issue, April/May 2003; http://img.bemil.chosun.com/nbrd/data/10040/upfile/201001/20100106104057.pdf (accessed March 2021).

[210] R. Kovar, *Environmentally Compliant Sprayable Low Observable Coatings that Facilitate Rapid Removal and Repair (Report: WP-1181)*, **2004**, https://serdp-estcp.org/index.php/Program-Areas/Weapons-Systems-and-Platforms/Surface-Engineering-and-Structural-Materials/Coatings/WP-1181 (accessed March 2021).

[211] S. Trimble, *F-22 Stealth Coatings Face Legal Scrutiny;* **2009**, https://www.flightglobal.com/f-22-stealth-coatings-face-legal-scrutiny/87622.article (accessed March 2021).

[212] H. Lv, Z. Yang, B. Liu, G. Wu, Z. Lou, B. Fei, R. Wu, *Nat. Commun.* **2021**, *12*, 834.

[213] T. Cui, M. Qi, X. Wan, J. Zhao, Q. Cheng, *Light Sci. Appl.* **2014**, *3*, e218.

[214] J. B. Pendry, *Phys. Rev. Lett.* **2000**, *85*, 3966.

[215] J. B. Pendry, *Contemp. Phys.* **2004**, *45*, 191.

[216] V. G. Veselago, *Sov. Phys. Uspekhi* **1968**, *10*, 509.

[217] J. Valentine, S. Zhang, T. Zentgraf, E. Ulin-Avila, D. A. Genov, G. Barta, X. Zhang, *Nature* **2008**, *455*, 376.

[218] N. H. Faisal, N. Sellami, F. Venturi, T. Hussain, T. Mallick, F. Muhammad-Sukki, A. Bishop, H. Upadhyaya, N. K. Katiyar, S. Goel, *Emerg. Mater.* **2021**, *4*, 1619.

[219] S. Zhao, H. Ma, T. Shao, J. Wang, Z. Yang, Y. Meng, M. Feng, M. Yan, J. Wang, S. Qu, *J. Alloys Compd.* **2021**, *874*, 159822.

[220] A. Boltasseva, V. M. Shalaev, *Metamaterials* **2008**, *2*, 1.

[221] Y. Xie, X. Fan, J. Wilson, R. N. Simons, Y. Chen, J. Q. Xiao, *Sci. Rep.* **2014**, *4*, 6301.

[222] F. Cao, J. Xu, Z. Zhao, X. Zhang, Q. Ouyang, C. Zhu, X. Zhang, X. Zhang, Y. Chen, *Carbon* **2021**, *185*, 177.

[223] N. Yang, Z. X. Luo, S. C. Chen, G. Wu, Y. Z. Wang, *ACS Appl. Mater. Interfaces* **2020**, *12*, 18952.

[224] C. L. Zhu, S. Zhang, Y. Sun, Y. J. Chen, *J. Alloys Compd.* **2017**, *711*, 552.

[225] T. Wu, Y. Liu, X. Zeng, T. Cui, Y. Zhao, Y. Li, et al., *ACS Appl. Mater. Interfaces* **2016**, *8*, 7370.

[226] P. P. Yang, X. C. Zhao, Y. Liu, X. H. Lai, *Adv. Powder Technol.* **2018**, *29*, 289.

[227] J. Su, W. Zhou, Y. Liu, Y. Qing, F. Luo, D. Zhu, *J. Mater. Sci. Mater. Electron.* **2016**, *27*, 2460.

[228] M. S. Venkatesh, G. S. V. Raghavan, *Canadian Biosyst. Eng.* **2005**, *47*, 15.

[229] *MarketWatch Thermal Spray Equiment Market Share 2021 Industry Size, Growth, Global Technology, Development, Trends And Forecast To 2023*, https://www.marketwatch.com/press-release/thermal-spray-equiment-market-share-2021-industry-size-growth-global-technology-development-trends-and-forecast-to-2023-2021-04-05 (accessed: April 2021).

[230] *Prescient and Strategic Intelligence Private Limited (P&S Intelligence), Thermal Spray Market Size*, https://www.psmarketresearch.com/market-analysis/thermal-spray-market (accessed: April 2021).

[231] J. P. Longtin, L. Zuo, D. Hwang, G. Fu, M. Tewolde, Y. Chen, S. Sampath, *J. Therm. Spray Technol.* **2013**, *22*, 577.

[232] M. R. Dorfman, in *Handbook of Environmental Degradation of Materials*, 3rd edn. (Ed: M. Kutz), William Andrew Publishing, Norwich, NY **2018**, pp. 469–488, Ch. 22.

[233] P. Fauchais, in *Future Development of Thermal Spray Coatings* (Ed: N. Espallargas), Woodhead Publishing, Swaston, UK **2015**, pp. 17-49, Ch. 2.

[234] S. Wijewardane, in *Future Development of Thermal Spray Coatings* (Ed: N. Espallargas), Woodhead Publishing, Swaston, UK **2015**, pp. 241–257, Ch. 10.

[235] *Electromagnetic spectrum (COSMOS - The SAO Encyclopedia of Astronomy);* https://astronomy.swin.edu.au/cosmos/E/Electromagnetic+Spectrum (accessed: March 2021).

Nadimul Haque Faisal (Ph.D., C.Eng, MIMechE, MIMMM, FHEA) is a professor of Surface Engineering and Micromechanics at Robert Gordon University. His interest includes micromechanical behavior analysis of thermal spray coatings and thin films, metamaterial manufacturing using thermal spray coating techniques, sensor-based instrumented mechanical testing, and acoustic emission (AE) sensor-based condition monitoring. He has 70 peer-reviewed journals, 1 USA Patent, 4 book chapters, and over 50 conference publications. He is member of Royal Society of Edinburgh's Young Academy of Scotland, EPSRC peer review College member, and member of UK's Metamaterials Network. Total research and commercial funding obtained is over £1.25M (as PI/Co-I). He is principal investigator of recently funded EPSRC grant 'METASIS' (EP/W033178/1).

Rehan Ahmed is the associate director of research and senior programme director for mechanical engineering at Heriot-Watt University. He is an internationally leading expert on surface engineering, mechanics, materials, and manufacturing and has published more than 100 refereed research papers. He has successfully secured more than 20 competitive research grants with value in excess of £2.2 million from Industry and Research Councils. He was featured in the "Global Pioneers" theme of Heriot-Watt University in 2016. He is a member of the EPSRC Peer-Review college and has been the guest editor for special issues in the Journal of Thermal Spray Technology.

Nazmi Sellami is an associate professor in mechanical engineering and research lead at Edinburgh Napier University. His research is rooted in the field of renewable energy systems, with a special focus on solar energy including the characterization and design of thermal and photovoltaic solar devices for various types of applications and especially for building integration. He has worked on various multidisciplinary projects including quantifying and monitoring potential ecosystem impacts of geological carbon storage and scalable solar thermoelectric, and photovoltaics. He has 36 peer-reviewed journal articles and over 16 conference publications.

Anil Prathuru is a lecturer in the School of Engineering, Robert Gordon University, and an early career researcher with experience in thermal spray coating development and characterization. Before joining RGU, he worked as a mechanical engineer for EC-OG, Aberdeen, a subsea renewables company. His research interests include thermal spray coatings for energy harvesting, hydrogen energy, and remote-sensing applications and application of machine learning in material development. He also worked on the development of structural health monitoring based on NDT techniques and associated data processing methods. He has worked on several commercial projects related to early-stage technology development as a research project on the digitalization of material development.

James Njuguna is the research strategic lead (engineering) and subsea engineering theme lead at National Subsea Centre. His research is focused on experimental research on composite materials reinforcement, materials design, and selection and structural–property relationship. Structural composite research is on evaluation of composites' integrity and durability evaluation primary structural applications in impact resistance and energy absorption management. A side stream of his research is a focus on exploiting materials failure behavior to investigate emission/diffusion/release of nanofillers from polymer fiber-reinforced nanocomposites, which contributes to research on their durability and on furthering NanoSafety of nanomaterials to human and environmental health.

Federico Venturi is assistant professor in materials and aerospace engineering at the University of Nottingham (UK). His interests and expertise encompass advanced materials characterization and surface engineering, including thermal spray, nanocomposite coatings, transmission electron microscopy, and additive manufacturing. He received his Ph.D. in Physics and Nanosciences from the University of Modena and Reggio Emilia (Italy) and then worked as a research fellow in surface engineering at the University of Nottingham. He has been a visiting researcher at EMAT University of Antwerp (Belgium) and ER-C Forschungszentrum Jülich (Germany). He holds B.Sc. and M.Sc. in physics from the University of Bologna (Italy).

Tanvir Hussain, C.Eng, FIMMM, FHEA, holds a Chair in coatings and surface engineering at the University of Nottingham, UK, and an EPSRC research fellowship (EP/V010093/1, £2.1 M) on ceramic coatings for aerospace propulsion. He was also awarded the Royal Academy of Engineering (RAEng) fellowship in conjunction with Leverhulme Trust. He has been a PI or CoI on £8.3 m grants from UKRI (UK Research and Innovation) and industry. With over 100+ peer-reviewed journal papers and 2100+ citations, he is in the top 2% of the scientists cited worldwide. He is an editor of the Journal of Thermal Spray Technology and served as an associated editor for the Journal of Engineering Tribology (IMechE). He is particularly interested in the understanding of novel materials processing techniques, especially thermal spray, and cold gas dynamic spray.

Hamed Yazdani Nezhad is an associate professor in aerospace structures at City, University of London, the director of the Advanced Composites Research Focused Group, and a member of the Aeronautics and Aerospace Research Centre. His research is focused on multiscale design, development, characterization, and structural analysis of multifunctional polymeric composites and composite structures under mechanical loading, electromagnetic field exposure, and environmental conditions. He has practiced fabrication techniques through conventional and unconventional nanocomposite and composite manufacturing, 4D printing, interrogation of materials/structures through fracture, high strain rate, impact, cyclic loading, fatigue, hygrothermal testing and in situ instrumentations, and numerical analysis through continuum damage mechanics and multiphysics finite-element analysis.

Nirmal Kumar Katiyar is a Newton International postdoctoral Fellow at London South Bank University, London, awarded by Royal society UK. He received his Ph.D. in materials science and engineering from Indian Institute of Technology Kanpur, Kanpur India. His interests are focused on nanomaterials preparation, characterization, and their functional applications, thermal spray coating, cryo-ball milling, high entropy alloys, and catalysis. His devotion is toward development of nature-inspired materials for ecofriendly sustainable development.

Saurav Goel (FHEA, FIMMM) is an associate professor of precision engineering at London South Bank University with visiting appointments at various Universities in India, China, and the UK. He is a passionate researcher working in the area of material-oriented manufacturing using digitalized approaches. He is an EPSRC ECF forum member in manufacturing and an associate director of the EPSRC NetworkPlus in manufacturing. He is currently serving as an associate editor for four international journals (Journal of Advanced Manufacturing Systems, Journal of Manufacturing Processes, BioMaterials and Polymers Horizons and Nanofabrication). He has published 85+ journal papers in various top-tier international journals including the prestigious Nature magazine.

Hari Upadhyaya is cofounder and former Head of London Centre for Energy Engineering at the school of Engineering, London South Bank University. He had held Chair positions at Brunel University (2014–2018), at Heriot-Watt University (2011–2014), and was instrumental in establishing the world class PV laboratory at CREST, Loughborough University (2005–2011). He is an expert in thin-film deposition using vacuum and nonvacuum processing methods toward a range of semiconducting junction device researches, which include transparent conducting oxides (TCOs), dye-sensitized solar cells (DSCs), perovskite solar cells, CdTe, and CIGS thin film solar cell technologies, including memristors and metamaterials antennae.

Shrikant Joshi is a professor in the Department of Engineering Science at University West, Sweden, with nearly 30 years of experience in areas spanning surface engineering, laser materials processing, and now also additive manufacturing. He is a chemical engineer by academic training, having obtained his M.S. and Ph.D. from the Rensselaer Polytechnic Institute and University of Idaho, respectively, in USA. Prior to moving to Sweden, he has had long stints as a scientist at a couple of premier federally funded materials' research laboratories in India. His work has led to many industrial applications, over a dozen patent submissions, and more than 200 publications in peer-reviewed journals.

Firdaus Muhammad-Sukki is a lecturer in Engineering Mathematics at the School of Engineering and Built Environment, Edinburgh Napier University. His research interest is in the area of renewable energy technology and policies and sustainable resources with specific focus on concentrator technology and solar cells. He has 98 peer-reviewed journals, 1 UK and 1 USA Patent, and 5 book chapters, and over 61 conference publications.

Radhakrishna Prabhu is a professor in Smart Sensors and Instrumentation. He has more than 25 years of research experience and generated strong research record in areas including optical instrumentation, sensing, spectroscopy, surface engineering and nanocoating, clean technology, and optical materials and electronic instrumentation. He has authored more than 150 publications in scientific journals, conferences, symposia, and books. He also has many patents related to optical security and biosensing. His research has led to many research collaborations both nationally and internationally including USA, Europe, Brazil, Malaysia, Turkey, and India.

Tapas Kumar Mallick is currently the chair in Clean Technologies (Renewables) within the Environment and Sustainability Institute (ESI) and he leads the Solar Energy Research at University of Exeter. He is also cofounder and chief scientific advisor to the Build Solar limited, a spin-out company from University of Exeter and adjunct professor of Mechanical Engineering at Indian Institute of Technology, Madras. He has secured research funding ($>£13.5m$) as PI and Co-PI of various national, European, international, and industrial funders. He has published over 340 research articles and holds two patents on solar technology and successfully supervised 25 Ph.D. candidates to completion in the wide range of problems associated with solar energy.

Will Whittow (AFWES, SFHEA, SMIEEE) is professor of Radiofrequency Materials at Loughborough University and leads the Wireless Communications Research Group in the Wolfson School of Mechanical, Electrical and Manufacturing Engineering. He is a named investigator on EPSRC grants totalling > £9m: 3D Metamaterials for RF, Microwave, and THz Applications (SYMETA) (PI, EP/N010493/1), Microfabricated anisotropic metasurfaces (PI, EP/S030301/1, EP/S030794/1), and 3D antennas (PI, EP/K011383/1). He has > 250 peer-reviewed publications (> 3,000 citations, H-index = 28), metasurfaces and metamaterials, frequency-selective surfaces (FSS), dielectric lenses, dielectric characterization, and inkjet printing and is currently editing an IET book on bioelectromagnetics.

Spyros Kamnis (C.Eng, FIMMM) is the R&D manager of Castolin Eutectic UK. Holds a B.Eng in mechanical engineering and an M.Sc. in thermal power and fluids engineering from the University of Manchester (UMIST). He obtained his Ph.D. in modeling of thermal spraying process and further developed his computational expertise in material modelling as a postdoctoral research associate at Aston University and later at the Energy Technology group in the University of Southampton (UK). He worked for Xi'an Jiaotong-Liverpool University as a lecturer for 4 years and he has published more than 45 papers.